THE DESIGN OF TWO APPARATI TO MEASURE SOLID-LIQUID AND LIQUID-LIQUID EQUILIBRIA DATA

By

Margreth Tadie

BEng (Hons)

National University of Science and Technology, Zimbabwe

Submitted in fulfilment of the academic requirements for the degree of Master of Science in Engineering to the Faculty of Engineering, School of Chemical Engineering, University of KwaZulu-Natal, Durban

2010

Preface

This work was carried out under the supervision of Professor D. Ramjugernath and Dr P. Naidoo from March 2009 up to November 2010, within the Thermodynamics Research Unit at the University of KwaZulu Natal.

I Margreth Tadie declare that;

(i) The research reported in this dissertation/thesis, except where otherwise indicated; is my original work.

(ii) This dissertation/thesis has not been submitted for any degree or examination at any other university.

(iii) This dissertation/thesis does not contain other persons' data, pictures, graphs or other information, unless specifically acknowledged as being sourced from other persons.

(iv) This dissertation/thesis does not contain other persons' writing, unless specifically acknowledged as being sourced from other researchers. Where other written sources have been quoted, then:

a) their words have been re-written but the general information attributed to them has been referenced;

b) where their exact words have been used, their writing has been placed inside quotation marks, and referenced.

(v) Where I have reproduced a publication of which I am an author, co-author or editor, I have indicated in detail which part of the publication was actually written by myself alone and have fully referenced such publications.

(vi) This dissertation/thesis does not contain text, graphics or tables copied and pasted from the Internet, unless specifically acknowledged, and the source being detailed in the dissertation/thesis and in the References sections.

Signed:

Margreth Tadie (Candidate)

"As the candidate's Supervisor I agree to the submission of this thesis."

Doctor P Naidoo (Supervisor)

Professor D Ramjugernath (Co-Supervisor)

Acknowledgments

I would like to acknowledge the following people who have made a significant contribution to my life during the period of this MSc and to the MSc work;

- My supervisors, Professor D. Ramjugernath and Doctor P. Naidoo, for their support and guidance throughout this work.
- Professor Dr Juergen Rarey whose advice on the way to go with the project was invaluable.
- Check-It-Systems, who developed the software for the apparati.
- Professor Eitelberg for assisting us in designing the software used for the apparati.
- My parents and sisters, without their love and support I would not have undertaken this master's degree.
- Mr J Chifamba and his wife who have continuously encouraged me to persevere and have been both family and mentors always encouraging me to push on.
- My colleagues and friends, Edson, Samuel, Ayanda, Lindinkosi, Travis, Kaniki, Jim, Mark, Thokozani, Xavier, Francois and Nadine.
- Finally and most importantly of all, my Lord and Saviour Jesus Christ, by His Grace I have made it this far. To Him I give the glory and praise and by His grace I will continue to another level in my life.

Abstract

Two new apparati have been developed to measure solid-liquid and liquid-liquid equilibria via a synthetic visual method by determination of thermal signatures. One apparatus adopts a technique of using Peltier modules for cooling, and the other is a well-known design that uses a cryogenic fluid in a thermostatted glass cell for cooling of the sample. The Peltier design is for small sample volumes, with a 10 cm^3 aluminium equilibrium cell and has a minimum operating temperature of 253.15 K. The glass design is developed to complement the Peltier and has a larger volume of 140 cm^3 and a minimum operating temperature of 223.15 K.

Both apparati have been semi-automated in order to increase the accuracy and improve the efficiency of data measurements. Therefore the experimenter no longer has to wait for many hours for the determination of equilibrium. This was done by incorporating software, which was specially designed for the apparati using Labview8^{TM}, for controlling the cooling and heating rates. The uncertainty of the temperature measurements was found to be ±0.03 K for the Peltier apparatus and ±0.02 K for the Glass apparatus.

Liquid-liquid equilibria data has also been measured on the Peltier apparatus, to demonstrate its versatility. This was done using a digital camera, controlled through the Labview software to identify cloud points. The results have been found to be comparable with literature values.

For solid-liquid equilibria new systems of n-alkyl carboxylic acid binary mixtures have also been measured: heptanoic acid + butyric acid and heptanoic acid + hexanoic acid. These systems were measured using both apparati and both systems exhibited eutectic behaviour. All eutectic temperatures were measured on the Glass apparatus. Experimental data for these systems was modelled using the local composition models: Wilson, NRTL and UNIQUAC models. The NRTL model was found to give the best results for both systems with root mean square deviations (RMSD) of 2.16 K and 1.27 K and absolute average deviations (AAD) of 0.61 K and 0.49 K, between temperature measurements of this work and those calculated from the models, for the heptanoic acid + butyric acid and heptanoic acid + hexanoic acid systems, respectively.

Table of Contents

List of Figures

Chapter 2

Chapter 3

Chapter 4

List of Photographs

Chapter 4

List of Tables

Nomenclature

a	activity
a_{12}	group interaction parameter in the UNIQUAC equation
Cp	specific heat capacity of the liquid [J/mol K]
$\hat{f}_i$	Fugacity of species *i* in solution [kPa]
f	fugacity [kPa]
f_i^o	Fugacity of species *i* at standard conditions [kPa]
G	molar Gibbs energy [J/mol]
$\overline{G_i}$	Partial molar Gibbs energy [J/mol]
G_{12} G_{21}	parameters in the NRTL model [cal/mol]
g_{12} g_{21}	energy interaction parameter between species in the NRTL model [cal/mol]
G*	molar Gibbs energy of pure species A [J/mol]
G^E	excess molar Gibbs energy [J/mol]
H	enthalpy [J/mol]
l	structural parameter in the UNIQUAC model
n	number of moles
P	pressure [kPa]
q	Pure component area parameter in the UNIQUAC model
q_1'	pure component area parameter in the UNIQUAC model
R	Universal gas constant [J/mol K]
r_1	pure component volume parameter in the UNIQUAC model
S	entropy [J/mol]
T	temperature [K]

Δu_{12} Δu_{21}	interaction energy parameters for the UNIQUAC model [cal/mol]
x	composition in the liquid phase
z	coordination number in the UNIQUAC model

Greek Letters

$\alpha_{12,21}$	non-randomness parameter in the NRTL model
β	denotes a form of crystal structure
Δ	denotes a change in a property
γ_i^{∞}	activity coefficient at infinite dilution
γ_i	activity coefficient
δ	denotes a form of crystal structure
ε	tolerance in the objective function
θ	area segment fraction in the UNIQUAC model
θ'	area segment fraction in the UNIQUAC model
$\lambda_{12,}$ $\lambda_{21,}$ λ_{11}	energy interaction parameters in the Wilson model [cal/mol]
Λ_{12}, Λ_{21}	Wilson model Parameters [cal/mol]
μ	chemical potential
π	total number of phases
σ	standard deviation
τ_{21}	energy interaction parameter in the NRTL model [cal/mol]
υ_1, υ_2	molar volume parameters in the Wilson Model [m^3/mol]
Φ^*	segment fraction in the UNIQUAC model

Subscripts

1,2	components 1 and 2 respectively
calc	denotes calculated
exp	denotes experimental
eut	denotes the eutectic
fus	denotes fusion
m	denotes melting
trs	denotes transition
t	denotes triple point

Superscripts

S	denotes the solid phase
L	denotes the liquid phase
E	denotes an excess property
mixt	denotes the mixture

Abbreviations

LLE	Liquid-Liquid Equilibria
SLE	Solid-Liquid Equilibria
VLE	Vapour-Liquid Equilibrium

Chapter 1

Introduction

1.1 Importance of Solid-Liquid and Liquid-Liquid Equilibria

The study of solid-liquid equilibria is essential for the design of separation processes, such as crystallisation. Solid-liquid equilibria is the study of melting and/or crystallisation temperatures of chemical mixtures or pure component chemicals. This data can be useful in a number of applications. These include either purification and separation processes, design of pipe-lines and equipment, and are also used for the determination of low temperature parameters for thermodynamic models. In separation processes solid-liquid equilibria is applied to separation of mixtures with a high separation factor (thermolabile components) that makes the components nearly impossible to separate by processes such as distillation (Lohmann et al., 1997).

Separation by crystallisation is commonly applied in the pharmaceutical industry where the chemicals used are sensitive to heat, for example separation of biological compounds such as amino acids. An example is the PhD work of Kurosawa (2004) which was to study the solubility of amino acids in solvents. Another application is the separation and purification of chemicals that are solid above room temperature such as fatty acids (Costa et al., 2007). A more recent study in solid-liquid equilibria has been the study of ionic liquids. These are salts that may tend to melt at temperatures close to or below 373.15 K (Arce et al., 2007), amongst them room temperature ionic liquids are liquid at room temperature (Marsh et al., 2004). Work has been done to investigate their solubility in various solvents in order to find an application for them in industry. These solvents may be alkanes, alkenes, aromatic compounds, water etc. Ionic liquids have low, almost negligible, vapour pressures for temperatures up to 400 K (Marsh et al, 2004). They are as a result under consideration as possible alternatives to volatile organic compounds (VOCs) as solvents (Poole and Poole, 2009 and Marsh et al, 2004).

Solid-liquid equilibria data are also often applied to the study of wax formation in the petroleum industry, for the design of pipe-lines and storage vessels containing or transporting crude oils with heavy hydrocarbon fractions (Hammami et al., 2003). Finally application of solid-liquid equilibria data is also used for the determination of parameters in thermodynamic models. Solid-liquid equilibria provide low temperature data that assists in defining the temperature dependence of the parameters for these models (Lohmann et al., 2001). Some liquid-liquid equilibria may be of interest with solid-liquid equilibria. Liquid mixtures may exhibit immiscibility in some temperature ranges, for example

1-butanol + water and 2-butanol + water mixtures (Lohmann et al., 1997). Immiscibility is a convenient method for chemical separation in extraction processes.

1.2 Background to Work and Objectives

The Thermodynamics Research Unit at the University of KwaZulu-Natal has been well established in measurement and modelling of phase equilibria; especially low to high temperature-pressure vapour-liquid equilibria and liquid-liquid equilibrium measurements. The Unit is currently focussed on the study of separation of fluorinated chemicals and work has been done in the area of vapour-liquid equilibria for fluorinated compounds. It was envisaged that the Unit would require solid-liquid equilibria for these types of compounds in the near future. However, there was no solid-liquid equilibria equipment in the research unit. The major objective of this work therefore was to develop apparati and expertise in SLE measurements and modelling.

The specific objective of this research is to develop an automated apparatus which utilises a synthetic technique to measure solid-liquid equilibrium data. The apparatus is to be diversified to measure liquid-liquid equilibrium data by a synthetic cloud point technique. The design and development of the apparatus is not a novel idea and has been adopted from the work of Torzo et al. (2007). They used Peltier modules as cooling devices in an apparatus to demonstrate and measure solid-liquid equilibria. The apparatus designed by Torzo and co-workers specifically measured solid-liquid equilibria. Their technique was adopted and improved in order to develop an apparatus that will accurately measure solid-liquid and liquid-liquid equilibria. The apparatus is also designed to be compact and have small sample volume. Low sample volumes allow for ease of handling of chemicals and lower costs in measurement of systems involving costly chemicals. A second apparatus which uses an already proven technique by Jakob et al. (1995) was also constructed to complement the SLE and LLE apparatus and so that the research unit would have two different SLE apparati for measurements. The Peltier apparatus provides the benefit of small sample size which is cost effective for measurement of expensive chemicals, whilst the glass apparatus may be applied to measurement of solid-liquid equilibria of larger chemical quantities.

In this work a thermodynamic description of solid-liquid and liquid-liquid equilibria is given from literature. Some equipment, which have been used to measure solid-liquid and liquid-liquid equilibria are reviewed and the key features and operation of these equipment have been highlighted. This is followed by a description of the apparati which has been commissioned, constructed, tested and used, including their experimental procedures. The method of analysis of results is also discussed. The apparatus performance, as well as experimental procedure was evaluated by measurement of test systems for SLE and LLE and through measurement of these systems, a reliable method for

determination of the phase equilibria data was developed. Finally new systems were measured for binary n-alkyl carboxylic acids and the SLE data and modelling are presented.

The measurement of SLE for carboxylic acids was an extension of an investigation which began in the Thermodynamic Research Unit by Sewnarain (2001). His investigation was into the possibility of crystallisation as a means for separation of carboxylic acid mixtures. He performed a feasibility study from which he found that there was potential viability in the application of freeze crystallisation for the separation of C2–C7 alky carboxylic acids. As a follow on from this work the measurement of solid-liquid equilibria for binary mixtures of carboxylic acids is made. The solid-liquid binary carboxylic acid mixtures that have been measured are shown in the matrix in Table 1-1 and the systems which remain to be measured are also indicated in this table.

Table1-1: The binary solid-liquid equilibrium experimental data available for C2-C7 alkyl carboxylic acid systems.

Carbon	***Number***	***2***	***3***	***4***	***4***	***5***	***6***	***7***
	Acid	**Acetic**	**Propionic**	**Butyric**	**Isobutyric**	**Pentanoic**	**Hexanoic**	**Heptanoic**
2	**Acetic**							
3	**Propionic**	a						
4	**Butyric**	b						
4	**Isobutyric**		f					
5	**Pentanoic**	c	g		h			
6	**Hexanoic**	d						
7	**Heptanoic**	e						

a. Abrman and Malijevska, (1999); b,c,d,e,f,g,h. Dortmund Data Bank Software (2009)

These measurements will contribute to data for the solid-liquid equilibria of binary carboxylic acid mixtures undertaken by the research unit. The work by Sewnarain was initiated as an investigation into the possibility of separating various carboxylic acids in a waste stream. The SLE data generated for these acid mixtures will provide valuable data for design of any future crystallisation equipment. It may also be used to determine operating conditions for any streams containing mixtures of acids at low temperatures. From modelling of the data, low temperature model parameters may be obtained. These will contribute to determination of the temperature dependence of the parameters for some of these systems at low temperatures and can be used for model predictions.

The focus of the work in this study has been on SLE measurements of carboxylic acids and the main objectives on building solid-liquid equilibria equipment and introducing solid-liquid phase equilibria

in the research unit. Future areas of research interest involving SLE and LLE include ionic liquids and fluorinated pharmaceutical components.

Fluorinated pharmaceuticals are becoming ever more common in the pharmaceutical industry. They have been applied in the manufacture of antidepressants, antibacterial agents and anti-cancer drugs (Kirk, 2006) to name a few applications. Fluorinated chemicals are being used to replace chlorinated and bromine pharmaceuticals due to the properties of fluorine (Müller et al., 2007). The properties of fluorine that have made it useful in biological processes are its small size, strong electronegativity and the low polarisability of the carbon fluorine bond (Bégué and Bonnet-Delpon, 2006). Due to fluorine technology and phase equilibria being a main research interest of this Unit, the study of solid-liquid equilibria of fluorinated pharmaceuticals is a future goal for the Unit.

Chapter 2

Theoretical Review of Solid-Liquid and Liquid-Liquid Equilibria

The theory relating to the thermodynamic modelling and regression of measured data for solid-liquid equilibria and liquid-liquid equilibria are discussed in this chapter. Popular thermodynamic models presented in literature are reviewed beginning with the explanation of a few basic principles and relations of thermodynamics. The reader is referred to Appendix A and to the references provided for further information regarding the derivation of the equations.

2.1 Criterion for Equilibrium

Equilibrium is described as a static state in which there is no macroscopic change in a system (Smith et al., 2001). For two phases to reach equilibrium the intensive properties of each phase do not undergo any changes. These intensive properties are properties that are independent of the mass, size, and shape of the phase (Prausnitz et al., 1999). The most common and useful of these properties are pressure (P), temperature (T) and composition (x). The description of a phase in equilibrium can then be given by the properties of the phase in equilibrium. Through thermodynamic relations a system may be described as a function of its properties. From these relations it becomes possible to calculate a single property of a system whilst the other properties are known. Real systems however are difficult to describe using simple equations. Through thermodynamics, real systems can also be described by abstract properties, such as chemical potential and fugacity that can then be related to measurable properties.

The basis for equilibrium of a heterogeneous system of π phases is expressed in terms of the chemical potential μ which is one of the abstract properties mentioned above. The condition for equilibrium is (Prausnitz et al., 1999);

$$\mu_m^1 = \mu_m^2 = \ldots = \mu_m^\pi \qquad 2\text{-}1$$

The equation applies for m components and π phases.

Fugacity (f_i) is an auxiliary function which translates chemical potential (μ) to a function with properties that can be measured within the system. This can be done through activity (a_i) which is defined as the ratio of fugacity to fugacity at its standard state (Prausnitz et al., 1999).

$$\frac{f_i}{f_i^0} = a \qquad 2\text{-}2$$

If fugacities in the standard states are equal then the following equation exists for two phases α and β in equilibrium and is known as the iso-fugacity criterion. This implies that the activity of species *i* in any two phases are equal provided that the standard fugacity is the same;

$$f_i^\alpha = f_i^\beta \qquad 2\text{-}3$$

The activity coefficient (γ_i) is a measure of the deviation of a system from the ideal solution state (Smith et al., 2001);

$$\gamma_i = \frac{\hat{f}_i}{x_i f_i} \qquad 2\text{-}4$$

2.2 Liquid-Liquid Equilibrium

Liquid-liquid equilibrium is a phenomenon in which a chemical species forms a non-homogenous phase (immiscible phases) when mixed with a certain composition of another or other chemical species, after sufficient equilibration has been allowed. The system at equilibrium will separate into distinct phases of a fixed composition (partially miscible). This equilibrium condition is one in which a minimum Gibbs energy is existent (Novak et al., 1987, Prausnitz et al., 1999).

2.2.1 Liquid-Liquid Equilibrium in Binary Systems

A two component two phase system has two degrees of freedom according to the Gibbs phase rule (Appendix A). The binary two phase system has two degrees of freedom and the two phase region is divided by a curve which is known as the equilibrium or binodal curve (Novak et al., 1987). The Binodal curve is a boundary which shows the transition temperature and composition for the miscible region and the immiscible region. The point on this curve that denotes the temperature beyond which there is complete miscibility between the liquids for all compositions is known as the critical solution temperature (CST). This is a significant temperature and composition for liquid-liquid equilibrium applications. Binodal curves are constructed under isobaric conditions. As seen in Figure 2-1 below, they can take various forms which are further explained in the following summary.

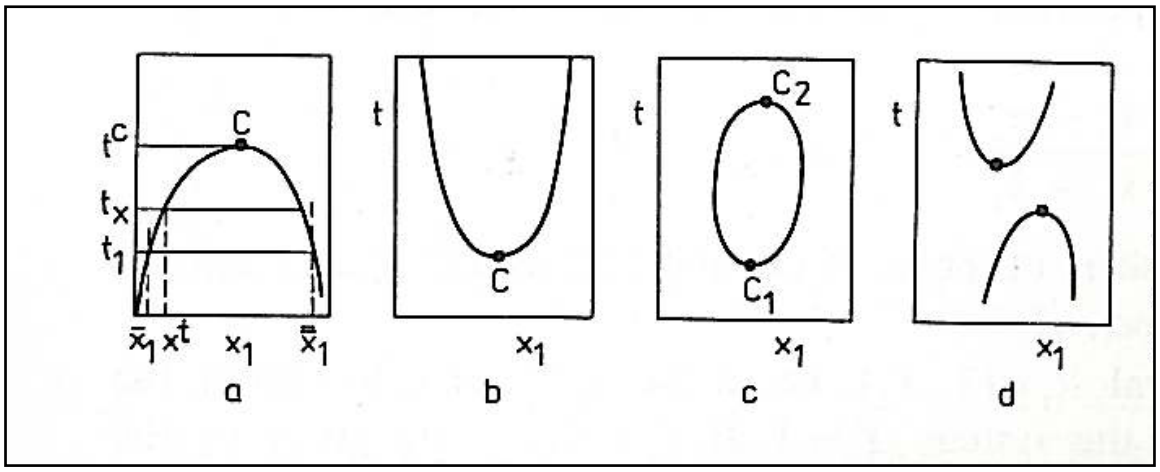

Figure 2-1: Binodal Curves for binary systems (Novak et al., 1987).

Diagram a – Upper Critical Solution Temperature (UCST)

A concave binodal curve indicates an upper critical solution temperature (UCST) (Novak et al., 1987). For such a curve the system is a homogenous solution (complete miscibility) above a temperature t_x corresponding to composition x_t on the binodal curve. At any temperature below t^C the solution forms two phases. For example at temperature t_1 the solution separates into two phases with equilibrium composition of $\bar{x}_1$ and this corresponds to composition $\bar{\bar{x}}_1$ in the corresponding phase (refer to (a) in Figure 2-1).

Diagram b – Lower Critical Solution Temperature (LCST)

In the second system (b), mutual solubility increases with decreasing temperature. Such a binodal curve has a lower critical solution temperature (LCST) (Prausnitz et al., 1999 and Novak et al., 1987), i.e., with increasing temperature the homogenous solution separates into two phases. An example of such a system is the behaviour of amines in water (Novak, 1987).

Diagram c – Lower and Upper Critical Solution Temperatures

A closed limiting solubility curve exhibits both an LCST and a UCST. An example is the binary mixture of tetrahydrofuran with water (Yoo et al., 1997and Lazzaroni et al., 2004)

Diagram d – Separate Lower and Upper Critical Solution Temperatures

Shown on diagram d is a less common occurrence, which is a system that has both upper and lower critical solution temperatures, but separate equilibrium curves are formed.

2.2.2 Thermodynamic Description of Binodal Curves

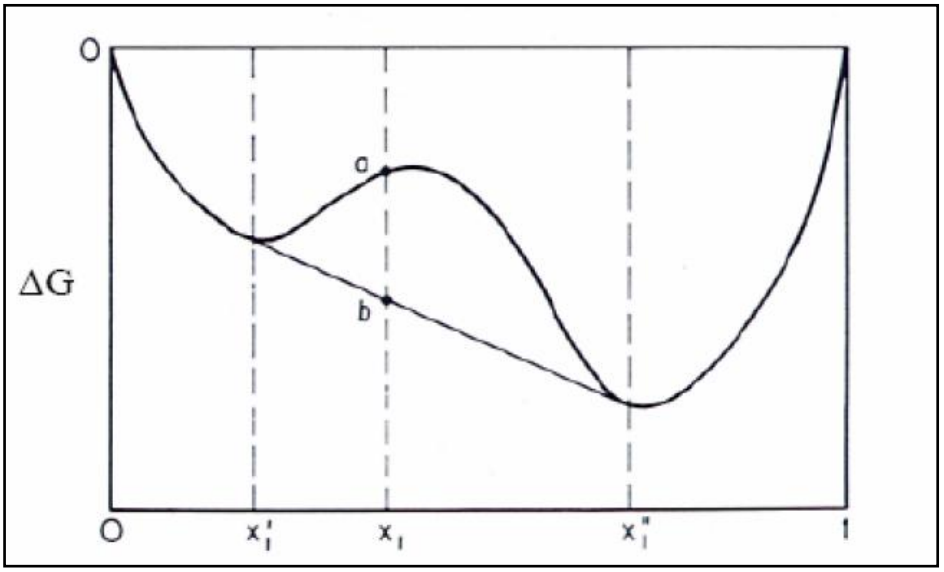

Figure 2-2: Gibbs energy of mixing versus composition (Prausnitz et al., 1999).

The equilibrium state is characterised by a minimum Gibbs energy. In liquid-liquid equilibrium the solution only forms two phases if the formation of the phases results in a lowering of the Gibbs energy of the mixture. The Gibbs energy of mixing is given by the following expression (Prausnitz et al., 1999);

$$G_{mixt} = x_1 G_1^* + x_2 G_2^* + \Delta G_b \qquad 2\text{-}5$$

where x_1 and x_2 are mole fractions of the two liquids and G_1^* and G_2^* are the Gibbs energy properties of the pure liquids and ΔG_b is the change in Gibbs energy at equilibrium.

Figure 2-2 shows a curve of Gibbs energy versus composition at constant temperature and pressure. For a mixture of composition x_1 the Gibbs energy is depicted by point (a). However the mixture can further lower its Gibbs energy to the value of point (b) lying in a tangent to the curve. When the mixture has achieved Gibbs energy at point (b) it is at equilibrium because this is a lower Gibbs energy value than point (a). The mixture separates into two phases which are the tangential points on the curve and the corresponding composition are formed. This is only applicable if the curves for

Gibbs energy are in part concave downwards (Prausnitz et al., 1999). The isobaric locus of points such as (b) for different temperatures yields the binodal curve.

2.2.3 Thermodynamic Treatment of Liquid-Liquid Equilibrium

At fixed temperature and pressure for a binary system containing n liquids in equilibrium, the phases will be denoted by superscripts of 1 up to π phases. The iso-fugacity criterion applies for component $i = 1$;

$$\gamma_1^1 x_1^1 = \ldots = \gamma_1^\pi x_1^\pi \qquad 2\text{-}6$$

For a given system at fixed temperature and pressure, the mutual solubility (liquid-liquid equilibria) in both phases can be calculated if the activity coefficient can be determined. The partial excess Gibbs energy is related to the activity coefficient by the following equation;

$$\overline{G}^E = \left[\frac{\partial n_T G^E}{\partial n_i}\right]_{T,P,n_j} = RT\ln\gamma_i \qquad 2\text{-}7$$

Equally important is the expression for molar excess Gibbs energy;

$$G^E = RT\sum x_i \ln\gamma_i \qquad 2\text{-}8$$

Activity coefficients can be obtained from the estimation of excess Gibbs energy. This can be modelled into a function that is composed of parameters that are dependent on temperature, i.e.

$$G^E = F(x, A, B, \ldots) \qquad 2\text{-}9$$

G^E is the excess molar Gibbs energy which is a function of composition and parameters A, B etc. (dependent on temperature) and to some extent on pressure as well. These are known as activity coefficient models.

When the excess Gibbs function has been defined it provides a means by which a relationship between activity coefficient and mole fraction can be obtained. When a single phase is richer in one component than the other then the composition of the corresponding component in each phase can be calculated (Prausnitz et al., 1999). The excess Gibbs function can be determined using theoretical

models e.g. the NRTL equation which is described at the end of this chapter along with other models. Conversely from experimental data the excess Gibbs function can be calculated.

2.3 Solid-Liquid Equilibrium

Solid-liquid equilibrium is the equilibrium relationship between solid and liquid phases. Phase diagrams are introduced and the different types of solid-liquid equilibrium are made mention of. The thermodynamic derivation of the equation for determining solid-liquid equilibrium is also shown.

2.3.1 Phase Diagrams

The solid-liquid phase diagram is constructed at constant pressure and is a plot of temperature against composition.

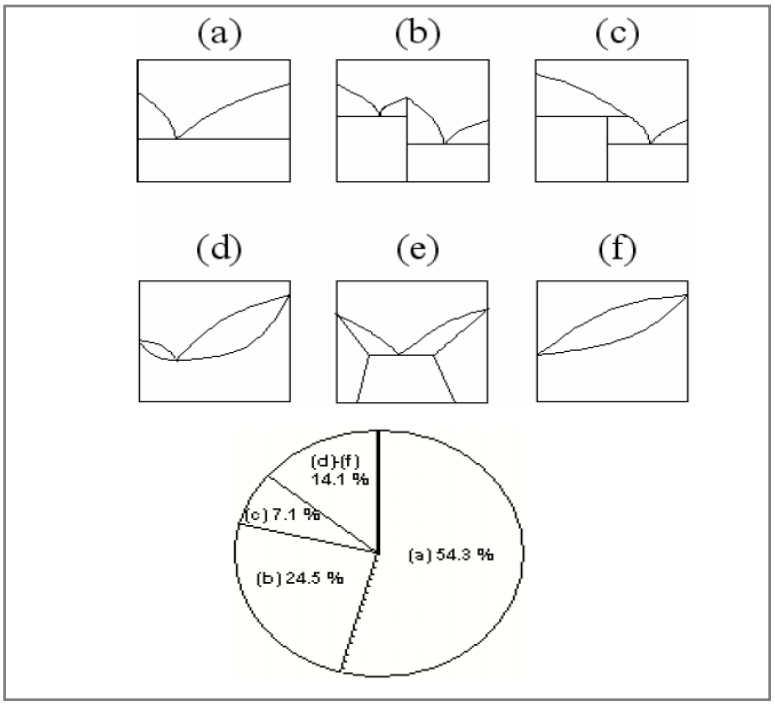

Figure 2-3: Types of organic binary SLE diagrams and the likelihood of their occurrence, (Kurosawa, 2004).

Figure 2-3 shows the different types of binary phase diagrams that can be exhibited by organic compounds. This investigation was done by Matsuoka (1991) and reported in the PhD thesis of Kurosawa (2004). The form of these phase diagrams may also apply to inorganic mixtures with some forms more common than others.

The simplest type of phase diagram formed is one in which a solid solution is formed. Such phase diagrams are represented in Figure 2-3 as (a), (d) and (f). A solid solution is a mixture of crystal structures from different components. A simple eutectic can be seen in (a) which is a mixture of a fixed composition that behaves as a pure component. On the eutectic point as shown in (d) the mixture will not exhibit a solidus and liquidus line. Most solid solutions exhibit isomorphism. For example in a binary solution, on crystallising, one of the molecules may fit into the crystal lattice of the other molecule without alteration of the crystal structure.

Phase Diagram (e) can take one of two forms. There is an intermediate region in which two crystal structures are in existence e.g. structures δ_1 and δ_2 crystals. On either side of this region, one crystal structure is dominant and that structure is specific to the component which is in abundance in the solution. As the solution becomes richer in the other component the crystal structure begins to change to the structure exhibited by that component. This is referred to as homeomorphism. If homeomorphism is weak then the crystals for the pure components can exhibit the same type of crystal structure i.e. for components 1 and 2, they exhibit structures δ_1 and δ_2. Strong homeomorphism, will result in the crystals being formed being of different structures e.g. δ_1 and β_2.

Finally (b) shows a phase diagram in which intermolecular compounds are formed on crystallisation. In phase diagram (b) it can be seen that a compound was formed which behaves as a pure component, this is known as a peritectic point. For (c) the left hand side of the phase diagram clearly shows that on crystallisation there is more than one type of crystal that can be formed. This is an example of polymorphism in which a component crystallises into more than one form of crystal structure.

2.3.2 Thermodynamic Description of Phase Diagrams

Recalling that equilibrium only occurs when minimum Gibbs energy is achieved, for solid- liquid equilibrium we consider the following equation for a binary mixture:

$$G(T,x)=(1-x)G_A^*+xG_B^*+(1-x)\ln(1-x)+x\ln x+G^E(T,x) \qquad 2\text{-}10$$

where G_A^* and G_B^* are the molar Gibbs energies for the pure components.

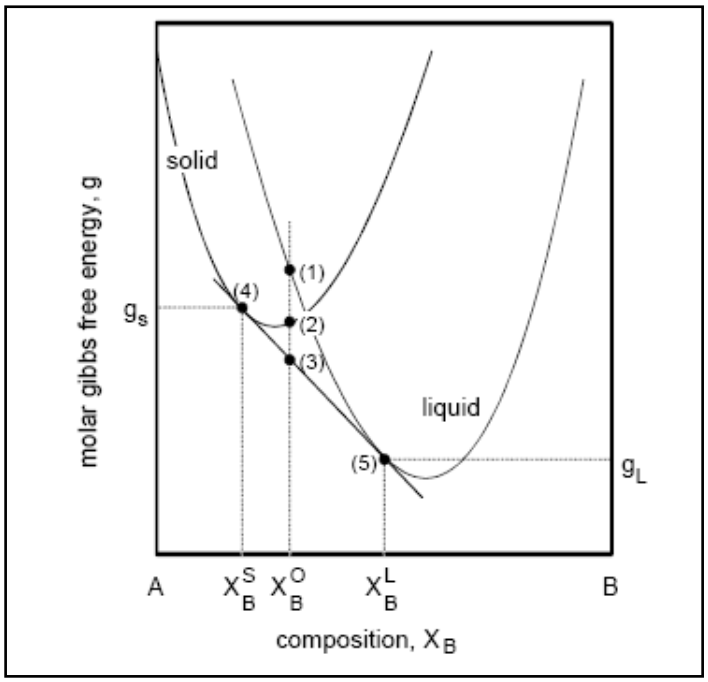

Figure 2-4: Gibbs energy of mixing against mole fraction for the solid-solid phase transition of a solid and liquid phase at constant temperature (Weir and De Loos, 2001).

Figure 2-4 shows the plot of Gibbs energy versus composition for a mixture of A and B at constant temperature and pressure. For a mixture of composition X_B^O at this temperature and pressure there are three states which can occur and these are denoted by (1), (2), and (3). It is evident that the minimum possible Gibbs energy is point (3), which is on a tangent to the two curves. From this graph, a mixture of composition X_B^O at this given temperature and pressure, will have a liquid of composition X_B^L in equilibrium with a solid of composition X_B^S. The locus of points X_B^L and X_B^S for varying temperature and initial composition X_B^O is a phase diagram that has a solidus and liquidus line. An example is phase diagram (f) in Figure 2-3.

The implication of such a phase diagram is that at a given temperature, a solid with a specific concentration is in equilibrium with a liquid of specific concentration. The region in between the two lines denotes the existence of a solid and liquid mixture. Below the solidus line the entire mixture is existent in crystal form and likewise, above the liquidus line the mixture is existent in liquid form.

2.3.3 Thermodynamic Description of Solid-Liquid Equilibria

The mole fraction of a component in a liquid phase which is in equilibrium with a solid is given in terms of fugacity of the solid and the liquid by the following equation:

$$x = \frac{f^s}{\gamma f^l} \qquad 2\text{-}11$$

x refers to the mole fraction in the liquid phase
γ is the activity coefficient of the liquid

A simplifying assumption that is usually made to calculate solid-liquid equilibria is that mixed crystals are not formed. This implies that the composition of the solid phase is 1, and the activity coefficient for a pure solid is $\gamma^s = 1$. In the transformation from solid to liquid, the thermodynamic cycle passes through the triple point of the system. The relationship between the molar Gibbs energy change and fugacity can be derived according to the following derivation (Prausnitz et al., 1999):

$$\Delta G_{sol\text{-}liq} = RT\ln\frac{f^l}{f^s} = \Delta H - T\Delta S \qquad 2\text{-}12$$

Where;

$$\Delta H = \Delta_{fus}H_{T_t} + \int_{T_1}^{T}\Delta Cp\, dT \qquad 2\text{-}13$$

$$\Delta S = \frac{\Delta_{fus}H_{T_t}}{T_t} + \int_{T_1}^{T}\frac{\Delta Cp}{T}dT \qquad 2\text{-}14$$

For; $\Delta Cp = Cp_{liq} - Cp_{sol}$

Substitution of Equations 2-13 and 2-14 into 2-12 and integration yields the following equation over the temperature range from $T \rightarrow T_t$;

$$\ln\frac{f^l}{f^s} = \frac{\Delta_{fus}H_{T_t}}{RT}\left[1-\frac{T_t}{T}\right] - \frac{\Delta Cp}{R}\left[1-\frac{T_t}{T}\right] + \frac{\Delta Cp}{R}\ln\frac{T_t}{T} \qquad 2\text{-}15$$

For most substances the triple point temperature and the melting point are not very different, therefore the triple point temperature T_t can be replaced by the melting temperature T_m. In addition, enthalpy of fusion at the triple point is replaced by that at the melting temperature $\Delta_{fus}H_{Tm}$. The temperature dependence of specific heat capacity can also be neglected, in the derivation of this equation (Prausnitz et al., 1999 and Jakob et al., 1995), and at these conditions ($T_t = T_m$) the last two terms in the equation are negligible (Prausnitz et al., 1999). According to Jakob et al., (1995), these last two terms will cancel in the region of the melting point because they are of similar magnitude and opposite sign. The resulting equation for solid-liquid equilibria is therefore:

$$\ln \frac{f^l}{f^s} = \frac{\Delta_{fus}H_{Tm}}{RT_m} \left[\frac{T_m}{T} - 1\right] \qquad 2\text{-}16$$

Solid-solid transitions can take place below the melting point and they need to be accounted for in the equation (Jakob et al., 1995). The equation for solid-liquid equilibria then becomes:

$$\ln x_i^L \gamma_i^L = -\frac{\Delta_{fus}H_{T,m}}{RT}\left[1-\frac{T}{T_m}\right] - \frac{\Delta_{trs}H_i}{RT}\left[1-\frac{T}{T_{trs,im}}\right] \qquad 2\text{-}17$$

x_i^L is the mole fraction of component i in the liquid phase,

γ_i^L is the activity coefficient of component i in the liquid phase,

$\Delta_{fus}H_i$ and $\Delta_{trs}H_{trs,i}$ are the molar enthalpy of fusion and transition of component i respectively,

T_m and $T_{trs,im}$ are the temperatures of melting and transition for component i,

and recalling that, $x_i^L \gamma_i^L = \frac{f^s}{f^L}$.

The solution of this equation is an iterative procedure because the activity coefficient is dependent on temperature and concentration (Prausnitz et al., 1999). Once calculated the activity coefficient can be used to construct the phase diagram through the lever rule or through mole fractions from Equation 2-17. Alternatively the activity coefficient can be calculated from experimental compositions and temperatures using Equation 2-17 and activity coefficient models used to fit experimental data.

2.4 Activity Coefficient Models

Activity coefficient models are mathematical relations, to calculate the activity coefficient in a non-ideal system. For ideal solutions $\gamma = 1$. Models have attempted to accurately describe the real behaviour of the system in thermodynamic terms. From activity coefficient models, solubility (mole fractions) in liquid-liquid equilibria and solid-liquid equilibria can be calculated as discussed in Sections 2.2 and 2.3.

The most commonly used activity coefficient models are the Wilson equation, NRTL (Non Random Two Liquid) equation and the UNIQUAC (Universal Quasi-Chemical theory) equation. These models are known as G^E models because the models describe the excess Gibbs energy function. These equations are based on the theory of local composition which was introduced by Wilson (1964). The theory says that within a solution pseudo compositions are formed. These compositions are responsible for non-randomness in orientation of molecules and short range order which result from differences in molecular size and intermolecular forces (Smith et al., 2001). This theory has proved to be very successful in prediction of systems, making the Wilson model one of the most widely used G^E

models. This is despite certain disadvantages and limitations. The NRTL model of Renon and Prausnitz (1968) and UNIQUAC model of Abrams and Prausnitz (1975) were later designed and are also based on the theory of local composition.

The models available for activity coefficient estimation and modelling of experimental data are numerous and the popular ones will be discussed in this work.

2.4.1 Activity Coefficient Models Used in this Work

Modelling of solid-liquid equilibria can be simplified if the solid phase is assumed to be ideal. The activity coefficient of a pure solid phase is 1. The equation for solid-liquid equilibria is given as Equation 2-17, however if non-idealities do exist then the expression in Equation 2-15 must be used to account for the non-idealities. These non-idealities are attributed to polymorphism - multiple crystal structure formation amongst others (Kurosawa, 2004).

In this work it has been found that the local composition models, Wilson, NRTL and UNIQUAC equations have proven to be sufficient for prediction and modelling of many solid-liquid equilibria data, with or without solid phase non-idealities. These models have limitations depending on the behaviour of the components. For example, Coutinho (1996) found that the Wilson model is not accurate in prediction and modelling of systems in which intermediate compounds are formed i.e. peritectic points. The local composition models have been applied for prediction of solid-liquid equilibria data for many organic compounds, and have produced satisfactory results for alkane mixtures and alcohol-carboxylic acid mixtures (Qingzhu et al., 2007).

In this work solid-liquid equilibrium data for binary carboxylic acid mixtures is to be measured. These are the C1 – C9 acids of which there have been few studies undertaken. One of the studies has been that of Abrmans et al. (1999), who have measured the acetic acid + propionic acid system and have regressed the experimental data using the Wilson model (1964). The solid–liquid equilibria phase behaviour depicted an almost ideal system therefore making the modelling fairly simple.

In terms of non-idealities for these systems, n-alkyl carboxylic acids are known to form dimers, especially in the gas phase and in polar solvents (Schröder et al., 2010). Work on the crystallisation of pure components by Bond, (2004) and Larsson (1966) have shown that the acids crystallise as dimers. Despite these possible non-idealities, Goff et al., (2005) measured the binary solid-liquid equilibria of stearic acid and methyl stearate with acetic acid and some other solvents. The Wilson, NRTL and UNIQUAC equations were used to model this data. The Wilson and NRTL equations gave good

calculation of activity coefficients but the UNIQUAC model was unable to give a good calculation of activity coefficients. In another work by Costa et al., (2007) binary mixtures of the fatty acids from C10 – C18 were measured. The NRTL equation was successfully used to fit the experimental data with an absolute average deviation from experimental data of 0.17. It can be concluded that the dimerisation of the acids, might not affect the ability of the models to fit the data in a significant way and hence the G^E models are regarded as sufficient for modelling of the acid systems in this work.

Using the Dortmund Data Bank (2009) Recval3 software, the experimental data measured in this work is regressed/fitted using the Wilson, NRTL and UNIQUAC equations. Each of the local composition models are described below.

2.4.2 Wilson Model

The model was developed by Wilson (1964), and the expression for a binary liquid mixture is given as (Prausnitz et al., 1999):

$$\frac{G^E}{RT} = -x_1 \ln(x_1+\Lambda_{12}x_2) - x_2 \ln(x_2+\Lambda_{21}x_1) \qquad 2\text{-}18$$

The activity coefficients for each component are given by:

$$\ln \gamma_1 = -\ln(x_1+\Lambda_{12}x_2) + x_2\left(\frac{\Lambda_{12}}{x_1+\Lambda_{12}x_2} - \frac{\Lambda_{21}}{x_2+\Lambda_{21}x_1}\right) \qquad 2\text{-}19$$

$$\ln \gamma_2 = -\ln(x_2+\Lambda_{21}x_1) - x_1\left(\frac{\Lambda_{12}}{x_1+\Lambda_{12}x_2} - \frac{\Lambda_{21}}{x_2+\Lambda_{21}x_1}\right) \qquad 2\text{-}20$$

The Wilson model for binary liquid mixtures has two adjustable parameters which are related to molar volumes of the pure components, as well as energy of interaction between the molecules of the different components. These parameters are λ_{12} and λ_{21} and are derived from the following relations (Prausnitz et al., 1999):

$$\Lambda_{12} \equiv \frac{\upsilon_2}{\upsilon_1}\exp\left(-\frac{\lambda_{12}-\lambda_{11}}{RT}\right) \qquad 2\text{-}21$$

$$\Lambda_{21} \equiv \frac{\upsilon_1}{\upsilon_2}\exp\left(-\frac{\lambda_{21}-\lambda_{22}}{RT}\right) \qquad 2\text{-}22$$

Over modest temperature intervals the Wilson model not only provides a relationship between activity coefficient and composition (mole fractions), but it also describes the relationship between activity coefficient and temperature (Raal and Mülbauer, 1998 and Prausnitz et al., 1999). This has proved useful for isobaric calculations. The Wilson has been found to be applicable to a wide range of systems for example polar components in non-polar solvents (Prausnitz et al., 1999).

Unfortunately the Wilson model has been found to be unable to predict partially miscible liquid mixtures (Prausnitz et al., 1999 and Raal et al., 1998). The model can only be applied to the regions in which the liquids are miscible and form one phase. Modifications to the Wilson model have been presented in order to improve its applicability to immiscible systems. One of the successful modifications is the T-K Wilson model by Tsuboka and Katayama (1975). The modified equation adds a new binary parameter to the Wilson equation which allows the model to be applicable to immiscible systems (Tsuboka and Katayama, 1975 and Hiranuma, 1983).

2.4.3 NRTL (Non Random Two Liquid)

This model was developed by Renon and Prausnitz (1968) and the expression for Gibbs energy is (Prausnitz et al, 1999):

$$\frac{G^E}{RT} \equiv x_1 x_2 \left(\frac{\tau_{21} G_{21}}{x_1 + x_2 G_{21}} + \frac{\tau_{12} G_{12}}{x_2 + x_1 G_{12}} \right) \qquad 2\text{-}23$$

$$\tau_{12} = \frac{g_{12} - g_{22}}{RT} \qquad \tau_{21} = \frac{g_{21} - g_{11}}{RT} \qquad 2\text{-}24$$

$$G_{12} = \exp(-\alpha_{12}\tau_{12}) \qquad G_{21} = \exp(-\alpha_{21}\tau_{21}) \qquad 2\text{-}25$$

g_{ij} is an energy interaction parameter between the two species and $\alpha = \alpha_{12} = \alpha_{21}$ is a parameter that relates the non-randomness of the mixture. All parameters in this model are independent of temperature. The parameter α is usually fixed and it has been found that the value ranges between 0.20 and 0.47 (Prausnitz et al, 1999). Usually the value of α can be set to 0.30 (Prausnitz et al, 1999). The NRTL model has been found to be most useful for modelling miscible systems and systems that exhibit strong deviations from ideal solution behaviour (Raal and Mülbauer, 1998). The expressions for the activity coefficients for this model are given by:

$$\ln \gamma_1 = x_2^2 \left[\tau_{21} \left(\frac{G_{21}}{x_1 + x_2 G_{21}} \right)^2 + \frac{\tau_{12} G_{12}}{(x_2 + x_1 G_{12})^2} \right] \qquad 2\text{-}26$$

$$\ln \gamma_2 = x_1^2 \left[\tau_{12} \left(\frac{G_{12}}{x_2 + x_1 G_{12}} \right)^2 + \frac{\tau_{21} G_{21}}{(x_1 + x_2 G_{21})^2} \right] \qquad 2\text{-}27$$

2.4.4 The UNIQUAC Model

The Universal Quasi-Chemical model was developed by Abram and Prausnitz (1975) and is based on a quasi-chemical theory that was developed by Guggenheim (Prausnitz et al, 1999). This model was developed in order to produce a two parameter model which has the flexibility of the Wilson model but is not limited to miscible systems only (Prausnitz et al, 1999). The UNIQUAC model is the sum of two parts, a combinatorial part and a residual part. The combinatorial part is dependent on the size and shape of molecules as well as the composition of the mixture. This is determined through pure components data. The residual part however is solely dependent on intermolecular forces. The molar excess Gibbs energy is thus represented by the expression (Prausnitz et al., 1999):

$$\frac{G^E}{RT} = \left(\frac{G^E}{RT}\right)_{\text{Combinatorial}} + \left(\frac{G^E}{RT}\right)_{\text{Residual}} \qquad 2\text{-}28$$

$$\left(\frac{G^E}{RT}\right)_{\text{combinatorial}} = x_1 \ln \frac{\Phi_1^*}{x_1} + x_2 \ln \frac{\Phi_2^*}{x_2} + \frac{z}{2}\left(x_1 q_1 \ln \frac{\theta_1}{\Phi_1^*} + x_2 q_2 \ln \frac{\theta_2}{\Phi_2^*} \right) \qquad 2\text{-}29$$

$$\left(\frac{G^E}{RT}\right)_{\text{residual}} = -x_1 q'_1 \ln(\theta'_1 + \theta'_2 \tau_{21}) - x_2 q'_2 \ln(\theta'_2 + \theta'_1 \tau_{12}) \qquad 2\text{-}30$$

z is the coordination number and when set equal to 10, then the segment fractions are defined as (Prausnitz et al, 1999):

$$\Phi_1^* = \frac{x_1 r_1}{x_1 r_1 + x_2 r_2} \qquad \Phi_2^* = \frac{x_2 r_2}{x_1 r_1 + x_2 r_2} \qquad 2\text{-}31$$

$$\theta_1 = \frac{x_1 q_1}{x_1 q_1 + x_2 q_2} \qquad \theta_2 = \frac{x_2 q_2}{x_1 q_1 + x_2 q_2} \qquad 2\text{-}32$$

$$\theta'_1 = \frac{x_1 q'_1}{x_1 q'_1 + x_2 q'_2} \qquad \theta'_2 = \frac{x_2 q'_2}{x_1 q'_1 + x_2 q'_2} \qquad 2\text{-}33$$

r, q and q' are dependent on molecular size and external surface areas. There are two adjustable parameters for any given binary mixture. These parameters are dependent on interaction energies Δu_{12}

and Δu_{21} which are usually weakly dependent on temperature. The parameters are (Prausnitz et al, 1999):

$$\tau_{12} = \exp\left(-\frac{\Delta u_{12}}{RT}\right) \equiv \exp\left(-\frac{a_{12}}{T}\right) \qquad 2\text{-}34$$

$$\tau_{21} = \exp\left(-\frac{\Delta u_{21}}{RT}\right) \equiv \exp\left(-\frac{a_{21}}{T}\right) \qquad 2\text{-}35$$

The expressions for the activity coefficients are given by the following equations (Prausnitz et al, 1999);

$$\ln\gamma_1 = \ln\frac{\Phi_1^*}{x_1} + \frac{z}{2}q_1\ln\frac{\theta_1}{\Phi_1^*} + \Phi_2^*\left(l_1 - \frac{r_1}{r_2}l_2\right) - q'_1\ln\left(\theta'_1+\theta'_2\tau_{21}\right) + \theta'_2 q'_1\left(\frac{\tau_{12}}{\theta'_1+\theta'_2\tau_{21}} - \frac{\tau_{12}}{\theta'_2+\theta'_1\tau_{12}}\right) \qquad 2\text{-}36$$

$$\ln\gamma_2 = \ln\frac{\Phi_2^*}{x_2} + \frac{z}{2}q_2\ln\frac{\theta_2}{\Phi_2^*} + \Phi_1^*\left(l_2 - \frac{r_2}{r_1}l_1\right) - q'_2\ln\left(\theta'_2+\theta'_1\tau_{12}\right) + \theta'_1 q'_2\left(\frac{\tau_{21}}{\theta'_2+\theta'_1\tau_{12}} - \frac{\tau_{21}}{\theta'_1+\theta'_2\tau_{21}}\right) \qquad 2\text{-}37$$

r and l are structural parameters where:

$$l_1 = \frac{z}{2}(r_1 - q_1) - (r_1 - 1) \qquad 2\text{-}38$$

$$l_2 = \frac{z}{2}(r_2 - q_2) - (r_2 - 1) \qquad 2\text{-}39$$

The UNIQUAC equation has been found to be applicable to a wide range of systems. According to Prausnitz et al. (1999) the model is applicable to mixtures containing non-polar and polar fluids such as hydrocarbons, alcohols, nitriles, ketones, aldehydes, organic acids and water to name a few. The UNIQUAC equation has also been found to be satisfactory in modelling partially miscible mixtures as well, making their range of application wide. According to Raal and Mülbauer (1998), and Prausnitz et al. (1999) the UNIQUAC equation is as applicable as the NRTL and an improvement on the original Wilson equation due to the ability to describe immiscible systems whilst retaining the temperature dependence of the parameters within the Wilson model.

Chapter 3

Review of Experimental Apparati and Methods

Experimental apparati and methods used for determining solid-liquid and liquid-liquid equilibrium data are reviewed in this chapter. The principles used in constructing the apparatus used in this study are also highlighted. Although the measurement of liquid-liquid equilibria data is different from that of solid-liquid equilibria data, the principles that are employed can be the same, allowing for an apparatus to measure both types of phase equilibrium data.

3.1 Experimental Methods for Determining Liquid-Liquid Equilibrium Data

Experimental methods for measuring liquid-liquid equilibria can be classified into two categories (Weir and de Loos, 2005):

- Analytical
- Synthetic (Turbidimetric/cloud point)

The apparati commonly used for measurement of LLE using both methods are jacketed glass vessels. A heating or cooling fluid is circulated within the jacketed vessel to raise or lower the temperature of the sample. The apparatus is usually transparent for visualisation of the contents either for the identification of the liquid phase boundary in analytical methods (which involve sampling of phases), or for detection of any changes in turbidity in the synthetic method.

3.1.1 Analytical Methods

The analytical method of determining liquid-liquid equilibria requires the measurement of the composition of the immiscible phases of the system. This is determined at constant temperature and pressure and is referred to as solubility.

In the apparatus a mixture of components is rigorously stirred and allowed to settle into separate liquid phases. At this state the sample will be in equilibrium. Sufficient time is required for equilibrium to be reached. The method relies on the presence of a distinct phase boundary appearing at equilibrium. At constant temperature the molecular fractions of each component in the phases are determined. Samples may be drawn from the apparatus by the use of a syringe (Raal and Mühlbauer, 1998), or in other equipment pipettes have been used (Weir and de Loos, 2005).

The determination of molecular fractions within the phases may be made by a number of different techniques. These techniques include: refractive index, identification by chemical reaction, boiling point differences (gas chromatography), solubility in solvents (liquid chromatography), density and others (Weir and de Loos, 2005). The most commonly used technique is gas chromatography.

An example of an analytical cell is the cell of Ndlovu (2005). The cell is a glass jacketed cell with temperature controlled from a constant temperature bath. The cell had two sampling points, one at the top of the cell to sample the lighter phase and one at the bottom of the cell to sample the heavier phase (Figure 3-1). Gas chromatography was used to analyse the samples.

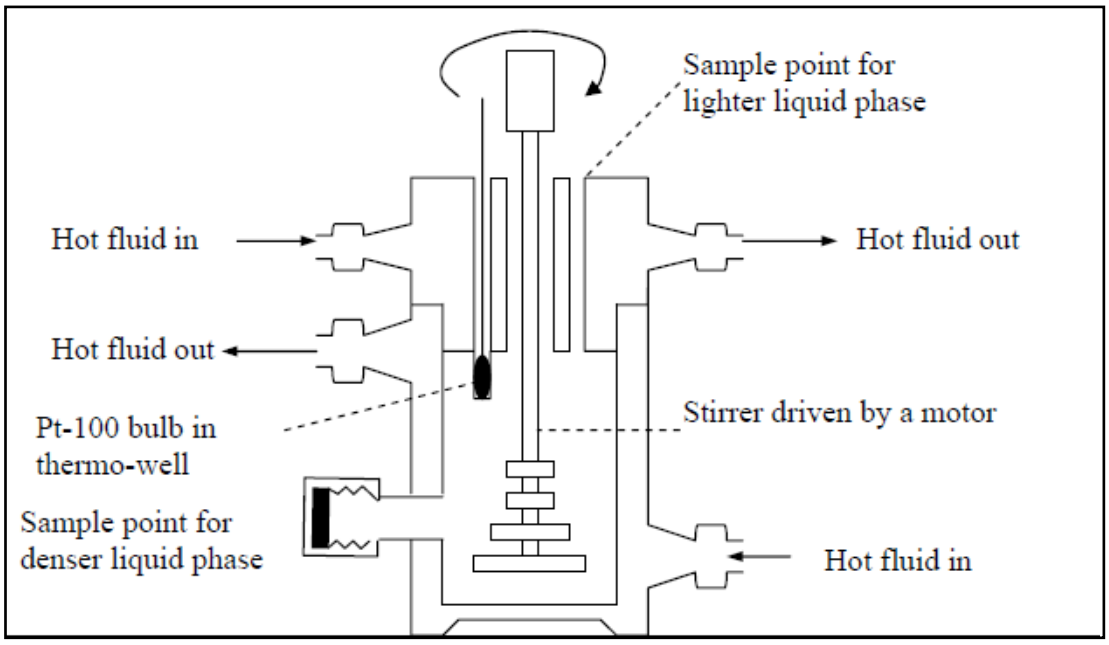

Figure 3-1: Analytical glass LLE cell of Ndlovu (2005). Adapted from Ndlovu, (2005).

3.1.3 Synthetic Methods

The synthetic method is an optical method or a visual technique in which LLE is observed through the disappearance or appearance of turbidity due to immiscible phases appearing in the mixture. These are either cloud-point or clear points, depending on which is the most reliable method of detection. Ochi et al. (1993) have preferred to use clear point detection. The change in turbidity in the mixture is achieved in one of two ways:

- By titration which is a change in composition until turbidity occurs, at fixed temperature. This is achieved by a gradual addition of one of the components as a known volume.

- By a change in temperature for a fixed/known composition until turbidity occurs. This is a more commonly used technique between the visual techniques.

The apparati used for synthetic methods is the same in design as that for analytical methods. These are typically glass jacketed vessels, with a cryogenic fluid flowing through the jacket for temperature control. The essential characteristic of these apparati is that they are transparent in order to enable visual identification of turbidity.

For the synthetic method there exist differences in the techniques used to identify the cloud/clear point (turbidity). A reliable technique is required to aid in identification of an accurate phase transition temperature. Some techniques that have been used to identify cloud point include laser scattering which has been used by Ochi and co-workers (1993), Hefter et al. (1991), and Schrödle et al. (2004). Laser scattering assists the experimenter in determining the transition temperature.

A schematic diagram of the apparatus by Ochi and co-workers (1993) is given in Figure 3-2 which is an example of an LLE cell for the synthetic method.

- The equilibrium cell they used was a double jacket glass cell which has temperature controlled by water flowing from a constant temperature bath through a jacket.
- They used an optical system to detect cloud point of the sample. This optical method was composed of a He-Ne laser for a light source and a light sensor which was a selenium photocell. The light was shone onto the cell from a 45^{o} angle.
- The light source and the equilibrium cell were all placed in a pressurized container.

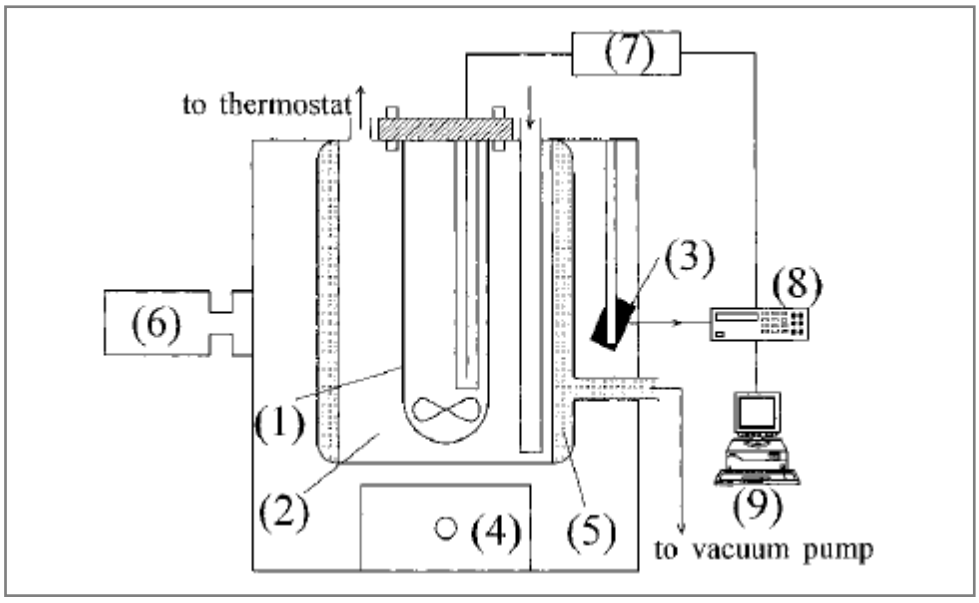

Figure 3-2: LLE cloud point apparatus of Ochi et al. (1993) using a laser scattering optical technique. Adapted from Ochi et al. (1996).

In Figure 3-2; 1. Equilibrium Cell; 2. Temperature Bath; 3. Light Sensor (Selenium Cell); 4. Magnetic Stirrer; 5. Adiabatic Jacket; 6. He-Ne laser; 7. Thermometer; 8. Digital Multimeter; 9. Personal Computer (Ochi et al., 1996).

Cloud and clear points were detected in this apparatus by the laser (6) shining onto the light sensor (3) which was connected to the computer. Ochi and co-workers determined the transition point based on the change in intensity of light detected by the sensor.

The apparati for LLE may include both techniques such as the apparati constructed by Haruki et al. (2000). A flow technique was also used for mixing and for provision of equilibration time. The apparatus constructed was for measurement of water and hydrocarbon systems which can have very low solubility. The apparatus which is schematically shown in Figure 3-3 consisted of a feed system, an effluent sampling system, and an equilibrium cell. The equilibrium cell had sapphire windows from which digital images were captured and phase behaviour was studied by means of a video camera attached to a microscope. The video camera was directed to view into the equilibrium cell through the side of the apparatus in a perpendicular angle to the He-Ne laser (not shown in Figure 3-3).

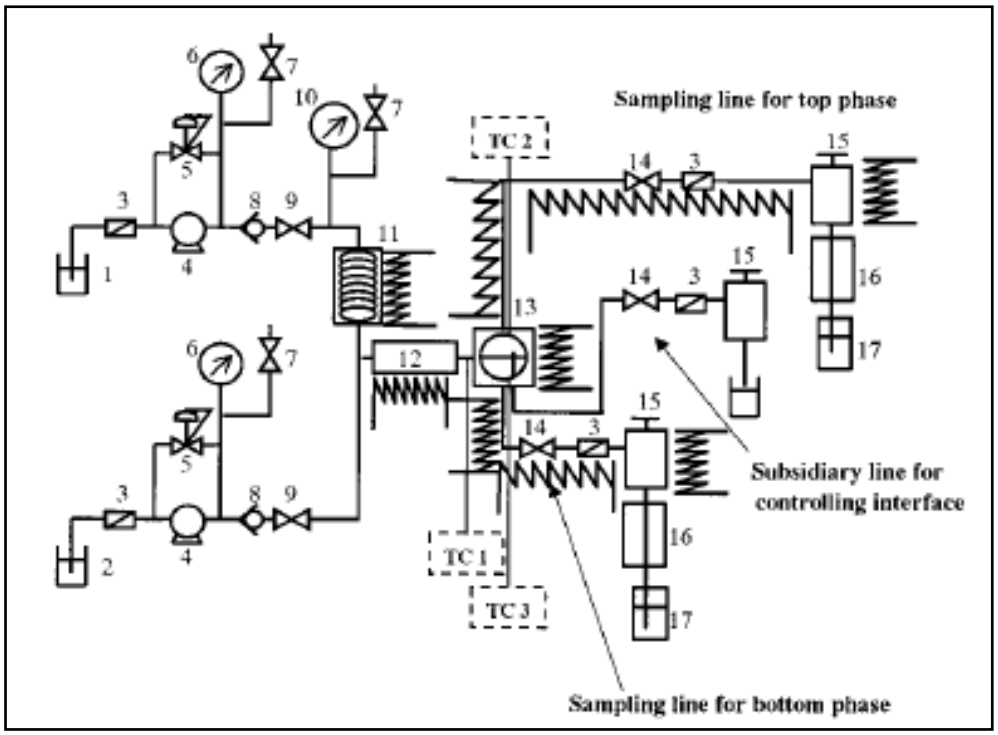

Figure 3-3: Flow diagram for flow cloud point method of Haruki et al. (2000). Adapted from Haruki et al., (2000).

In Figure 3-3: 1. Water Reservoir; 2. Hydrocarbon Reservoir; 3. Hydrocarbon Reservoir; 4. Feed Pump, 5. Back Pressure Regulator; 6. Pressure Gauge; 7. Safety Valve; 8. Check Valve; 9. Stop Valve; 10. Precision Gauge; 11. Preheating Coil; 12. Line Mixer; 13. Equilibrium Cell; 14. Stop Valve; 15. Expansion Valve; 16. Water Bath; 17. Collecting Bottle; TC1-TC3. Resistance Temperature Detector (Haruki et al., 2000).

From the feed supply both components were released into a line mixer which was preheated before introduction of the components (water and hydrocarbon). Water was preheated before being fed into the line mixer. From the line mixer the components which were well mixed, entered into the equilibrium cell and were observed through sapphire windows by a video camera. The residence time in the equilibrium cell for the apparatus was 6-15 min after which the sampling lines, two lines at the top and bottom of the equilibrium cell were opened to sample the two phases. The component feed lines; line mixers, as well as the sampling lines were maintained at a fixed temperature by preheating them to the required temperature. These temperatures were controlled by an electric heater to ±1 K of the equilibrium temperatures. The interface level between the two phases was controlled in order to ease the separation of the two phases by controlling the feed flow rate.

3.2 Experimental Methods for Measuring Solid-Liquid Equilibrium Data

In the same manner as liquid-liquid equilibria, experimental methods for the determination of SLE are divided into two categories (Weir and de Loos, 2005):

- Synthetic
- Analytical

The apparati used are usually glass jacketed vessels with a cryogenic fluid flowing through the jacket for temperature control, (similar to the LLE apparati). This design is more flexible for SLE, as will be seen in the examples which follow.

3.2.1 Analytical Methods

The technique uses the same concept as the analytical method of LLE measurements, discussed previously. Lohmann et al. (1997) have used an analytical technique, alongside a synthetic technique for solid-liquid equilibria measurements of viscous binary organic mixtures. In their analytical technique a binary mixture was prepared and cooled to a predetermined temperature so that partial crystallisation was exhibited within the sample. Equilibration time was allowed and at these conditions a sample of the liquid phase was removed and analysed by gas chromatography to determine the composition. The phase diagram was therefore determined by analysing the composition in the liquid phase which was in equilibrium with the solid phase. The composition of the solid phase was therefore calculable from the liquid phase composition. Lohmann and co-workers used this technique to measure viscous mixtures which were difficult to measure by synthetic methods due to high viscosity. The analytical technique they used was more accurate for regions of high viscosity in the phase diagrams than a comparative synthetic method. The type of apparatus used for this technique may be a glass cell such as that by Lohmann and co-workers (Figure 3-4) or a non transparent cell. The advantage of using a glass cell in an analytical technique is the ability to visualise the phase boundary during sampling.

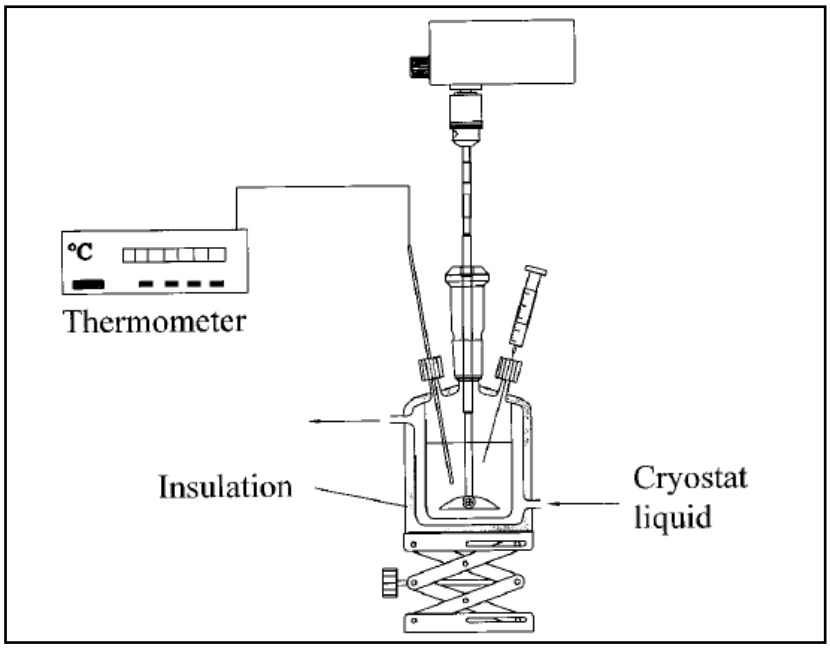

Figure 3-4: Analytical solid-liquid equilibria cell of Lohmann et al. (1997). Adapted from Lohmann et al. (1997).

3.2.2 Synthetic Method

The synthetic method allows for the measurement of the solid-liquid equilibrium of a known composition of sample. There are two techniques in which the synthetic method is applied. The phase change can be detected through thermal signature changes, or visual observation (synthetic visual method) of the transition between the liquid and the solid state (Nyvlt, 1977 and Weir and de Loos, 2005). The samples in a synthetic method are usually made up by weighing the chemicals and charging them into the equilibrium cell. The temperature in the cell is then gradually reduced if the sample is liquid at room temperature, or increased if the sample is solid at room temperature. The apparati are therefore always equipped with a mechanism for cooling or heating at a controlled rate. The temperature at which crystallisation occurs or the temperature of melting is taken to be the equilibrium temperature (Weir and de Loos, 2005).

3.2.2.1 Thermal Signatures

In the determination of SLE by thermal signatures the phase transition occurs as a result of the latent heat evolved or absorbed, (depending on whether the sample is being melted or crystallised). An analysis of the plot of temperature versus time for the experiment can be performed. This is because during phase transition, temperature remains constant (latent heat evolved/absorbed), resulting in phase transition being identified by either a break or an arrest in the temperature-time profile. An

arrest is a region of constant temperature (plateau) and a break is a distinguishable change of gradient in the temperature profile of the sample. Equilibrium is determined by identifying the temperature at which the arrest/break occurs (Nyvlt, 1977). Using thermal signatures accurate/precise temperature data logging is essential for the experimental technique or method.

Apart from using the temperature profile as a method of identifying thermal signatures, the heat flux, caused by latent heat during transition, may also be used to identify the phase transition. This is done using heat flux diagrams, in the technique of calorimetry. A thermogram is generated from a calorimeter (graph of heat flux against temperature). The phase change is identified by a peak on the thermogram due to the evolution of latent heat during phase transition (Wahayudi et al., 1989 and Hohne, 2003). Calorimeters are sensitive to any transition taking place and therefore can be used to identify when the SLE transition begins and when it ends (Wahayudi et al., 1989). Very small heat fluxes can easily be detected and other transitions such as solid-solid transitions, after the solid-liquid transition has taken place, are easily identifiable. The types of calorimeters most common for measurement of SLE are: adiabatic calorimeters, differential thermal calorimeters, and differential scanning calorimeters. Many types of calorimeters are also available but the most common are the differential scanning calorimeters. The caloric measurement is based on the differential energy input between the sample and a reference; when integrated this yields the enthalpy change of the sample (Hohne, 2003). This enthalpy change is used to construct the thermogram. Heating rates are controlled by a gradual increase of energy to the sample. Some examples of these calorimeters in literature are described in Appendix B.

3.2.2.2 Visual Method

For the synthetic visual method, the initial crystal appearance or the last crystal disappearance is detected. The synthetic visual method usually refers to the detection of the final crystal disappearance. This method has been used by Domanska et al. (1996) and by Lohmann et al. (1997) amongst others. The experimenter is required to wait for the transition to occur and record the temperature. As a result the technique takes practise and patience. Transparency of the equilibrium cell or some form of visualisation technique into the cell is necessary.

For both techniques in the synthetic method, the key features of the apparati are the same. The same way that temperature is important for detecting thermal signatures; temperature readings are also important for the visual technique. However, like cloud point detection a reliable technique for identifying crystal disappearance is required. The same techniques may be applied to solid-liquid equilibria as were applied to determining liquid-liquid equilibria. An example is the technique of

measuring turbidity used in the apparatus by Schrödle et al. (2004). The apparatus used a circuit of light emitting diodes, light dependant resistors, and photo-detectors to determine the turbidity within the equilibrium cell. This was applied for an apparatus that measures both solid-liquid and liquid-liquid equilibria.

3.2.3 Apparati requirements for the measurement of SLE and LLE

The apparatus requirements are the same for all types of phase equilibria measurement. A very slow rate of melting and cooling is required for solid-liquid equilibria, not only to ensure that equilibrium is reached, but also to reduce the effects of super-cooling and superheating (Nyvlt, 1977). This is when the sample exceeds the equilibrium temperature without having undergone phase change. Usually the highest temperature reached after super-cooling is recorded as the crystallisation temperature (Ochi et al., 1996), and the final temperature before the melting curve changes in gradient after an arrest is taken as the melting temperature (Provost et al., 1998). Some apparati have been designed to measure melting point because the effect of superheating usually has less effect on the accuracy of the equilibrium temperatures than super-cooling (Rossi et al., 1963). However, apparati measuring the crystallisation temperature are also available and found to be reliable. These apparati will be made mention of in the following sections.

Temperature control is also very important for LLE measurements because just like SLE measurements they are also sensitive to temperature (Raal and Mühlbauer, 1998). They can also be sensitive to the temperature rate, especially for cloud point measurements. This was found by Ochi and co-workers (Ochi et al., 1993) who discovered that the difference between the cloud point and the clear point temperatures could be minimized by reducing the rate of temperature change within the sample. Slower rates of temperature change made the transition easier to visualize.

The basic requirements of a solid-liquid equilibria apparatus and a liquid-liquid equilibria apparatus are (in summary):

- a controlled heating and cooling system (elimination of super-cooling and super-heating in SLE),
- a mixing device to eliminate temperature gradients within the sample,
- and a mechanism/technique for the identification of phase change (this includes data capture of temperature where necessary).

3.2.4 Solid-Liquid equilibria apparatus of Jakob et al. (1995)

The solid-liquid equilibria apparatus of Jakob and co-workers is an example of a glass jacketed equilibrium cell using the synthetic visual method. The apparatus is described in greater detail because the design was adopted to develop a solid-liquid equilibria apparatus in this work for large volume measurements. The schematic diagram of the apparatus is shown in Figure 3-5.

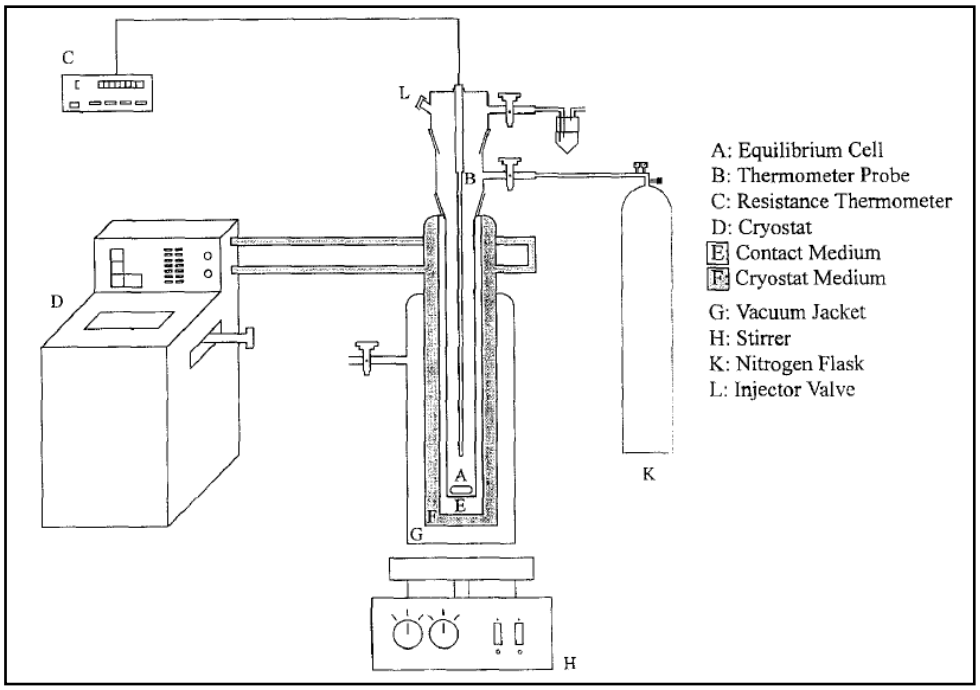

Figure 3-5: Solid-liquid equilibrium apparatus of Jakob et al. (1995). Adapted from Jakob et al. (1995).

The apparatus consisted of a three jacketed glass vessel that encased the equilibrium cell. The capacity of the equilibrium cell was 160 cm^3 and it was also glass. A platinum resistance thermometer was immersed in the equilibrium cell and had an accuracy ± 0.005 K across the temperature range of the apparatus which was 213.15 K to 373.15 K. It was a Model 1506 Metrology thermometer. Nitrogen gas was circulated above the sample in the equilibrium cell to prevent humidity at lower temperatures. The three jackets of the vessel were for; contacting fluid in the inner jacket (for uniform heat transfer), cryogenic fluid in the middle jacket, and a vacuum jacket on the outside (for insulation).

In the operating procedure the sample was partially super-cooled by immersion of the equilibrium cell in liquid nitrogen, and then allowed to solidify whilst inside the thermostat. The mixture was then heated at a rate of approximately 0.3 K/h and the last crystal disappearance was observed as the melting point. Observation of last crystal disappearance was observed by the experimenter. The

equilibrium cell was charged with a known composition. The composition was varied and measurements of the melting point obtained. From this apparatus Jakob and co-workers reported a degree of accuracy of ± 0.015 K for solid-liquid equilibria measurements.

3.2.5 Apparatus of Torzo et al. (2007)

The solid-liquid equilibria apparatus that was developed in this work was based on the design of Torzo and co-workers. The schematic diagram of the apparatus is given in Figure 3-6. The apparatus they designed was to measure solid-liquid equilibria measurements for undergraduate experiments, to demonstrate the super-cooling phenomenon and other phase equilibria phenomena. The concept that was adopted for cooling/and heating was the use of thermoelectric modules. A data acquisition system was also used to obtain temperature data points and generate cooling/heating curves, in a synthetic method which identified thermal effects. They used the apparatus to investigate freezing point depression and boiling point elevation of NaCl + water and ethanol + water. Experiments were also conducted to illustrate the freezing point of Sodium Acetate and to determine latent heat by analysis of the cooling curve. Finally they performed experiments to illustrate the difference between the Peltier effect and the Seebeck effect (Torzo et al., 2007). Results obtained from their work were compared against literature values and deviations of 1 K were recorded between their measurements and the literature data. Apart from that designed by Torzo and co-workers, such a mechanism has not been directly applied for the measurement of phase equilibria. Thermoelectric modules have been employed in experiments to investigate the second law of thermodynamics (Cvahte et al., 1998), because of the heat pump and heat engine capabilities of the thermoelectric module.

Apparatus Description

The equilibrium cell was a rectangular aluminium cell with the following dimensions:

- Three walls 40 x 3 mm thickness.
- One Wall 40 x 8 mm thickness, this thickness allowance was to enable a hole for a temperature sensor to be inserted.
- Inner depth of sample holder was 9 mm.
- Base thickness was 2 mm thick.

The sample holder was positioned on top of a stack comprising two Peltier modules (cooling mechanism). The equilibrium cell and the modules formed a stack which was secured between a PVC (Poly Vinyl Chloride) cover that secured the equilibrium cell and an aluminium heat sink. The PVC flange had four screws through it, which were used to secure the sample holder and the Peltier

modules to the aluminium heat sink base. Heat conductivity at both junctions was enhanced by addition of a thin layer of heat conductive paste.

The Peltier modules were connected thermally in parallel with the equilibrium cell and electrically in series. Thermal energy was drawn from the cold side of the Peltier's (sample side) and dissipated through the hot side (heat sink side). The Peltier modules that were used were Pke128a0020 modules (40 x 40 x 4.7 mm), with a maximum power of 33W (Torzo et al., 2007). Heat was dissipated through a CPU heat sink which had a 12 V standard PC fan assisting to maintain low temperatures in the sink by forced convection. Finally the equilibrium cell was insulated with a cap made of neoprene foam that was removable.

Three temperature measurement sensors were incorporated in the apparatus. The first sensor was inserted in a hole drilled into the 8 mm thick wall of the equilibrium cell. The hole was positioned close to the base of the cell. This was so that when the sensor was inserted, it could be assumed to measure the temperature of the cold plate of the Peltier modules. Another hole was drilled in the top of the heat sink directly below the Peltier modules to measure the temperature of the hot plate of the Peltier modules. The last sensor was suspended horizontally on the top surface of the sample inside the equilibrium cell. The sensor was fixed to a wire and a loop was made using heat shrink, which allowed the sensor to be secured by one of the retaining screws for the apparatus. All the sensors were National LM61 integrated-circuit sensors which were covered by a plastic envelope. They were 4.5 mm in diameter and 5 mm in length. These sensors had an accuracy of 1 K for a temperature measurement range of 243.15 K to 373.15 K. In Figure 3-6 the apparatus of Torzo and co-workers is shown.

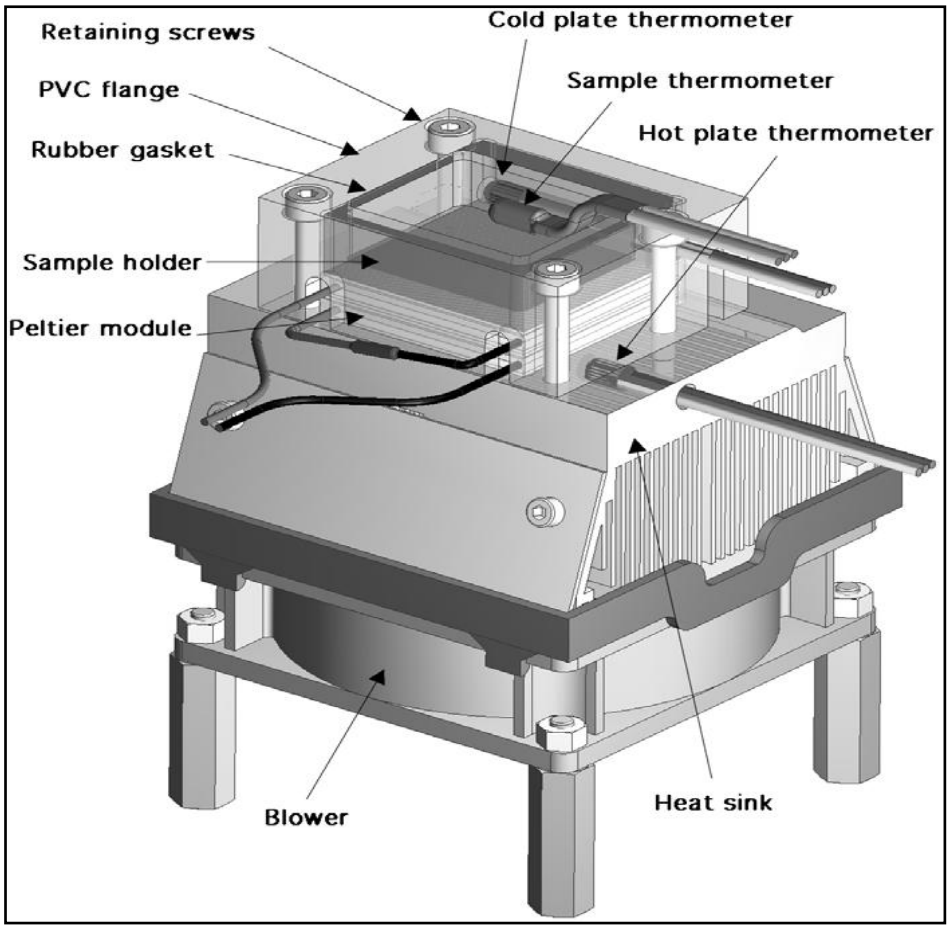

Figure 3-6: Diagram of the apparatus designed Torzo et al. (2007) which uses Peltier modules as a cooling and heating mechanisms. Adapted from Torzo et al. (2007)

3.2.6 Other SLE and LLE Apparati

Table 3-1 lists some of the LLE and SLE apparati reported in literature. Some of the interesting features of the apparati have been highlighted.

Table 3-1: Review of SLE and LLE Apparati.

Reference	Phase Equilibria	Method of Equilibria Determination	Temperature a) Range b) Accuracy	Cooling/ Heating Mechanism	Equilibrium Cell a) Type b) Size c) Agitation	Comments
Domanska, 1986 (Domanska, 1996)	SLE	S Visual, Last Crystal Disappearance	a) N/S b) ± 0.1 K	CTB	a) Pyrex cell b) N/S c) Magnetic Stirrer	Melting rates were < 2 K/h
Wahayudi et al. (1989)	SLE	S DSC (C-80 Setaram Calorimeter)	a) N/S b) ± 0.3 K	EH (calorimeter heater)	a) Glass Tubes b) N/S c) No mixing	Samples melted at a rate of 0.02 K/min
Ochi et al. (1993)	LLE	S, Cloud point detection by laser diffraction	N/S	CTB	a) Glass Cell b) 120cm^3 c) Magnetic stirrer	Cloud and clear points measured within 0.1 K of each other

A	Analytical
CTB	Constant Temperature Bath
DSC	Differential Scanning Calorimetry
EH	Electric heater
N/S	Not Specified
S	Synthetic

Reference	Phase Equilibria	Method of Equilibria Determination	Temperature a) Range b) Accuracy	Cooling/ Heating Mechanism	Equilibrium Cell a) Type b) Size c) Agitation	Comments
Jakob et al. (1995)	SLE	S Visual method, Last crystal Disappearance	a) N/S b) ± 0.015 K	CTB	a) Glass Cell b) 160cm^3 c) Magnetic stirrer	Melting rates of 0.3 K/h used
Coutinho et al. (1998)	SLE	S, (DSC, Mettler TA 3000)	a) 150 K - 320 K b) N/S	EH (calorimeter heater)	a) Aluminium trays b) 150µl c) No mixing	Samples were melted at a rate of 1 K/min
Raal and Brouckaert (Raal and Mühlbauer, 1998)	LLE	S, GC used for analysis	N/S	CTB	a) Glass Cell b) N/S c) Mechanical Stirrer	-
Zhiang et al. (1998)	SLE	S, Visual detection of equilibrium, Cloud Point Determination	a) N/S b) ± 0.1 K	CTB	a) Glass Flask b) N/S c) Mechanical Stirrer	Analytical determination of equilibrium compositions, with the assistance of a visual technique to identify SLE.

Reference	Phase Equilibria	Method of Equilibria Determination	Temperature a) Range b) Accuracy	Cooling/ Heating Mechanism	Equilibrium Cell a) Type b) Size c) Agitation	Comments
Haruki et al. (2000)	LLE	A, for internal observation, GC used for analysis	N/S	EH	a) Hastelloy Cell b) 31 cm^3 c) Flow mixing	Flow of the sample was used for agitation, The cell was equipped with sapphire windows for viewing with a microscope and video camera
Schrödle et al. (2003)	SLE/LLE	S, Visual method with use of photo-detectors for visual identification	a) 253 K – 353 K b) ± 0.01 K	EH (Resistance heater)	a) N/S b) 2.75 cm^3 c) Magnetic stirrer bar	Apparatus measures up to six samples simultaneously.
Di Nicola et al. (2008)	SLE	S, Crystallisation temperature obtained from the temperature profile	a) up to 132 K b) ± 0.023 K	Liquid nitrogen and cold air heat exchange	a) Stainless Steel cylinder b) 47 cm^3 c) Mechanical stirrer	-

Reference	Phase Equilibria	Method of Equilibria Determination	Temperature a) Range b) Accuracy	Cooling/ Heating Mechanism	Equilibrium Cell a) Type b) Size c) Agitation	Comments
Wachter et al. (2008)	SLE	S, Visual method with, melting and crystallisation curve analysis	a) N/S b) ± 0.001 K -0.003 K	CTB (Silicone oil)	a) Pyrex tube b) 2cm^3 c) Magnetic stirrer	Automated apparatus measuring 30 samples simultaneously.

The apparati listed in Table 3-1 are some of the SLE and LLE apparati from the literature, more detailed descriptions of these apparati may be found in Appendix B. Some of the characteristics that can be seen are that through measurement of cloud points it is possible to measure both SLE and LLE with the same apparatus. Both SLE and LLE glass apparati had the same design features, such as the thermostatted glass jacket.

The size of the equilibrium cells vary from 160 cm^3 to as low as 150 µl for the calorimeters. Naturally a larger volume equilibrium cell requires large volumes of chemical, which would not be advantageous for the measurement of expensive chemicals. However it can also be a disadvantage to have a very small volume for the equilibrium cell. According to both Wachter et al. (2008) and Schrödle et al. (2004), the very low volumes of sample used in calorimetry make their measurements vulnerable to contamination. This is because a small amount of contamination in a small sample will result in a large concentration difference. Another disadvantage of calorimeters that is pointed out by both researchers is the lack of mixing in calorimetric samples. This introduces error into any measurements of multi-component mixtures.

It is very important for all SLE measurements to be made at very low rates of heating/cooling in solid-liquid equilibria measurements. In the equipment reviewed all rates of temperature change were lower than 2 K/h, for the solid-liquid equilibria apparati (for the rates that were specified). Similarly Ochi and co-workers used a rate of 0.1 K/min for their liquid-liquid equilibria cloud point measurements.

Wachter et al. (2008) summarised in their work some of the important errors that should be eliminated in the design of any solid-liquid equilibria apparatus. These should be (Wachter et al., 2008):

- Heat conduction through the thermometer if it is immersed in the sample.
- Joule heating of the thermometer.
- Insufficient equilibration time, rates that are too large are prone to errors from superheating and super cooling. Very low rates can result in unclear curves, due to the effect of heat from the surroundings; typical rates are from 0.5 to 3 K/h.
- Impurities in chemicals can cause freezing point depression of the chemical sample
- Crystal formation around the temperature sensor, results in joule heating of the sensor. This can be eliminated by effective mixing.

Chapter 4

Equipment Description and Operating Procedures

In this chapter descriptions of the apparati that were built are given, including the operating procedures for each apparati in measurement of both SLE and LLE. Two sets of apparati were set up, the first apparatus is a large volume glass apparatus and the second is a new apparatus that operates using Peltier modules for cooling. The apparati have both been semi-automated to ease the operability and to increase the accuracy of measurements. Both of these equipments adopt the synthetic method. Visual observations of the experiments were made with a camera.

Apart from the mode of operation, the major difference between the apparati and the reason for the two apparati is that the Peltier apparatus (as it shall be referred to) has a small sample volume. This makes it useful for measurements of more costly chemicals, and chemicals which are difficult to handle in large quantities. The Glass apparatus, as it shall be referred to, has a large cell volume.

4.1 Glass Apparatus

The design of the glass cell was based on the apparatus of Jakob and co-workers (Jakob et al., 1995). The apparatus of Jakob and co-workers has been described in the previous chapter. This type of apparatus has been modified by introducing a programmable circulator. The programmable circulator is able to increase or decrease the temperature of the circulating fluid in order to achieve a specified rate of melt or crystallisation. In addition solid-liquid equilibria were detected through thermal signatures i.e. melting or cooling curve instead of crystal disappearance as undertaken by Jakob and co-workers. A camera was also used to record visually the crystallisation/melting process.

4.1.1 Equipment List:

1. Glass Equilibrium Cell
2. Insulated heating and cooling glass chamber
3. 350 mm x Ø 6 mm stainless steel encased 4 wire RTD (Glass Pt-100)
4. Teflon coated magnetic stirrer bar
5. Snijders model 34532 hotplate magnetic stirrer
6. 12 litre bath with ethanol as the cryogenic fluid
7. Polyscience Model 7312 Programmable Circulator
8. Polyscience VLT 100 Chilling Unit (173.15 K-233.15 K)
9. USB module NI-USB 9219 (resistance converter)

10. LabVIEW^{TM} software from National Instruments
11. 752 x 480 Resolution Firefly MV camera.

4.1.2 Equilibrium Cell and Apparatus Assembly

In the description of the equipment, reference is made to Figure 4-1, Photograph 4-1 and Photograph 4-2. The numbers refer to features in Figure 4.1 and the letters of the alphabet refer to features shown in Photograph 4-1 and Photograph 4-2.The equilibrium cell is a cylindrical glass vessel with a height of 200 mm and a diameter of 30 mm. The active volume of the cell is 141.30 cm^3 i.e. a capacity of approximately 140 ml. The cell includes, nitrogen gas inlet (7/C) and outlet valves (8/D), positioned above the equilibrium chamber. Nitrogen gas creates an inert environment. The sample is introduced into the equilibrium cell by injection through a sample point with a septum, located above the equilibrium chamber (6/G). Temperature measurement is via a stainless steel encased Pt-100 (1) which is in direct contact with the sample, and positioned through the centre of the equilibrium cell.

The equilibrium cell sits in a double jacketed thermostat (B). This thermostat comprises of an oil well in which the equilibrium cell is immersed (3). Silicon oil (SI-044) was used as a contact medium in order to achieve uniform heat transfer. A double jacket covers the oil well. The inner jacket (4) contains the heating/cooling fluid and the outer jacket (5) is a vacuum jacket for insulation. A cryogenic liquid is supplied from a bath (B), from where it has been chilled using a chilling unit (A). The glass apparatus is transparent and allows for visual observation of the sample within the equilibrium cell.

Photograph 4-1: The Glass apparatus equilibrium cell positioned within its thermostat jacket.

A. Equilibrium Cell; B. Thermostat jacket; C. Nitrogen Gas Inlet; D. Nitrogen Gas Outlet; E. Cyrostat Liquid Inlet; F. Cryostat Liquid Outlet; G. Sample Injection Point.

The thermostat is positioned on a hotplate magnetic stirrer (9/E) which is used to turn the Teflon coated magnetic stirrer bar (2) which sits in the equilibrium cell. All the glassware on the apparatus was made up from a specified design by a professional freelance glass blower (Mr Peter Siegling).

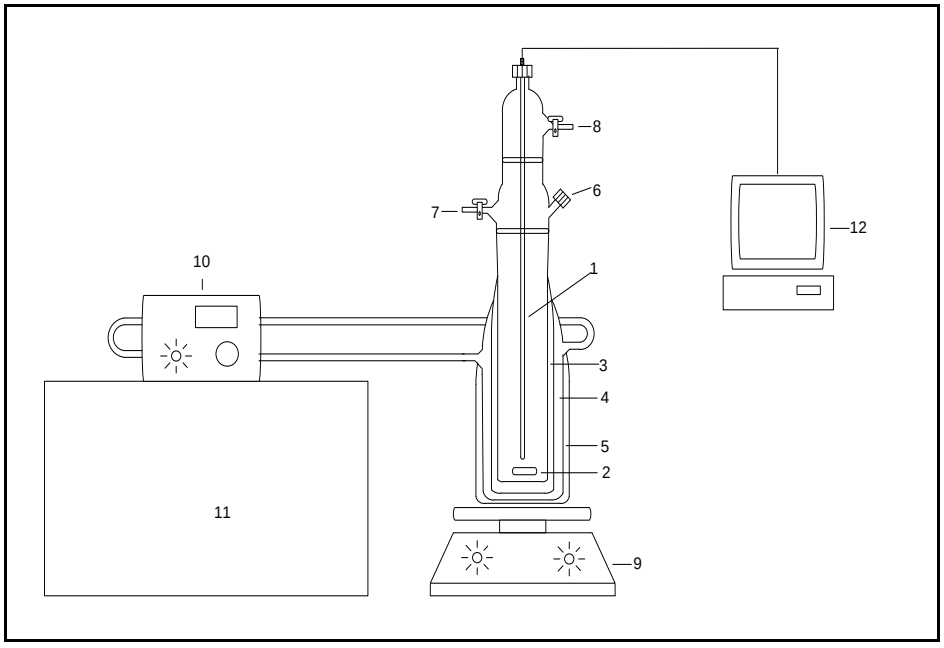

Figure 4-1: Schematic diagram of the layout of the Glass apparatus.

1. Stainless steel Pt-100; 2. Magnetic stirrer bar; 3. Contact medium chamber; 4. Cryogenic Fluid Chamber; 5. Vacuum Jacket; 6. Sample Injection point; 7. N_2 Inlet; 8. N_2 Outlet; 9. Hotplate Magnetic Stirrer; 10. Programmable Circulator; 11. Cryogenic bath; 12. Computer for data capturing.

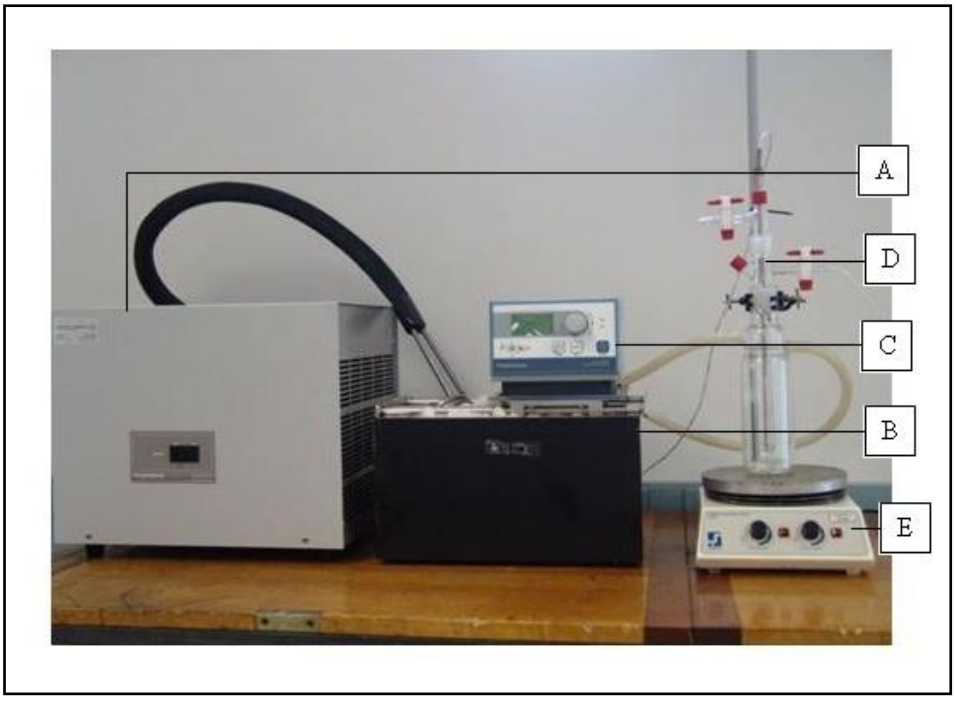

Photograph 4-2: The layout of the Glass apparatus.

A. Immersion Chilling Unit; B. Bath; C. Programmable Power Supply; D. Equilibrium Cell and Thermostat; E. Hotplate magnetic stirrer

4.1.3 Temperature Measurement and Data Capture

Temperature measurement of the sample is by means of a platinum resistance thermometer immersed within the sample. The temperature sensor is a 4 wire WIKA model REB 1/10 Din RTD. It is a straight stainless-steel encased probe with a diameter of 6 mm and a length of 35 mm. The tip of the probe is suspended 15 mm above the base of the equilibrium cell when positioned inside the equilibrium cell. The temperature reading on the Pt-100 is estimated to have an uncertainty of ± 0.02 K.

The temperature probe is connected to a computer through a USB device NI-USB 9219, and the temperature output is read through a specifically designed software using LabVIEW 8™. The software outputs temperature at data rate of up to 60 data points per second and precision to two decimal places. An output (real time graph) of temperature versus time plot is created, with data points being logged to a file at an operator prescribed rate. The data capture network is shown in Figure 4-2.

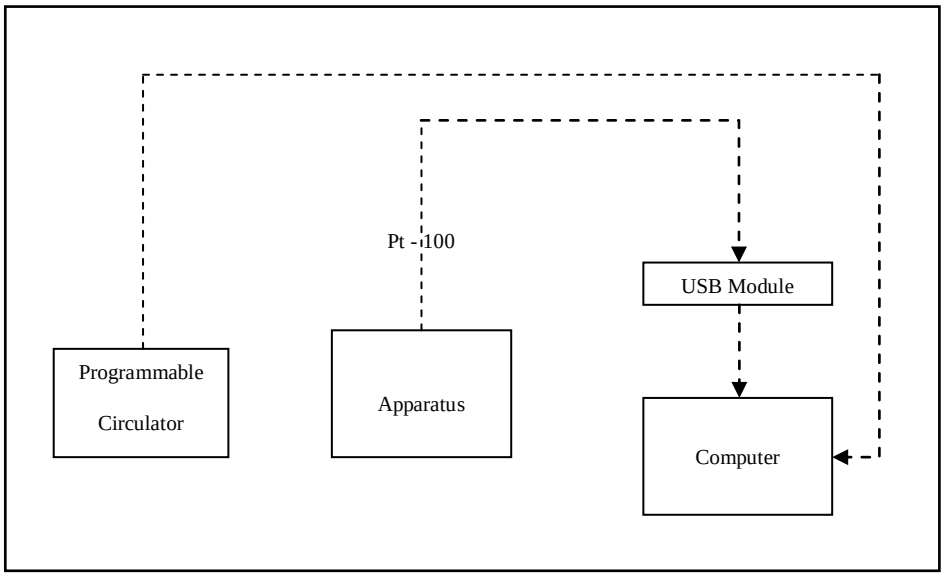

Figure 4-2: Block diagram of data capture network on the Glass apparatus.

4.1.4 Cooling and Heating

The cryogenic fluid used in this setup is ethanol; it has a melting point of 158.85 K (Dortmund Data Bank, 2009). The cryogenic fluid can be changed to vary the temperature range of operation of the apparatus. The cryogenic fluid is chilled in a 12 litre Grant GE water bath (11). The chilling unit used is a VLT 100 immersion cooler (A) purchased from Polyscience. This can be controlled in a temperature range from 173.15 K to 233.15 K, when a suitable cooling medium is used such as

ethanol. Temperature is controlled in the apparatus using a programmable circulator (10). The circulator is capable of programming 10 different programs with 55 steps per program; each program can loop up to 999 times. The programs can be input directly into the circulator or through an RS232 connection to the computer using suitable software such as LabVIEW^{TM} and Microsoft excel^{R}.

4.2 The Peltier Solid-Liquid Equilibrium Apparatus

The second apparatus built, was based on the design of Torzo et al. (2007). The apparatus uses thermoelectric (Peltier) modules for cooling the sample in a metal equilibrium cell. This concept was adopted for this apparatus. The apparatus by Torzo and co-workers was designed to demonstrate super-cooling. The requirement of the apparatus in this work is for accurate SLE to be measured, and therefore super-cooling should be minimised. This is achieved by controlling the rate of cooling and melting of the sample. The control of the apparatus was done electronically, through specially designed computer software by Check-It systems, (a software design company and distributors of National Instruments products). The software used was written in Labview 8^{TM}. A camera is incorporated into the apparatus for visual observation of the sample within the cell. Due to the fact that SLE and LLE experiments are long in duration, because of slow rates of heating and cooling, the objective of building this apparatus was to reduce the amount of time spent by the experimenter observing the experiment, through automation.

4.2.1 Equipment List:

1. One aluminium (40 mm x 40 mm x 30 mm) equilibrium cell with 4 (8 mm) thick walls and an 8 mm thick base.
2. 40 x 40 mm glass air chamber.
3. 40 x 40 mm Viton gasket.
4. 60 x 70 mm Perspex Cover.
5. Neoprene foam insulation.
6. Teflon Coated magnetic stirrer bar.
7. Ø 0.15 mm and 15 mm exposed probe 1/10 DIN RTD (sample Pt-100).
8. Ø 0.5 mm x 40 mm stainless steel encased Class A RTD (hot Pt-100).
9. 1.5 mm x 3 mm exposed probe, Class A RTD (cold Pt-100).
10. 2 (40 mm x 40 mm) Peltier modules.
11. 12 V DC stirrer motor.
12. GP 30-5 DC power supply.
13. 12 V white LED lights.

14. 752 x 480 Resolution Firefly MV camera
15. One (National Instruments) NI-USB-219 module (temperature resistance measurement).
16. Delta Electronika ES015 – 10 Programmable power supply
17. One (National Instruments) NI-USB-9263 USB module (power supply to PC connection).

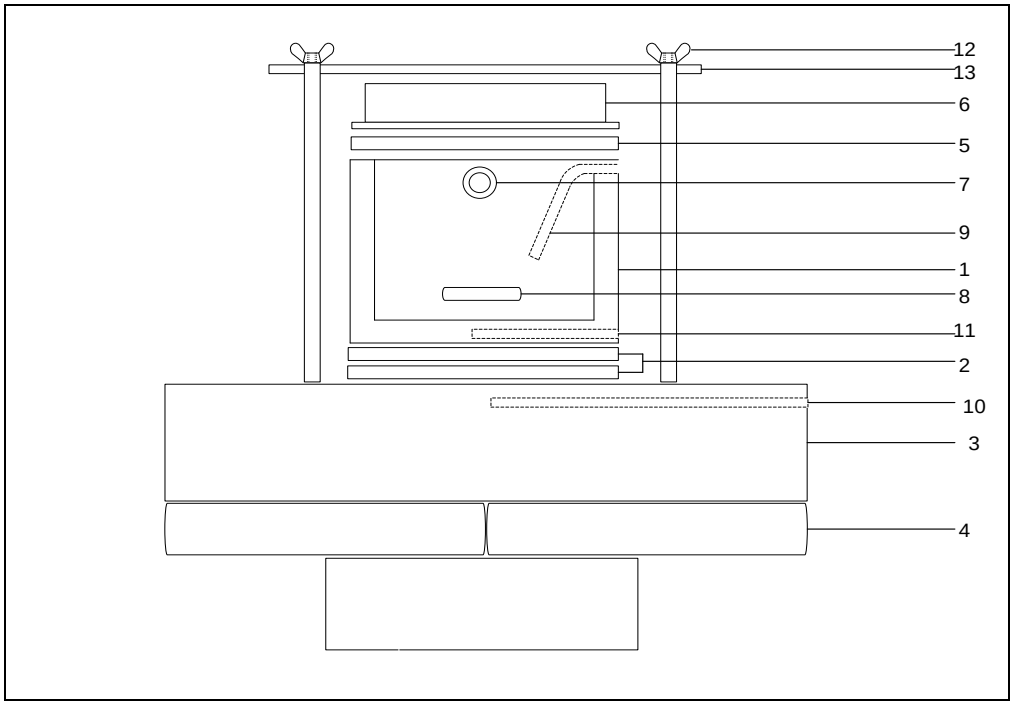

Figure 4-3: A schematic diagram of the cross-sectional view of the Peltier apparatus.

1. Aluminium equilibrium cell; 2. 2 x Peltier modules; 3. Aluminium finned heat sink; 4. Fans; 5.Viton Gasket; 6. Glass Air Chamber; 7. Nitrogen Gas Inlet; 8. Magnetic Stirrer Bar; 9. Sample Pt-100; 10. Insertion of Hot Pt-100; 11. Insertion of Cold Pt-100; 12. Support screws 13. PVC Cover.

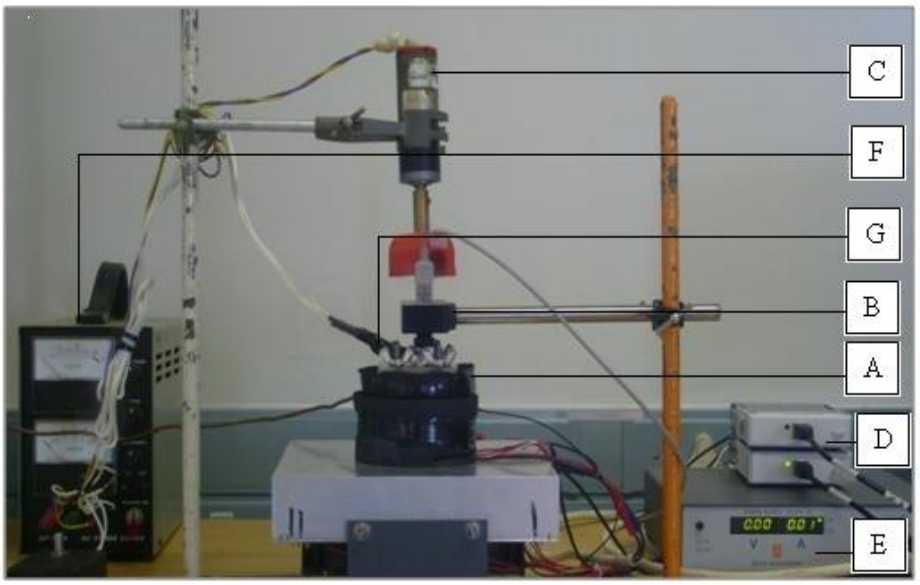

Photograph 4-3: The Peltier Apparatus Assembly

A. Insulated equilibrium cell; B. Camera; C. Stirrer Motor; D. USB modules; E. Programmable Power Supply; F. Analogue Power Supply; G. two x white LED bulbs.

4.2.2 The Equilibrium Cell and Apparatus Assembly of the Peltier Setup

The equilibrium cell is a rectangular aluminium block (1) (Refer to Figure 4-3 and Photograph 4-3). The walls of the cell are 8 mm thick. Fittings for nitrogen gas inlet and outlet (7) are located on the sides of the cell. Nitrogen gas is fed into the cell through a copper gas line. Two Pt-100s are located in the cell, the first Pt-100 which measures the approximate temperature of the Peltier module is placed inside the base of the cell through a drilled hole Ø 5mm (11, cold Pt-100). The sample Pt-100 (9) (which measures the temperature of the sample within the cell), fits in a 2 mm deep groove on one of the walls. Mixing within the equilibrium cell is achieved using a 15 mm, Teflon coated magnetic stirrer bar (8). The stirrer bar is driven by a magnet and motor (C). A Firefly camera (B) is positioned with the lens facing downward onto the equilibrium cell (A). Light is provided for the camera by two white LED bulbs which fit on either side of the camera lens (G). The magnetic stirrer and the LED bulbs are powered by a DC power supply (F), whilst the camera is powered by the computer through a fire wire card. The camera is not used to directly identify solid-liquid equilibria but is used to observe the contents of the cell during measurements. For liquid-liquid equilibria measurements the camera is used to detect the cloud points.

The equilibrium cell has a width of 40 mm, the same size as the Peltier modules. The Peltier modules (2) use the thermoelectric effect to withdraw energy from the equilibrium cell and sample (top face)

when a current is passed through them. They then dissipate that thermal energy through the bottom face. To ensure a constant flow of thermal energy, the heat dissipation face (bottom) of the Peltier, requires constant flow of energy to the surroundings. This is achieved by having the Peltier modules compacted between the equilibrium cell and a heat sink. The heat sink (3) operates by forced convection induced by four fans (4), attached underneath it. A hole is drilled into the top of the heat sink for a third Pt-100 (10, hot Pt-100). This temperature sensor approximates the temperature of the Peltier on the heat dissipation side. The temperatures of the cold and hot sides of the Peltier are an indicator of the efficiency of heat transfer in the apparatus. The temperature uncertainty for the Peltier apparatus, which is the uncertainty of the Sample Pt-100, was found to be ± 0.03 K.

The equilibrium cell is sealed at the top with a square Viton gasket (5), and a glass air chamber (6) covers the cell (1) providing further insulation. These are secured onto the heat sink using a perspex covering (13) which fits into four screws (12) drilled into the heat sink, and locked using wing-nuts. A neoprene foam cover insulates the sides of the equilibrium cell, for two reasons:

- to minimize external energy drawn into the cell and energy lost to surroundings
- to create a dry operating environment which is required for the Peltier modules

The equilibrium cell and the heat sink assembly were made and assembled in the School of Chemical Engineering workshop at the University of KwaZulu Natal, and the glass air chamber for insulation was specially made by Mr Peter Siegling. All other parts were ordered and purchased from various sources.

4.2.3 Data Capture

The Peltier apparatus is controlled by software which is described in the following section. Figure 4-4 shows how the apparatus is connected to the computer. The resistance from each RTD is read and converted to temperature through a USB module (D) which is connected to the computer. The power supplied to the Peltier modules is proportional to the amount of energy drawn and to the temperature of the sample. The programmable power supply (E) which is connected to the computer via another USB module is controlled through the computer. In this way, by adjusting the power supplied to the Peltier modules, the temperature of the sample can be controlled. Software was written using LabVIEW 8^{TM} which allows the experimenter to control the rate of temperature change within the sample. The software was developed by Check-It Systems, a software company that is also a distributor for National Instruments. All hardware to connect the apparatus to the computer was bought from National Instruments through the company Check-It Systems.

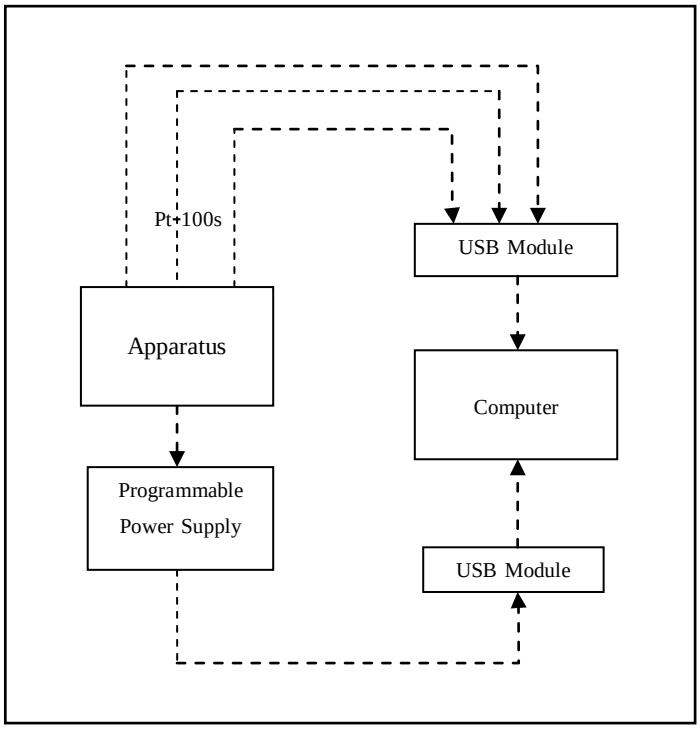

Figure 4-4: Block diagram of the data capture network for the Peltier apparatus.

4.3 Software – Peltier and Glass Apparati

Both apparati are connected to the same software interface. For the Glass apparatus the software only outputs the temperature profile and logs temperatures to file. When the camera is used with the apparatus then the image of the apparatus is output in real time and the frames are also logged to a file. On the Peltier apparatus the software is configured by the user to control the heating and cooling stages and to control the rate. There are two interfaces on the software; a configuration interface and an image display and temperature interface. One of the interfaces serves as an input interface (configuration) and the other is an output interface (image display and temperature graph).

In the configuration interface the operation of the software is either manual or automatic for the Peltier apparatus. The manual mode is useful to the user for determining the required parameters for the operation of the automatic mode i.e. power settings and time for accurate generation of the required rate. This is because in the automatic mode the user is required to input start and stop power settings, which will be ramped to generate a temperature differential. The operation is such that the change in power is proportional to the rate of change of temperature. The constant of proportionality is not the same for all systems because there are a number of factors affecting the rate of temperature change within the sample. These are for example:

- Specific heat capacity of the sample.
- Ambient temperature of surroundings, which can also be a factor because of insufficient insulation.

The image display and temperature graph interface displays the resulting experimental temperature profiles from the program, written in the configuration interface. This includes visual images from the camera.

4.3.1 Description of Interfaces

Figure 4-5 shows an image of the configuration interface. On this interface is a start (2) and stop button (3), which start and stop the SLE/LLE software. Temperature channels 1 – 4 (7), represent the Pt-100s connected to the software. When these channels are switched on the buttons appear as lit on the software, and the temperature profile can be viewed on the image display and temperature graph interface. The user is able to assign names to each temperature channel as seen on Figure 4-5.

Image and data acquisition intervals (1) are set to a value in milliseconds and the temperature at which the software will start logging images is also set by the user (4). The software logs images for all temperatures below the specified temperature, and at the same rate as temperature is logged. This data is logged by the software in an image file (picture frames from camera) and a log file (temperatures), which are located in user specified directories on the computer (8). The paths for the temperature log file and the image folder are requested when the software is first opened and may be changed during the course of operation of the software.

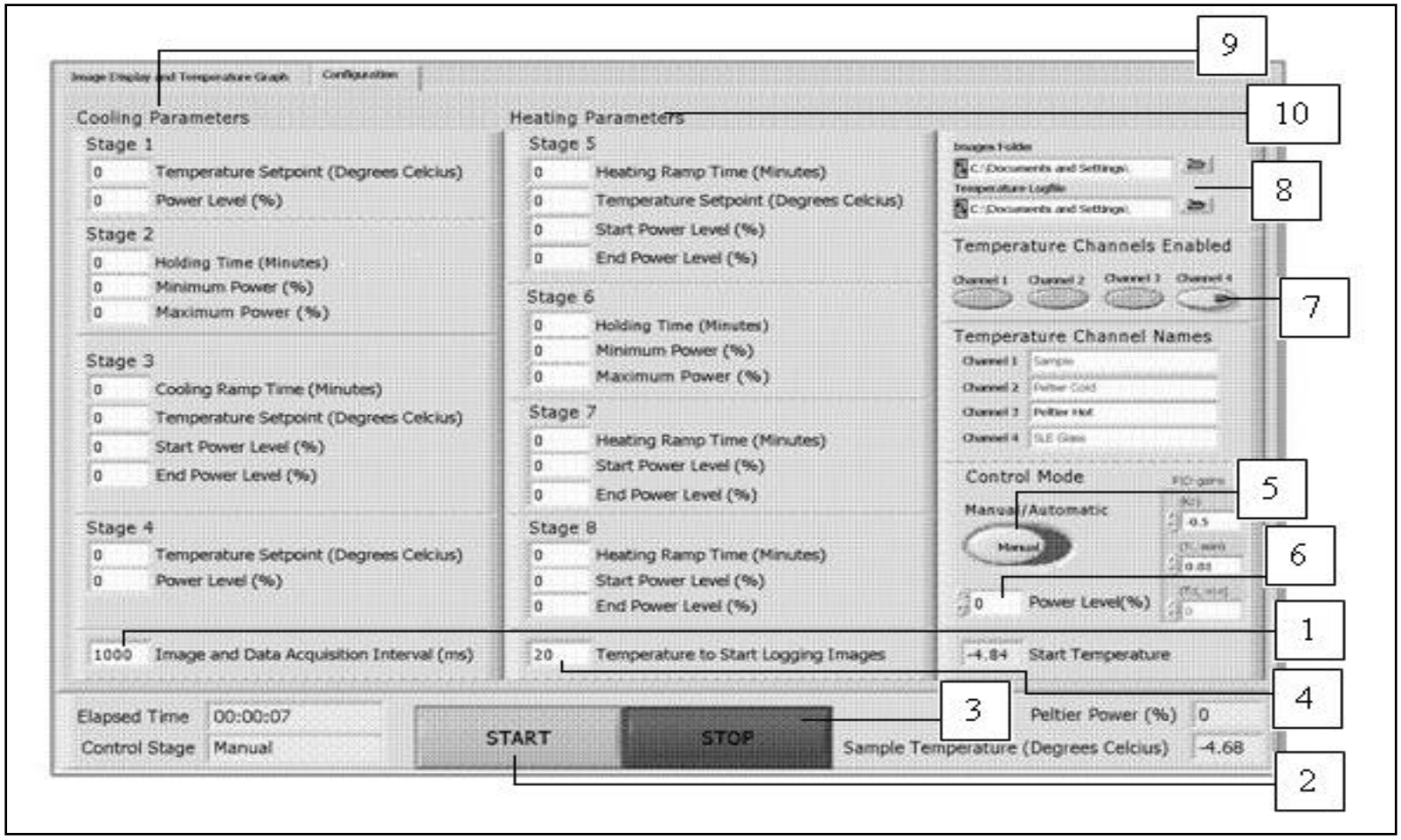

Figure 4-5: Configuration (SLE Software).

1. Image and Data acquisition rate is set in milliseconds; 2. Start button; 3. Stop Button; 4. Temperature at which images start logging is set; 5. Manual or automatic mode is set; 6.Power Level (%); 7. Temperature sensor on/off buttons; 8. Folder path for the temperature log-file and image file; 9. Cooling Parameters for a four stage cooling process; 10. Heating parameters for a four stage melting process.

The software is operated in two control modes, automatic and manual (5). The power level (from 0 – 100%) in the manual mode, is set beneath the mode control button (6). The automatic mode is controlled in two cycles; a heating and a cooling cycle. The cooling cycle is input with cooling parameters (9), from stages 1 to 4 and the heating cycle is input with heating parameters (10), from stages 5 to 8. The parameters in these cycles are time duration for each stage and power levels. Each stage allows the software to determine the power supplied to the Peltier modules and the time interval between consecutive power levels. Each of the stages is further explained:

- **Stage 1.** The controlling parameter is the temperature set-point for the sample. It is a quick cooling stage which brings the sample to a temperature above the equilibrium temperature (set-point). The input parameters are temperature set-point and the power level (%) which will produce the temperature set-point.
- **Stage 2.** This stage is time controlled. It is a holding stage in which the temperature is held constant through feedback control. The input parameters are time duration for the stage, and maximum and minimum power settings, which provide hysteresis on the temperature control. The purpose of this stage is to hold the temperature in the sample before a slow cooling stage.
- **Stage 3.** This stage is time controlled. It is a slow cooling stage at the required rate (<1 K/h). Input parameters are time, start and end power level (%), and temperature set-point. The power is gradually increased (ramped) in intervals until the specified time and final power are reached. Each power level results in a specific temperature being achieved in the sample. The power levels are set so that the temperature range covers the equilibrium temperature. In the ramp, the power range is divided into increments of time. This is specified by the user when the ramping time is input. It should be noted that the temperature profile does not necessarily follow the profile of the power, due to thermal effects caused by phase transition. This is illustrated in Figure 4-6.
- **Stage 4.** This stage is temperature set-point controlled. The temperature of the now solid sample is reduced to a temperature well below equilibrium, by a single power level. The purpose of the stage is to bring the sample to a temperature low enough to prevent difficulties in controlling the subsequent heating cycle.
- **Stage 5.** This stage is temperature set-point controlled. It is a quick melting stage and brings the temperature of the sample to a temperature close to and below the equilibrium temperature. The parameters required are time, start and end power level, and temperature set-point.
- **Stage 6.** The controlling parameter is time. This is a holding stage, controlled through feedback control. Input parameters are time and maximum and minimum temperatures, which control the hysteresis. The stage has been incorporated in order to control the rate of temperature change in the sample and in order to allow the crystals within the sample to re-orient into the equilibrium crystal phase before a slow melting stage.

- **Stage 7.** The controlling parameter is time. This is a slow melting stage through the equilibrium temperature. The input parameters are time, and start and end power levels. The power levels are gradually reduced in order to induce slow melting within an interval of time until the specified time is complete. These power levels are the reverse of the power levels in stage 3, with the same ramping time being applied.
- **Stage 8.** The controlling parameter is time. It is meant to be a quick melting stage in which the sample is heated to ambient temperature. The input parameters are time, and start and end power levels. The time that is set is a short time and the power level is set to zero in order to bring the sample back to ambient temperature quickly.

Figure 4-6 shows the power and temperature profiles that arise as a result of each of the above stages being applied to a sample in the Peltier apparatus. More details and the values that can be input are provided in the operating procedures of the apparati.

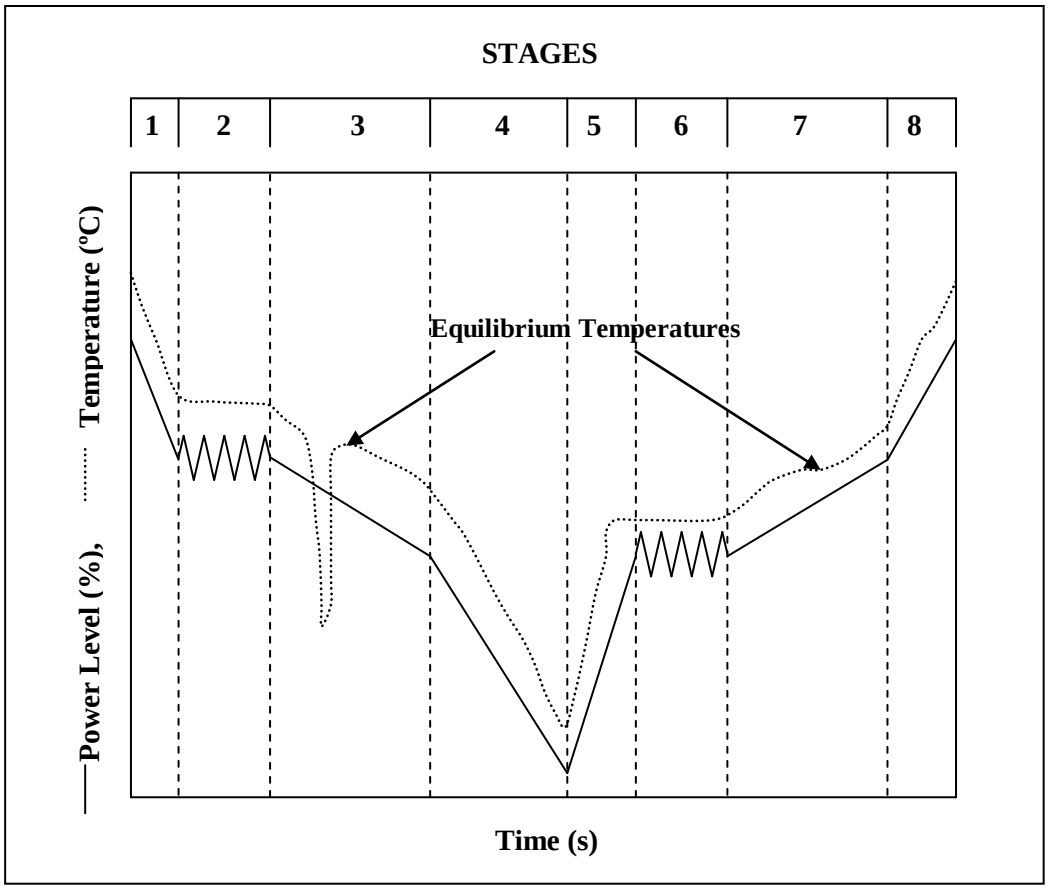

Figure 4-6: Graph of the stages described in the configuration section of the software; (—), power level profile and (·····), temperature profile.

The display of temperature profiles such as that shown in Figure 4-6 can be seen on the image display and temperature graph interface. A real time image from the camera is also shown beside the temperature profiles. An image of this interface can be seen in Figure 4-7.

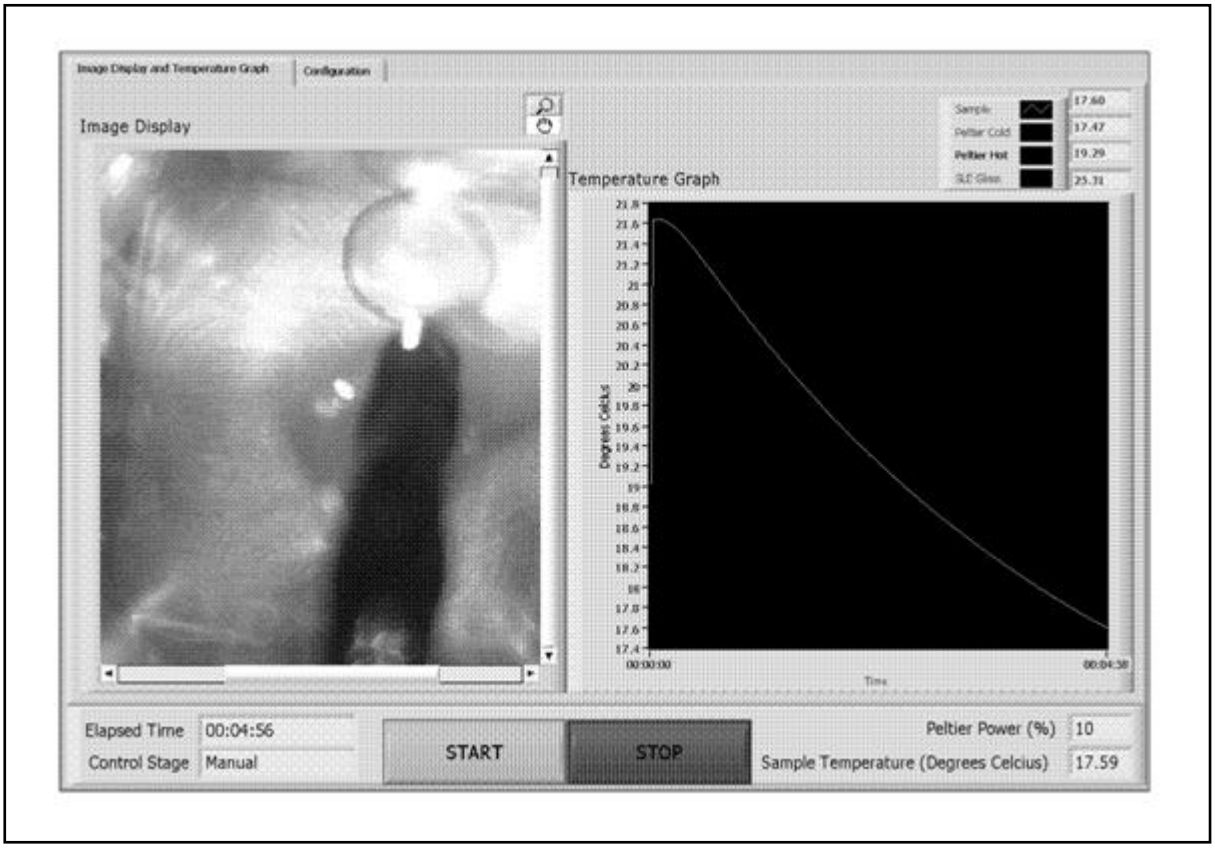

Figure 4-7: Image Display and Temperature Graph (SLE Software)

4.4 Operating Procedures for the Apparati

4.4.1 Cleaning of the Apparati

The cleaning procedure for each equilibrium cell is the same. The equilibrium cell is first removed from the apparatus assembly. The cell can be cleaned initially rinsing with water and detergent. It is thereafter rinsed in high purity acetone and dried using compressed air. The Pt-100s are rinsed with acetone and allowed to dry to prevent contamination of the sample during the experiment. This is because the Pt-100s are in direct contact with the sample. All parts of the equilibrium cell which are in contact or may have contact with the sample, are cleaned before loading fresh chemicals.

For the glass apparatus, the equilibrium cell may be removed without stopping the circulating fluid in the thermostat. For the Peltier apparatus it must be ensured that the power supply is switched off. This is to protect the Peltier modules from condensing moisture from the atmosphere, which can cause

short-circuiting in the wiring. The surface between the Peltier modules and the heat sink, as well as the surface between the Peltier modules and the equilibrium cell, must always be kept clean. The surface can be wiped clean using a cloth and then applying fresh heat conductive paste. The paste ensures effective heat transfer.

4.4.2 Temperature Sensor Calibrations

The temperature probes were calibrated against a standard probe which was a WIKA CTH 6500 precision measurement instrument. The sensor is a resistance thermometer Pt-100, with a temperature range from 73.15 K to 1123.15 K. It has an accuracy of ± 0.03 K for a range from 73.15 K to 423.15 K. The resolution of the sensor is 0.01 K for the range from 73.15 K to 473.15 K. Calibrations were made in a WIKA 9100 temperature calibration bath using silicon oil as the fluid medium (SI-044). The bath temperature was set and the temperature was allowed to stabilize for one hour. The temperature reading from each Pt-100 was then recorded. This was done over the temperature range being measured. At least six points were measured over the temperature range. Calibration points were repeated at least three times for reproducibility. The Pt-100s used in the experimental apparati were calibrated over a temperature range from 243.15 K to 303.15 K for the Peltier apparatus and a range from 243.15 K to 223.15 K for the Glass apparatus.

4.4.3 Purity of Chemicals and Sample Preparation

The purity of all chemicals was tested by two methods before use, viz., refractive index and gas chromatography injection. The refractometer used was an ATAGO Model RX-7000 and measured refractive indices with precision up to 5 decimal points. The chemical purity was also tested by gas chromatography using, a Shimadzu GC Series 2010 that uses a thermal conductivity detector (TCD). The GC was used to determine the percentage purity of the dominant chemical and identify the presence of other impurities.

All mixture compositions were measured in a syringe with the use of an OHAUS digital mass balance to obtain the required molar fraction. The precision on the balance is ±0.01 mg. The syringe was weighed before the chemical was drawn. The mass of the syringe with the sample was measured and the mass of the syringe was also measured after injection of the sample into the equilibrium cell, to determine the actual mass of chemical loaded into the cell. The resultant uncertainty in the mole fraction composition was calculated to be ± 0.00003.

4.4.2 Experimental Procedure for the Peltier Apparatus (SLE)

The general procedure which is followed when measuring solid-liquid equilibria is as follows for both apparati:

1. The sample is shock cooled to form small crystals, by subjecting the sample to very low temperatures, and then allowed to crystallise slowly to prevent formation of metastable crystals.
2. The equilibrium temperature is estimated from the plateau of the cooling curve.
3. The sample is melted at a fast rate up to a temperature which is estimated to be just below the equilibrium temperature.
4. The temperature is held constant at this temperature to allow for the kinetics of the crystals to stabilise within the sample.
5. The sample is then heated gently, through the equilibrium temperature using a low rate, approximately in the range of <1 K/h.
6. The equilibrium temperature is recorded as the temperature at which the last equilibrium crystal disappears.
7. The cycle is repeated at least three times to verify the equilibrium temperature.

The procedure for obtaining the solid-liquid equilibrium of a synthetic sample is described. For solid-liquid equilibria measurements the camera is not a necessity for the identification of equilibrium using both apparati. It is convenient for observing the cell contents, which can only be viewed from above for the Peltier apparatus and from the side for the Glass apparatus. The camera enables the experimenter to not be present whilst the experiment is in progress, and provides visual information of the experimental progression, should it be required.

4.4.2.1 Apparatus Start Up and Operating Procedure

1. Assemble the equilibrium cell and Peltier modules onto the heat sink. Use heat conductive paste, on the surfaces between the Peltier modules and the heat sink, on the surface between Peltier modules, and on the surface between the Peltier modules and the equilibrium cell base.
2. Switch on the programmable power supply and the heat sink fans.
3. Fill the equilibrium cell with sample, and position onto the Peltier modules.
4. Seal the equilibrium cell with the gasket, glass air pocket and Perspex cover.
5. Flush the cell with nitrogen:
    - Open the nitrogen gas valve on the nitrogen cylinder for 15 seconds.
    - Shut the Nitrogen gas valve.

6. Secure the apparatus by tightening the screws by hand.
7. Position a fan to blow onto the surface of the Perspex and switch it on. This aids removal of any condensation on the surface, which would reduce visibility.
8. Position the camera, lights and the stirrer motor, above the cell.
9. Switch on the stirrer to begin stirring the sample, the lights are switched on with the same switch on the DC power supply.
10. Open the software program on the computer and set the directory paths for the images and the temperature log files.
11. Set the temperature and image logging rate; 1000 ms is sufficient and set the temperature at which images should start logging. This temperature is usually 253.15 K, to prevent any images from being logged until the experiment is underway.
12. Switch the software to manual mode.
13. Set the power level for this mode to 0%.
14. Press the start button; the images of the cell contents appear on the screen and the program starts logging temperature.
15. Determine the equilibrium temperature T_{Eq} so that the parameters for the automatic mode may be obtained. (This is in manual mode.)
    - Change the power level in the manual mode from 0% to 100% and allow the sample to cool.
    - Determine T_{Eq} as the highest temperature reached on the arrest/break, (it is not necessary to obtain an accurate temperature value).
    - Keep the sample as a solid by leaving the power level at 100%.
16. Determine the power level required to achieve temperature T_1 ($T_1 \approx 2$ K below T_{Eq}) and temperature T_2 ($T_2 \approx 2$ K above T_{Eq}).
    - Starting with the solid sample from the previous step, increase the power level in increments of 10% and allow temperature to stabilise at each power level.
    - Take note of power level and corresponding temperature.
    - Reduce increments as the temperature approaches T_1 and determine P_1, the corresponding power level and P_2, the power corresponding to T_2.
    - Allow the sample to return to ambient temperatures by setting the power level back to 0%.
17. Input the parameters for the cooling and heating cycle on the configuration interface using the information obtained in Steps 15 and 16.

Cooling Parameters:

- Stage 1 – Set power level to P_2 and set temperature set point to T_2.

- Stage 2 – Set maximum power to P_2 + 1%, minimum power to P_2– 1% and holding time to 20 minutes (experimenter may use their discretion).
- Stage 3 – Set temperature set point to T_1, cooling ramp time to 240 minutes, start power to P_2 and end power to P_1.
- Stage 4 – Set temperature set point to T_{low} which is a temperature ≈ 10 K below T_1 or more, and power level to 100%.

Heating Parameters:

- Stage 5 – Set heating ramp time to 20 minutes, temperature set point to T_1, start power level to 100% and end power level to P_1.
- Stage 6 – Set maximum power to P_1 + 1%, minimum power to P_1 - 1% and holding time to 20 minutes.
- Stage 7 – Set heating ramp time to 240 minutes, start power level to P_1 and end power level to P_2.
- Stage 8 – Set heating ramp time to 20 minutes, start power level to P_2 and end power level to 0%.

18. Switch the configuration mode to automatic. The software begins to run through each stage. The experimenter can now set the temperature to start logging images as T_2.
19. At the end of the experiment, press stop on the software and restart (start button) to repeat the cycles. Repeat the cycle at least 3 times to reproduce results.

The rate of cooling or melting specified in this procedure should produce a rate of ≈ 1 K/h. The experimenter can change the rate by adjusting ramping times in Stages 3 and 7 of the software. The experimenter may also choose to measure only melting points making the cooling stage unnecessary. In this case, all power levels may be set to 100% in the cooling parameters and times minimised, in order to allow the software to advance through these stages quickly. The temperatures may remain unchanged. Similarly the heating cycle can also be bypassed in the same way, with all power levels set to 0% in order to bypass the stages.

4.4.2.2 Analysis of Results

A method was developed in which the rate of change of temperature can be identified, for data from both the Peltier apparatus and the Glass apparatus. This enables an analytical method of determining solid-liquid equilibria temperature. The data acquisition software records the temperature every second, depending on the data rate that is set. These temperatures are corrected to actual temperature using the temperature calibrations, which are unique for each Pt-100. The data points have then been

averaged over every 180 data points i.e. every 3 minutes. The temperature differences of these data point intervals have been calculated and represented on a graph of ΔT versus time (in seconds).

From this graph the temperature of phase change is identified by identifying the change of gradient in the transition region. Where the temperature of the sample remained constant, ΔT on the graph was very low due to small changes in temperature. When the temperature changes from constant temperature to a steady increase/decrease in temperature, ΔT on the graph also shows a corresponding change (the change is significant enough to be seen on the trend on the graph). The SLE temperature is the point on the ΔT versus time graph (in the region known to be the equilibrium region) where there is a significant change in ΔT. For systems in which the melting point temperature is indicated by constant temperature then this point can also be identified as the lowest value of ΔT, in the observed equilibrium temperature region.

The analysis of the results follows the following procedure:

1. Export data points from the log file onto a spread sheet.
2. Correct the temperatures to actual temperature using calibrations.
3. Calculate an average of the sample temperatures for every 180 seconds.
4. Calculate ΔT, for the averaged temperatures (from step 3). $\Delta T = T_i - T_{ii}$, for temperatures i and ii, which are consecutive temperatures.
5. Plot a graph of sample Pt-100 temperature and cold Pt-100 temperature versus time e.g. Figure 4-8 for the Peltier apparatus. The same applies for the sample temperature versus time for the Glass apparatus. Region A indicates existence of a solid phase, region B is a melting region and region C is a liquid state of the sample. Line E on Figure 4-8 and point E on Figure 4-9 indicate the equilibrium temperature. This temperature region is taken as equilibrium because it denotes the temperature at which the sample has completely melted. The final melting stage is considered to be the equilibrium region.
6. Plot a graph of ΔT versus time e.g. Figure 4-9.
7. Using the temperature - time graph locate the expected equilibrium region.
8. Using the ΔT versus time graph locate the point where the inflection in the curve is represented by a change in ΔT or the point where the constant temperature is represented by a minimum (e.g. Figure 4-9), this is the equilibrium temperature. According to step 4, Point E on Figure 4-9 is defined as $\Delta T = T_i - T_{ii}$. The SLE temperature is therefore T_i. The ΔT versus time graph is a tool to assist the experimenter to determine an exact SLE temperature.

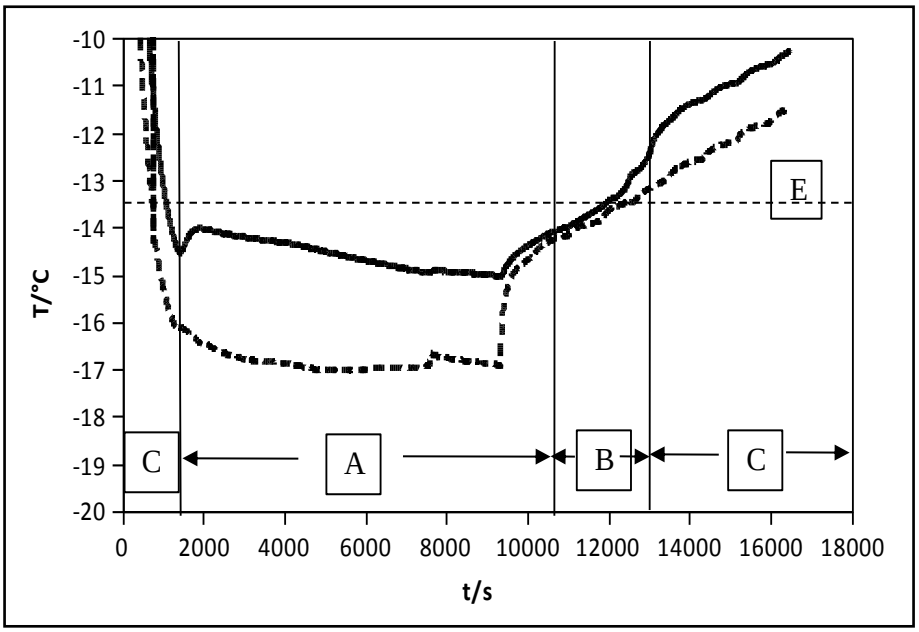

Figure 4-8: A Temperature profile generated from an experimental run on the Peltier apparatus: (—), Sample Temperature and (·····), Cold (Peltier module) Temperature. Region A indicates the existence of solid, region B is the melting region and region C is a liquid state of the sample. Point E indicates the equilibrium temperature.

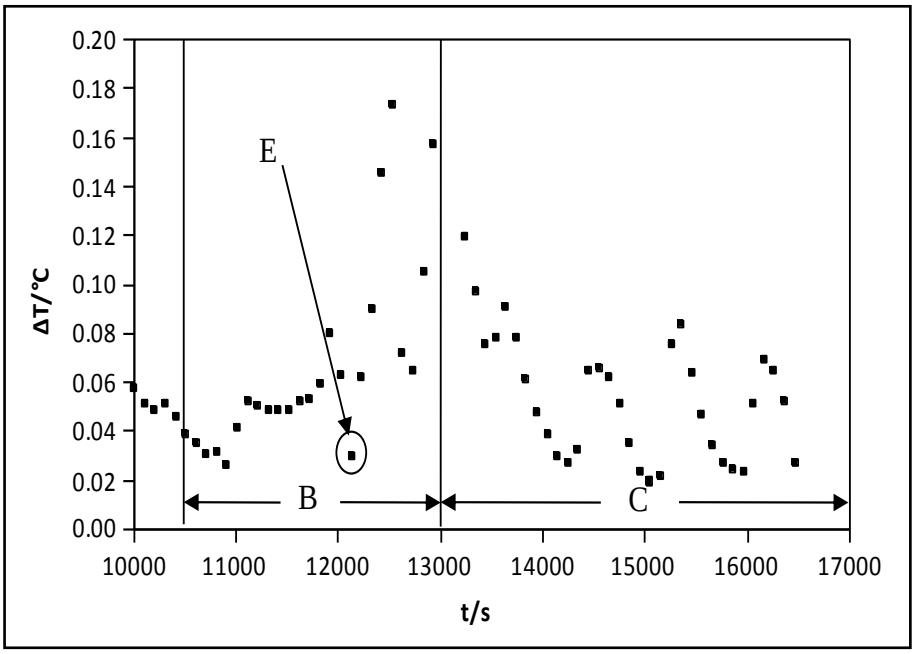

Figure 4-9: Graph of ΔT against time (s) for determination of SLE point.
Region B is the melting region and region C is a liquid state of the sample. Point E indicates the equilibrium temperature.

4.4.2.3 Shut-Down Procedure

At the end of an experiment the apparatus is returned to ambient temperature, and no power supplied to the Peltier modules.

1. Press the stop button on the software.
2. Switch off the magnetic stirrer and lights and remove them from the apparatus.
3. Switch off the programmable power supply.
4. Remove wing-nuts and remove the cover to the equilibrium cell.
5. Remove the nitrogen gas line and Pt-100s, (sample and cold) from the cell.
6. Remove the equilibrium cell and empty the chemicals into a waste bottle and clean the equilibrium cell.
7. Switch off the fans underneath the heat sink and the fan removing moisture from the top surface of the Perspex.
8. When not in use keep the equilibrium cell fully assembled on the heat sink.

4.4.3 Experimental Procedure for the Glass Apparatus (SLE)

4.4.3.1 Start up Procedure

1. Fill the cryogenic bath with cryogenic liquid.
2. Switch on the chilling unit and set it to temperature T_{low} which is well below the intended operating temperature range.
3. Fill oil well in thermostat jacket with silicon oil.
4. Switch on circulator and set the set-point to a low temperature T_{low}, this will maintain temperature in the thermostat jacket.
5. Flush equilibrium cell with nitrogen gas:
    - Open inlet and outlet valves.
    - Open nitrogen gas cylinder valve for 30 seconds and shut valve.
    - Shut nitrogen outlet valve on equilibrium cell.
6. Inject sample into the equilibrium cell through a septum. Raise the Pt-100 above the level of the septum so that no chemicals come in contact with it whilst loading the cell. Immerse the Pt-100 and wash down any chemical residue on the walls of the equilibrium chamber by swirling the contents of the cell.
7. Flush the equilibrium cell once again with nitrogen as described in step 5.
8. Switch on the hotplate magnetic stirrer.
9. Press start on the software to start recording the temperature. When the glass apparatus operates independently then the software configuration must operate in manual mode, with

the power level set to 0% to ensure that the Peltier modules are not damaged. In addition switch off the display buttons for all the Pt-100s on the Peltier apparatus. Alternatively the glass apparatus can operate simultaneously with the Peltier apparatus.

10. Place equilibrium cell inside the thermostat jacket. The magnetic stirrer will begin to homogenise the sample during crystallisation. The temperature T_{low} is low enough so that the sample can crystallise quickly. The value of T_{low} used was 225.15 K, due to the control limits of the programmable circulator.

    Alternatively, the equilibrium cell is shock cooled by immersing the cell in a flask of liquid nitrogen (replacing steps 9 – 10). The level of liquid nitrogen should cover the sample, for uniform heat transfer from the sample. This cell is held in liquid nitrogen until small crystals are seen to form within the sample in the equilibrium cell. The cell is then carefully transferred from the liquid nitrogen to the thermostatted vessel. The sample is then allowed to crystallise at a lower rate than in liquid nitrogen which is at a much lower temperatures than the thermostat.

    From this process an equilibrium arrest/break can be observed on the cooling curve for a temperature T_{Eq} during crystallisation. This gives an indication of the region of the equilibrium temperature.

11. Input a program in the programmable circulator which will determine the rate of melting, based on the knowledge of T_{Eq}. This program requires time and temperature set points.
    Step 1 Raise temperature from T_{low} to T_1 a temperature below the equilibrium temperature T_{Eq}.
    Step 2 Hold temperature at T_1 for a short period of time (≈30 minutes) for stabilisation and to allow crystals to transform to equilibrium crystals.
    Step 3 Slowly raise temperature from T_1 through T_{Eq} to final temp T_2.
    Step 4 Bring temperatures back from T_2 to low temperature T_{low}.
    For details on how to program the circulator the experimenter is referred to the operating manual (Operators manual programmable/digital controller model 7412, Polyscience).
    It is assumed that the rate of heat transfer to the sample is constant and uniform throughout the sample such that, the rate of increase in the temperature of the cryogenic fluid is equal to the rate of increase of temperature within the sample.

Change of composition is achieved by addition of a known mass of one of the components. The equilibrium cell may be emptied and cleaned before charging with a new composition; however with the size of the equilibrium cell this will waste chemicals.

4.4.3.2 Shut-Down Procedure

1. Stop the program on the programmable circulator and leave the set point at temperature T_{low}.
2. Remove the equilibrium cell from the thermostat.
3. Switch off the chilling unit.
4. Remove the Pt-100 from the equilibrium cell.
5. Empty the equilibrium cell contents into a waste bottle and clean the cell.
6. Switch off the programmable circulator.
7. Switch off the chilling unit.

4.4.4 Liquid-liquid Equilibria Experimental Procedure Using the Peltier Apparatus

1. Follow steps 1 to 14 of the solid-liquid equilibria start-up procedure for the Peltier apparatus.
2. Set the temperature to start logging images at ambient temperature, if the experiments are expected to be cooling experiments and set to 100 ºC, if the experiments are expected to be heating experiments. This ensures that the software records all images below the set temperature.
3. Determine the equilibrium temperature T_{Eq} (cloud point), so that the parameters for the automatic mode may be obtained, this is done in manual mode. This method is dependent on whether the sample is initially miscible or immiscible (clouded).

   Cooling:

   - Decrease the power level in the manual mode from 0%, in increments of 10%.
   - Determine T_{Eq} by comparing images recorded with temperature recorded. This is done by matching the time on the image to the time corresponding to a temperature data point.
   - Obtain power levels P_1 and P_2 which are power levels that give temperatures T_1 and T_2 (2 K above and below the equilibrium temperature T_{Eq} respectively).

   Heating:

   - Switch off the power supply and change the positive and negative terminals connecting the Peltier modules to the power supply. This will reverse the mode of operation from cooling to heating.
   - Change the power supply slowly, in increments of 5% until a change is observed on the screen. It is important to control heating because the modules over-heat easily and will become damaged.
   - Determine the transition temperature T_{Eq} by comparing images recorded with temperature recorded. This is done by matching the time on the image to the time on a data point.

- Obtain power levels P_1 and P_2 which are power levels that give temperatures T_1 and T_2 (2 K above and below the equilibrium temperature T_{Eq}).

4. Input the parameters for the cooling and heating cycle on the configuration interface using the information obtained in Step 3.

   Cooling Parameters:

   - Stage 1 – Set power level to P_1 and temperature set point to T_1.
   - Stage 2 – Set maximum power to $P_{1,Eq}$, minimum power to $P_{1,Eq}$ and holding time to 0 minutes (user has the option of by-passing the stage).
   - Stage 3 – Set temperature set-point to T_2, cooling ramp time to 60 minutes, set start power to P_1 and end power to P_2.
   - Stage 4 – Set temperature set-point to T_2 and power level to P_2 (user has option of by-passing the stage).

   Heating Parameters:

   - Stage 5 – Set heating ramp time to 0 minutes, temperature set-point to T_2, start power level to P_2 and end power level to P_2.
   - Stage 6 – Set maximum power to P_2, minimum power to P_2 and holding time to 0 minutes (user has option of bypassing the stage).
   - Stage 7 – Set heating ramp time to 60 minutes, start power level to P_2 and end power level to P_1.
   - Stage 8 – Set heating ramp time to 20 minutes, start power level to P_1 and end power level to 0%.

   If the Peltier module is operating in reverse mode (heating), then the cooling parameters become heating parameters and the same applies for the heating parameters.

   The rate of change of temperature is approximately 0.1 K/min.

5. The cloud point and clear point measurements are repeated 3 times for reproducibility.

Measurement of a new composition is made by emptying and cleaning the cell, by following the shut down procedure. This shut down procedure is the same as previously mentioned for the Peltier apparatus. The equilibrium cell can be charged with a fresh sample of known composition.

4.4.4.1 Analysis of LLE Results

Equilibrium temperatures or cloud point temperatures were obtained using the camera in a visual analysis. The camera was used to take frames of the equilibrium cell contents during experimentation, every second. After the experiment the frames were analysed to determine which frame showed the transition between turbidity and clarity of the sample. Each frame is identified according to time and

this is compared to temperature logs which are also identified by time. The frame and temperature of the sample can therefore be matched. The same procedure applies to clear points. The clear points were considered, in this work, to be the equilibrium temperature. Photograph 4-4 shows a series of frames taken by the camera on the Peltier apparatus. These frames show the transition of turbidity within the sample.

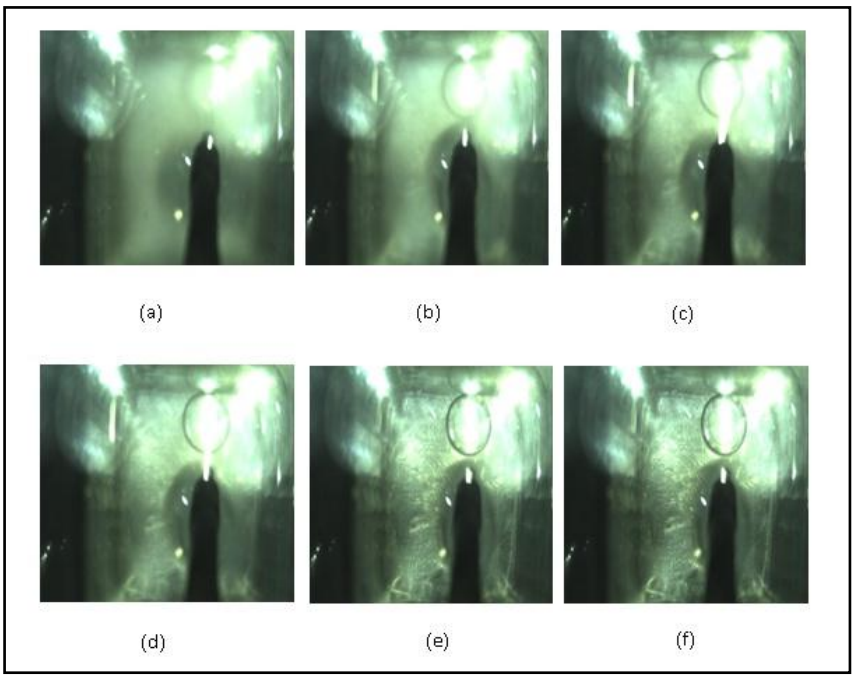

Photograph 4-4: Clear point picture frames taken using a camera in the Peltier apparatus. Frame (a) is turbid and frame (f) shows a clear sample.

The frames, (a) to (e) do not directly precede one another but have been chosen to illustrate the visual changes that take place within the cell. The frames are recorded at the same rate as temperature is logged and hence at very low rates of temperature change, more picture frames will be analysed before the phase change is detected. In Figure 4-4 frame (a) is turbid and frame (f) shows a clear sample.

4.4.5 Experimental (LLE) Procedure Using the Glass Apparatus

1. Steps 1 to 9 for the Peltier apparatus are followed in charging the equilibrium cell. An important note is that T_{low} is ambient temperature for the Glass apparatus.
2. Align the camera to the side of the equilibrium cell so that the sample may be viewed from the software interface.

3. The temperature to start logging images is set to a temperature which will ensure that frames for the entire experiment are logged.
4. Set a temperature T_2 on the programmable circulator which will allow the sample to either increase in temperature or decrease in temperature whichever way the experimenter requires. Identify T_{Eq} which is the clear or cloud point.
5. Program the circulator to proceed gradually, raising or decreasing the temperature at a rate of 0.1 K/min through the equilibrium temperature.
6. The temperature at which images are to be taken should be set at a temperature above that which is expected for the cloud point, so that images are recorded for each phase transition. The same camera from the Peltier apparatus is used to view into the glass apparatus from a horizontal angle.
7. The cloud point and clear point measurements are repeated for reproducibility by programming the circulator to loop about the same program for a set number of times.

Change of composition is achieved by addition of a known mass of one of the components. The equilibrium cell may also be emptied and cleaned before charging with a new composition. The method of analysis of results is the same as that used for the Peltier apparatus to determine cloud and clear points.

4.5 Evaluation of Equipment

4.5.1 Design and Operation of Equipment

A summary of the apparati designed, constructed and tested is given in Table 4-1. The design features of each apparatus which are unique to the apparatus and which have a significant role in the operation of the apparati are given in this table and then discussed thereafter.

Table 4-1: Key features of the Peltier and Glass apparati.

	Peltier Apparatus	**Glass Apparatus**
Equilibrium Cell	Aluminium square cell	Glass cylindrical cell
Capacity	10 cm^3 maximum	143 cm^3 maximum
Temperature Operating Range	253.15 – 373.15 K Maximum temperature limited by operating range of the Peltier modules. Minimum temperature limited by the heat sinks thermal capacity.	223.15 – 473.15 K Temperatures limited by the operating range of the chilling unit.

	Peltier Apparatus	**Glass Apparatus**
Temperature measurement device	1/10 DIN ceramic encased Pt-100, accuracy of ±0.03 K at 273.15 K.	1/10 DIN stainless steel encased Pt-100, accuracy of ±0.03 K at 273.15 K.
Mode of Cooling and Heating	Peltier modules used for heating and cooling.	Cryogenic fluid.
Moisture Condensation in Cell	A nitrogen gas inlet into the equilibrium cell allows the airspace above the sample to be filled by an inert gas.	
Insulation	Equilibrium cell is insulated from the sides and top. The Peltier modules also compensate for heat loss and heat addition from the heat sink.	Equilibrium cell is insulated by a vacuum jacket, however extra insulation is needed for very low temperatures.
Homogenisation of sample	Teflon coated magnetic stirrer bar in sample.	
Temperature Control	Semi-Automated Open loop control, through the computer.	Semi-Automated Open loop control, through the circulator or the computer.
Cleaning	Cleaning is required after each new composition.	Cleaning can be undertaken after a complete system or part of a system is measured.

4.5.1.1 Peltier Apparatus

The Peltier apparatus was designed to have a small sample volume for accurate data measurement. This enabled the apparatus to use low volumes of chemical during measurements of the system. This is a financial advantage to the laboratory. In terms of construction, the equilibrium cell was constructed of aluminium because of the high thermal conductivity of aluminium, which was required for effective heat transfer from the sample to the Peltier modules and vice versa.

The equilibrium cell was designed to have a nitrogen gas inlet and outlet. The purpose of the gas was to remove any moisture from the cell which would otherwise contaminate the sample, by keeping the sample in an inert environment. The only disadvantage of this design was that volatile substances could not be measured at high temperatures because of a loss of sample in the liquid phase resulting in a change in composition.

Peltier modules (which are also known as thermoelectric coolers), were used for cooling. The use of Peltier modules was very useful as a mode of cooling for various reasons. Firstly the modules are cheap and can easily be acquired, and the modules are easily manageable and compact, making the entire apparatus compact and easily movable. Their use also does not require special handling of chemicals and movement of large equipment.

Temperature measurement was by use of a ceramic encased Pt-100. The diameter of the probe was 1.5 mm and the length was 15 mm. The small diameter of the probe was chosen to improve the sensitivity of the probe to temperature changes and the length of the probe allowed it to fit well into the small volume of sample. A 1/10 DIN RTD was chosen because of its high accuracy.

From Chapter 3 it was found that an essential design feature for any SLE and LLE apparatus is mixing. To achieve this, a motor driven magnetic stirrer bar was used for stirring within the equilibrium cell. The square shape of the cell would have caused problems of dead zones in the mixture, but this was eliminated by varying the speed of the stirrer motor and having a small sized equilibrium cell. Stirring and visualisation of the equilibrium cell contents could only be done from the top of the cell because of the solid aluminium walls. Viewing into the equilibrium cell was achieved by the use of a camera interfaced to a computer. With sufficient lighting this was found to give adequate images of the cell contents. The experimenter was able to view the images of the experiment at the end of a measurement for further information regarding how the sample behaved during the experimental run, and for analysis of LLE data during LLE experiments.

The air gap was sufficient for insulation for temperatures down to 263.15 K, beyond which moisture began to condense on the perspex cover. In order to prevent moisture condensation, a fan was used to blow air onto the surface of the apparatus and continuously remove the condensation. This feature was incorporated after the design of the apparatus. Further insulation on the sides of the cell using neoprene foam was added. The neoprene foam was used mainly for protecting the Peltier modules. Peltier modules draw heat energy from their surroundings, which results in moisture condensing onto them. The modules are part of an electric circuit and hence it is not safe to have moisture present in the environment as it may cause short circuiting and reduce efficiency in heat removal or damage the modules.

The temperature range of operation of the apparatus was limited, as seen in Table 4-1 to a minimum temperature of 253.15 K. This was limited by the heat dissipation from the heat sink to the surroundings. At this temperature it was found that equilibrium was reached, between the amount of heat withdrawn from the sample and the amount of heat dissipated to the surroundings. It was found that if the temperature of the surroundings could be reduced then the temperature of the sample could

be reduced. If this was not possible then accumulation of heat within the heat sink resulted in heat being transferred back into the sample, due to heat conduction through the Peltier modules. The apparatus was operated in hot weather (summer in Durban - KwaZulu Natal) with the temperature of the surroundings reaching up to + 30 ºC (303.15 K). It was therefore found to be of importance to control the temperature of the surroundings by operating in an air-conditioned room. The cooling capacity in ΔT, as a result of control of external temperatures, was resultantly approximately equal to 40 – 45 K.

Control of the sample temperature was the most important design feature of the apparatus. This was done through the software, which has already been previously described. The software was designed in such a way that the user was able to specify a desired rate of melting or cooling through the parameter input to the software. The disadvantage was the amount of extra work that was required to determine the necessary parameters to input into the software for effective control. With continuous use it was found that this calibration became less of a time consuming exercise, due to expertise with the apparatus.

The operation of the Peltier apparatus required that the apparatus be cleaned between each consecutive measurement. This was because the design of the equilibrium cell did not have provision for sample injection, once the cell had been sealed. The small size of the cell reduced the amount of work done in cleaning and preparation for the next experiment.

4.5.1.2 Glass Apparatus

Many of the design features of the Glass apparatus were adapted from the apparatus of Jakob et al. (1995) (refer to Chapter 3). The major change that was made with the cell was to control the temperature rate for the apparatus through the use of a programmable circulator. Through the programmable circulator it was possible for the experimenter to set the rate of melting or heating required.

4.6 Analysis of Results

4.6.1 Analysis of Solid-Liquid Equilibria Results

One of the methods commonly used for solid-liquid equilibria determination is the determination of the temperature of the disappearance of the last crystal (Domanska, 1996, Jakob et al., 1995). This method is a visual method and the identification of the last crystal disappearance has often been observed by the naked eye. This method requires the experimenter to wait for long periods of time to

identify the disappearance of the crystals. In addition, the equilibrium temperature is subject to the interpretation of when the disappearance of the final crystal is observed by the experimenter. Another method of analysis is the melting curve. Provost and co-workers (Provost et al., 1998) developed a method to determine the melting point from the melting curve. The technique analysed the change in gradient of the melting curve. This is shown in Figure 4-10. Three points were determined: A, B and C. These were the onset of melting, final phase transformation and return to linear heating respectively. Point B denoted the region of the equilibrium temperature; this was determined by calculating the intersection point of the two lines AB and CB.

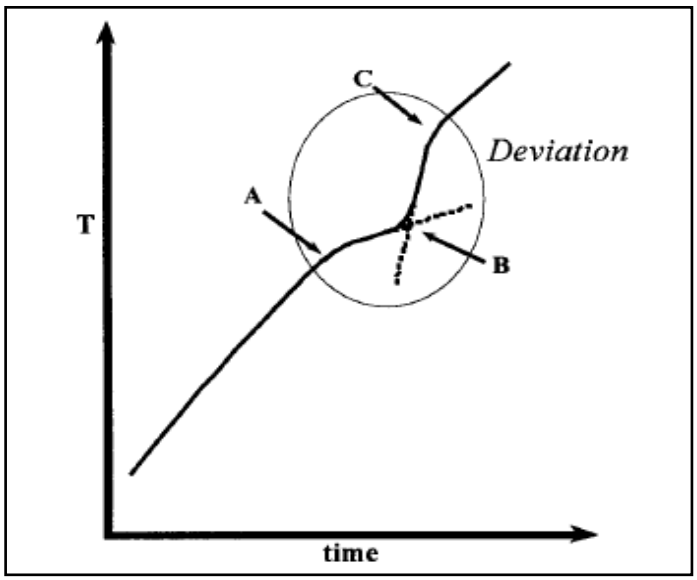

Figure 4-10: Melting curve for an n-alkane + solvent mixture denoting the onset of phase transition A, the final transition temperature B, and the return to linear melting point C (Provost et al., 1998).

In order to reduce errors introduced by the experimenter, it was initially proposed to implement the use of a camera to record the phase transition of the sample from solid to liquid phase. There were difficulties encountered with this method of determining the SLE temperature and that led to the method being adapted. It was observed that the crystals being formed within the sample exhibited different melting kinetics. This was mainly due to the fact that crystals were formed around the immersed Pt-100 which acted as a nucleation site. Crystals of a different structure may form at the surface of a sample whilst the crystals in the centre may be different, the crystals may melt at a temperature between the liquid temperature and the equilibrium melting temperature (Sirota, 1998). result of the difference in kinetics was a crystal mass within the sample which had a different melting point to the bulk of the sample. This was towards the end of the melting process. It was observed that the deviation between the last crystal disappearance and recorded literature data was up to 2 K on the Peltier apparatus, for the pure component melting point of cyclohexane. According to literature

values, this deviation was too large. Analysis of the melting curve showed a region in which the temperature within the sample began to fluctuate due to melting of the crystal. Attempts were made to minimise the formation of this crystal, by increasing the speed of the magnetic stirrer bar and applying different rates of cooling to the sample in order to produce uniform crystals throughout the sample.

Further analysis of the melting curve generated for the experiment showed that there was a demarcation from which the bulk of the sample was completely melted and where the final remaining solid with different kinetics, had melted. Figure 4-11 shows one of the melting curves generated (cyclohexane + hexadecane system). The point circled and labelled M on Figure 4-11 shows a change in temperature that resulted from the bulk crystal detaching from the magnetic stirrer bar and proceeding to melt with different kinetics.

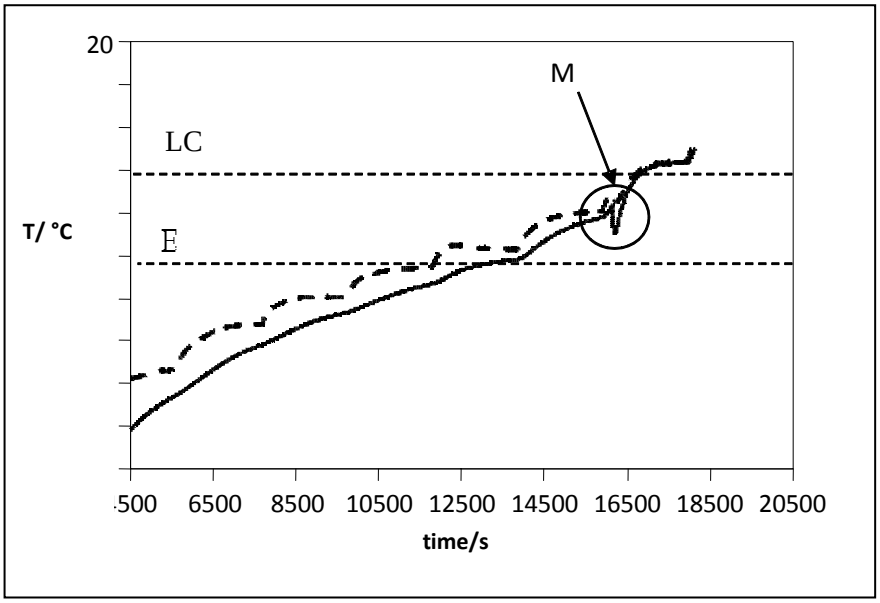

Figure 4-11: Melting curves generated for the Peltier apparatus in a cyclohexane + hexadecane system: -----, Peltier module temperature profile and ——, sample temperature profile; LC, last crystal disappearance, E, equilibrium temperature and M, melting of final crystal.

Line E on Figure 4-11 represents the equilibrium temperature and LC represents the last crystal disappearance. The composition of the sample was 0.2 mol fraction of cyclohexane and the equilibrium temperature was recorded as 288.06 K (14.91 ºC), the final crystal disappearance was observed at 290.05 K (16.9 ºC) a recorded literature value was 288.0 K (Tanaka et al., 1996). The deviation between the literature and the two temperatures can be observed to be very large, for the temperature at which the crystal disappears.

Based on this observation a different method for analysis of the equilibrium temperature, based on the technique used by Provost and co-workers (1998) was developed. The temperature of bulk crystal disappearance was taken as equilibrium. The final method of analysis was described previously. The method aimed at allowing the experimenter to effectively treat the large bulk of data points that were generated from each experimental run (up to 20 000 data points). It also enabled the experimenter to search for the thermal signature changes effectively, through analysis of the change in slope of the temperature profile. The main requirement in this method of analysis was for the experimenter to be aware of the physical significance of each section of the generated temperature curve. For example the correct identification of the onset of melting and the final transition from solid (refer to Figure 4-12, points A and B).

The final melting stage was defined experimentally by either a constant temperature or an inflection in the gradient of the temperature curve, depending on the system. This occurred in the same way that crystallisation is identified by either an arrest (constant temperature) or a break (change in the gradient of the curve). Figures 4-12 and 4-13 show the two different types of melting curves that were observed during experiments for two different systems. For both figures, point A denotes the onset of melting and point B denotes the equilibrium temperature.

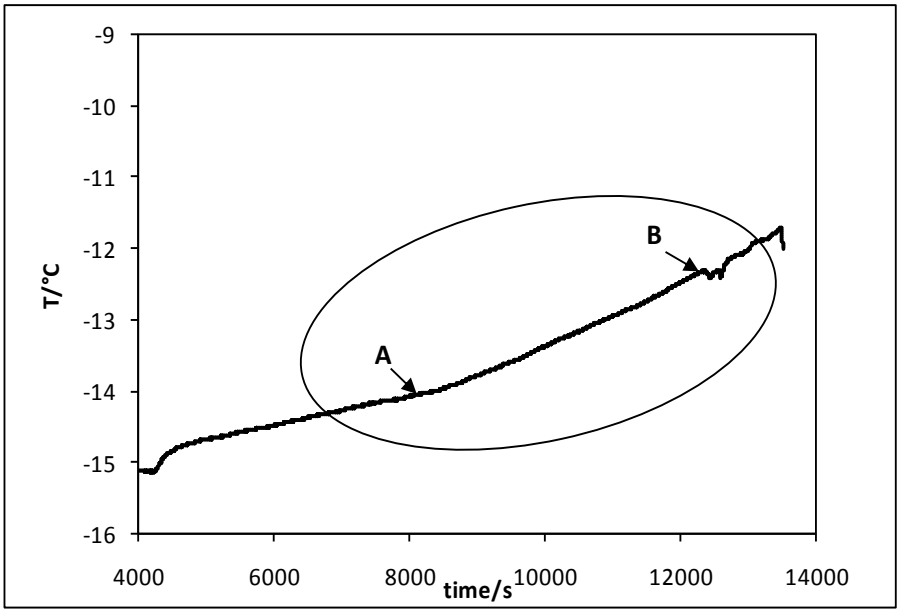

Figure 4-12: Melting curve of heptanoic acid + hexanoic acid on the Peltier apparatus showing a constant final transition temperature; A, beginning of melting of the sample and B, end of melting of the sample.

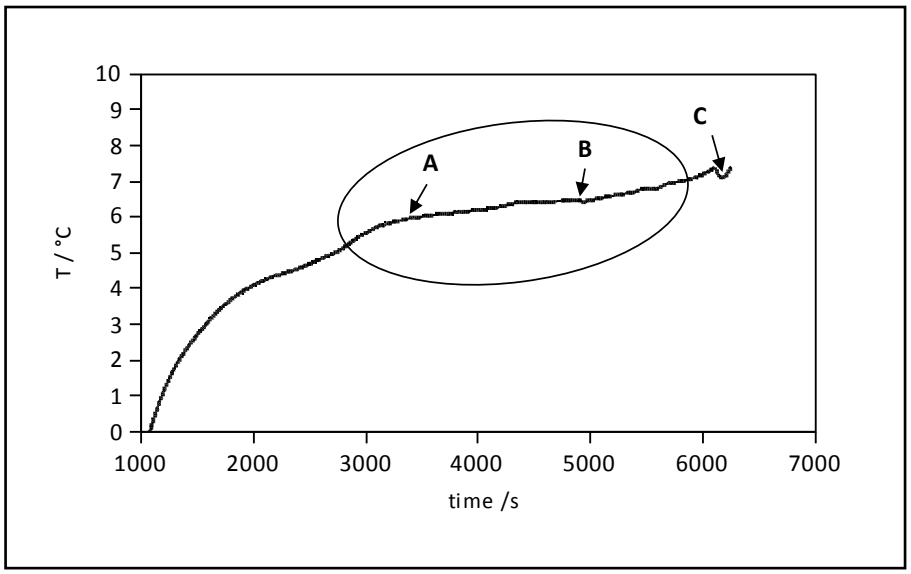

Figure 4-13: Melting curve for pure cyclohexane on the Peltier apparatus showing a change in gradient as the final transition temperature; A, beginning of melting of the sample, B, end of melting of the sample, and C bulk crystal phase disappearance.

In Figure 4-12 the temperature fluctuations around point B were a result of the final crystals melting and in Figure 4-13 point C denotes the disappearance of the final crystal, exhibiting different melting kinetics to the bulk of the sample as discussed previously.

4.6.2 Analysis of LLE Results

The LLE results were analysed from images stored by the software during the experiment. Images were taken by the camera at intervals of 1 second. The technique was time consuming because of the large number of picture frames generated, but allowed for the experimenter to not be present during the experimental run. It was difficult to identify the onset of the cloud point and therefore clear points were determined. This method was also used by Ochi et al. (1993), in which they too determined liquid-liquid equilibrium as the change from a turbid immiscible state to a clear miscible state. The visual method of cloud point determination could not be compared to the analytical techniques of determining liquid-liquid equilibria because the determination of phase transition is dependent on the interpretation of the experimenter and therefore subject to greater uncertainty.

Chapter 5

Results and Discussion

In this chapter the results and a discussion of the measurements that were made on both apparati are presented. The equipment was evaluated through SLE measurements of known systems (test systems), by comparing with the data in the literature. These systems were also modelled using thermodynamic models. An LLE system was also measured and the results are presented for measurements on the Peltier apparatus. New SLE systems were also measured and modelled using both apparati for SLE data, the results of which are also presented and discussed.

5.1 Systems Measured

Pure component melting points were measured over the temperature range of the apparatus. These were followed by binary test systems. Both these measurements were compared with published literature values. The pure component test systems for melting points were cyclohexane, hexadecane, 1-octanol, distilled water, and hexanoic acid. The binary test systems for melting points were the cyclohexane + hexadecane system, measured on the both apparati separately and the 2-butanol + water system, which was measured on the Peltier apparatus only, for solid-liquid equilibria measurements. Since the 2-butanol + water system has a region of immiscibility, liquid-liquid equilibria were also measured to demonstrate the versatility of the apparatus. In addition two binary aliphatic carboxylic acid mixture systems were also measured. These measurements constituted new systems whose solid-liquid equilibria had previously been unmeasured and are part of an ongoing research into the solid-liquid equilibria of carboxylic acid mixtures. They were; heptanoic acid + butyric acid and heptanoic acid + hexanoic acid. Both systems were measured by a combination of the Peltier and the Glass apparati.

The motivation for measurement of these systems extends from the fact that extensive vapour-liquid equilibria work has been done on the carboxylic acids (Sewnairan, 2001, Clifford, 2004, and Iwarere, 2009), but no investigation has been done into the solid-liquid equilibria. As previously mentioned in Chapter 1, Sewnairan (2001) has suggested that there is a possible viability in separating carboxylic acid mixtures by freeze crystallisation. In addition to the phase equilibria data (VLE and LLE) for separation, solid-liquid equilibria may contribute significantly to obtaining low temperature parameters for the various systems and thereby improve thermodynamic predictions made for these systems and like systems. The solid-liquid equilibria data for carboxylic acid mixtures is minimal in literature with only a few combinations having been measured for the C1 to C7 acids (refer to Table 1-1).

5.2 Temperature Calibrations

Temperature sensor calibrations were performed on each of the Pt-100s in order to determine the uncertainty on the temperature measurements. The results presented and discussed in this section are for the sample Pt-100s for the Glass and Peltier apparati. The uncertainties on these Pt-100s determine the uncertainty of the equilibrium temperatures measured. These uncertainties are given in Figures 5-1 and Figure 5-2.

The uncertainty in the temperature measurements from the calibrations was found to increase at low temperatures. The major contributing factor was possibly a result of the fluid used in the calibration bath, which was silicon oil. The calibrations were performed for a temperature range from 243.15 to 303.15 K. It was observed that the viscosity of the oil became higher in the lower temperature range and temperature stabilisation was not as fast in the lower temperature range as in the higher temperature range. The effect of the high viscosity at low temperatures can be seen in Figure 5-1 and 5-2, which are the scatter plots of the deviations between the temperature reading of the sample Pt-100s from the standard probe, for both apparati. The temperature deviations (absolute errors) in the low temperature region for both apparati are of the same magnitude in both apparati, and are also significantly higher than those observed at high temperatures, thus showing the effect of low temperatures on the oil within the calibration bath. This effect was more pronounced for the Glass apparatus as is indicated in Figure 5-1.

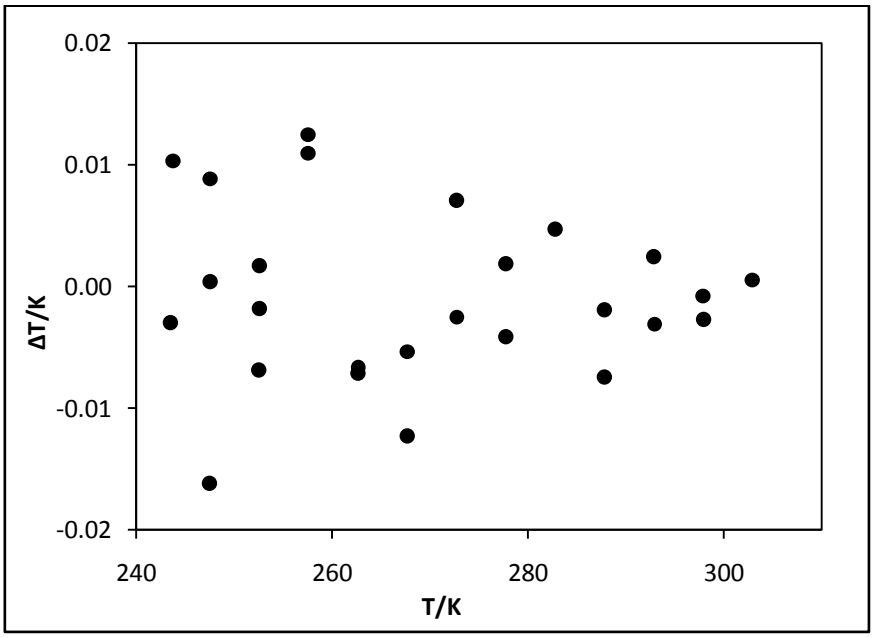

Figure 5-1: Temperature deviations between the Glass sample Pt-100 and the standard temperature probe for the calibration. $\Delta T = T_{standard} - T_{Sample\ Pt\text{-}100}$.

The scatter plot for the Peltier Pt-100 (Figure 5-2) shows a less even scatter to that of the Glass apparatus. One of the contributing factors was the positioning of the Pt-100s in the calibration bath. The standard probe was a long straight probe as was the sample Pt-100 for the Glass equipment. The sample Pt-100 for the Peltier apparatus however was in an L-shape and was shorter in comparison to the other two probes. The probes were fastened together within the calibration bath in order to have them measure the same temperature region in the bath. However, the shape of the Peltier apparatus's probe may have caused it to shift, thereby causing the tip of the probe to not be aligned with that of the standard probe. This would result in the higher errors recorded on the Peltier sample Pt-100 as compared to the Glass apparatus, despite the fact that both Pt-100s were of the same type and accuracy.

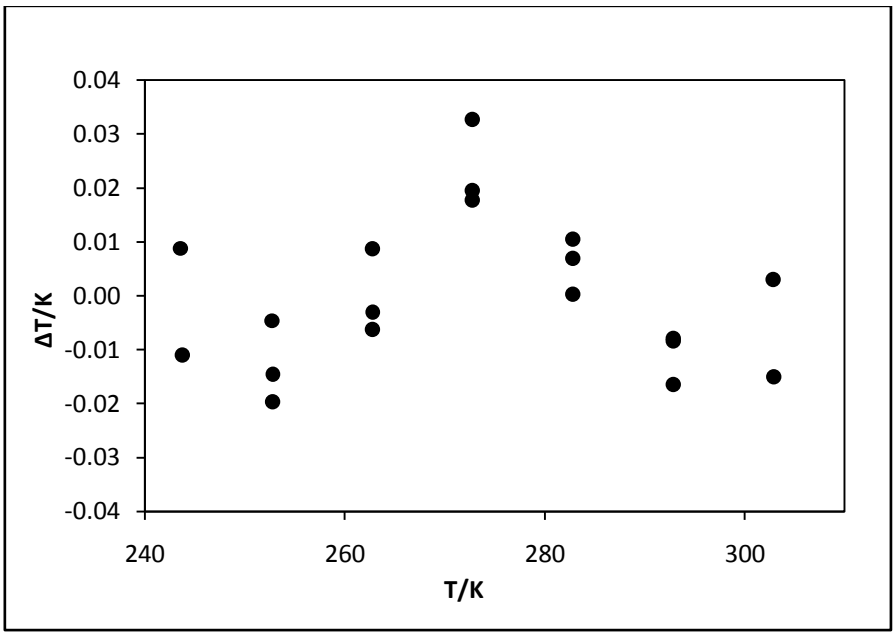

Figure 5-2: Plot of the deviations of the calculated temperature of the Peltier sample Pt-100 from the standard temperature. $\Delta T = T_{standard} - T_{Sample\ Pt\text{-}100}$.

The final calibration results showed the Peltier sample Pt-100 to have an uncertainty of ±0.03 K and the Glass apparatus an uncertainty on temperature reading of ±0.02 K. The final calibration equations are shown in Figures 5-3 and 5-4.

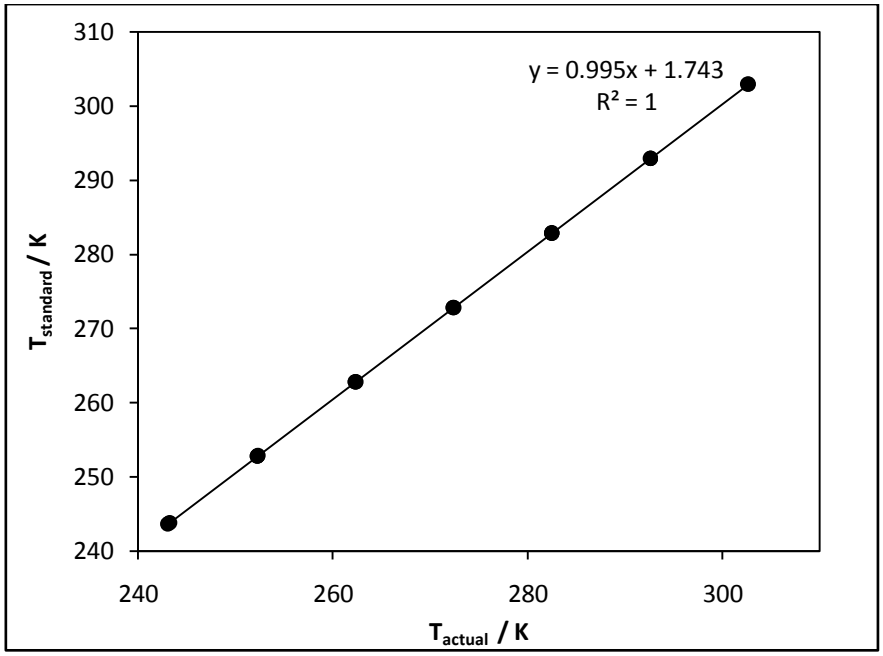

Figure 5-3: Temperature calibration results of the Peltier apparatus sample Pt-100.

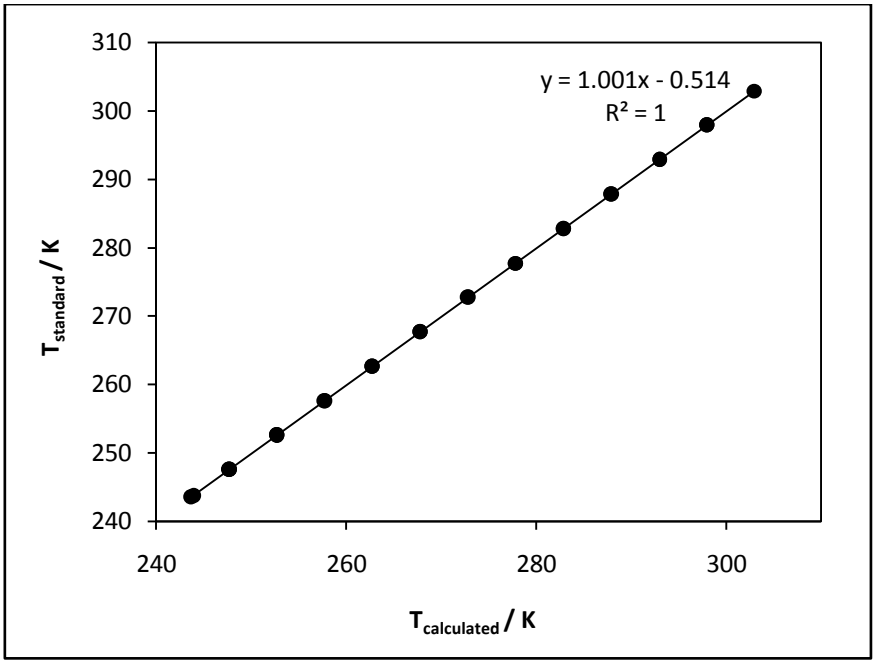

Figure 5-4: Temperature calibration results of the Glass apparatus sample Pt-100.

5.3. Purity of Chemicals

The supplier details and purities of the chemicals used are provided in the Table 5-1.

Table 5-1: Results of experimental purity tests by refractive index and gas chromatography.

				Refractive Index @ 20 °C	
Chemical	**Supplier**	**Specified Purity / %**	**GC % ***	**Experimental**	**Literature[a]**
Cyclohexane	Merck	≥99.5	99.87	1.42631	1.42660
2-Butanol*	Fluka	≥99.5	99.90	1.39730	1.39750
Butyric Acid	Fluka	≥99.5	99.47	1.39808	1.39800
Heptanoic Acid	Fluka	≥99	98.60	1.42290	1.41700
Hexadecane	Merck	≥99	99.90	1.43461	1.43450
Hexanoic Acid	Fluka	≥98	99.10	1.41692	1.41630
Distilled Water	-	-	99.90	1.33298	1.33298
Octanol	Fluka	≥99.5	99.90	1.42920	1.42950

[a]Weast (1983-1984),
* - GC % is area under peak.
*Molecular sieves were placed inside the 2-Butanol bottle after opening to absorb any moisture.

5.4. Test Systems

5.4.1 Pure Component Melting Points

The results of the melting points measured using the Peltier apparatus and the Glass apparatus are given in Table 5-2.

Table 5-2: Experimental results of the melting points for the pure components measured on the Peltier and Glass apparati.

Compound	T/K				
	Peltier	**σ**	**Glass**	**σ**	**Literature**
Water	273.38	±0.09	273.21	±0.01	273.15*
Hexadecane	291.15	±0.03	291.09	-	291.30[a]
					291.00[b]
					291.33[c]
Cyclohexane	279.80	±0.03	279.66	±0.08	279.73[d]
					279.84[e]
					279.70[f]
Heptanoic Acid	266.21	±0.02	265.94	±0.18	265.65[g]
Octanol	258.38	±0.26	257.97	±0.18	258.10[h]
					258.90[i]
Butyric Acid	268.64	±0.24	-	-	267.45[g]
Hexanoic Acid	270.69	±0.05	-	-	269.55[g]

*Weast (1983-1984), method not specified; [a]Erkey et al. (1989), method not specified; [b]Huang et al. (1995), method not specified; [c]Lobbia et al. (1983), synthetic method; [d]Goates et al. (1979), synthetic method; [e]Knauth et al. (1990), analytical method; [f]Aston et al. (1943), analytical method; [g]DDB PCP Data (2009), method not specified; [h]Yang et al. (2003), synthetic method; [i]Domanska et al. (2002), synthetic method.

Standard Deviation ,$\boldsymbol{\sigma} = \sqrt{\sum \left(T_{exp} - \mu\right)^2 / N}$

μ is the mean of T_{exp} and N is the number of data points measured

As indicated in Table 5-2 the largest uncertainty in temperature reading of the pure component measurements was 0.26 K for octanol, on the Peltier apparatus. The value of 0.26 K is σ and refers to the uncertainty in temperature reading. The largest uncertainty in temperature reading measured on the Glass apparatus was 0.18 K for octanol and heptanoic acid. This value is related to σ. The value for the comparison with literature is 0.56 K Peltier and 0.29 Glass for the heptanoic acid. Corresponding values for octanol are less. The higher deviation for octanol are less; this is possibly due to the purity of heptanoic acid being <99%. For the Peltier apparatus it was observed that the largest uncertainty in temperature reading recorded was for the measurement of octanol which has a melting point that is close to the limiting temperature of the apparatus. On the apparatus octanol was measured to have a melting point of 258.38 K. The limiting temperature of the Peltier apparatus was 253.15 K and the melting point of octanol, 5.23 K above the minimum temperature. During the measurements, crystallisation of octanol was observed to take much longer to achieve due to temperatures being in close proximity of the limiting temperature of the apparatus. This was because

super-cooling would take place before crystallisation occurred, and the temperature of the super-cooled liquid was below the temperature observed to be the minimum operating temperature. In these circumstances crystallisation was never achieved and the experiment had to be repeated and an attempt made to reduce the effect of super-cooling. The temperature of the surroundings played a significant role in the measurement of the melting point because as discussed in the previous chapter the lowest temperature attainable was determined by the temperature gradient between the apparatus and the surroundings. The temperatures of the surroundings during these measurements were unfortunately very high due to the season. As a result the measurement of octanol could not be repeated in cycles, as the operating procedure indicates.

The reason for the repetitive melting and crystallisation cycles was due to the observation that the uncertainty in determining the SLE point (temperature) reduced with each repetitive measurement. The same observation was also made by Domanska (1996). To verify the equilibrium temperature, multiple measurements of a single cycle per measurement were made for the octanol melting point, unlike for the other chemicals. For the Glass apparatus the temperature range of the apparatus had no effect on the measurements taken because the limits of operation of the apparatus were well below the temperature measurements made for the pure components.

The objective of measuring the melting points in the range of the Peltier apparatus was also to determine the accuracy of the temperature measurements. According to the calibrations it was seen that at lower temperatures the Peltier showed greater uncertainty in temperature readings, the same as for the Glass apparatus. It is also evident in the melting point measurements that the largest errors were recorded for the melting points measured below 273.15 K.

It is clear from comparison with the references that despite the deviations in the SLE temperatures measured between both apparati that the results obtained from both apparati fall within the range of measurements reported in the literature.

5.4.2 The Cyclohexane (1) + Hexadecane (2) System

This system was previously measured by Tanaka et al. (1996), Domanska et al. (1990), and Snow et al. (1986). Domanska and co-workers and Tanaka and co-workers used a synthetic visual method (last crystal disappearance) to determine the solid-liquid equilibria temperature. Snow and co-workers used a visual method similar to that used in this work (identification of thermal effects by analysis of the melting curve). The system was measured using both apparati.

The data measured were compared to the literature, graphically. This graph is shown in Figure 5-5. From this graph, the data obtained in this work follows the trend of that by Snow and co-workers, and Tanaka and co-workers; however it does not follow that of Domanska et al. (1990) from the range of 255 - 270 K.

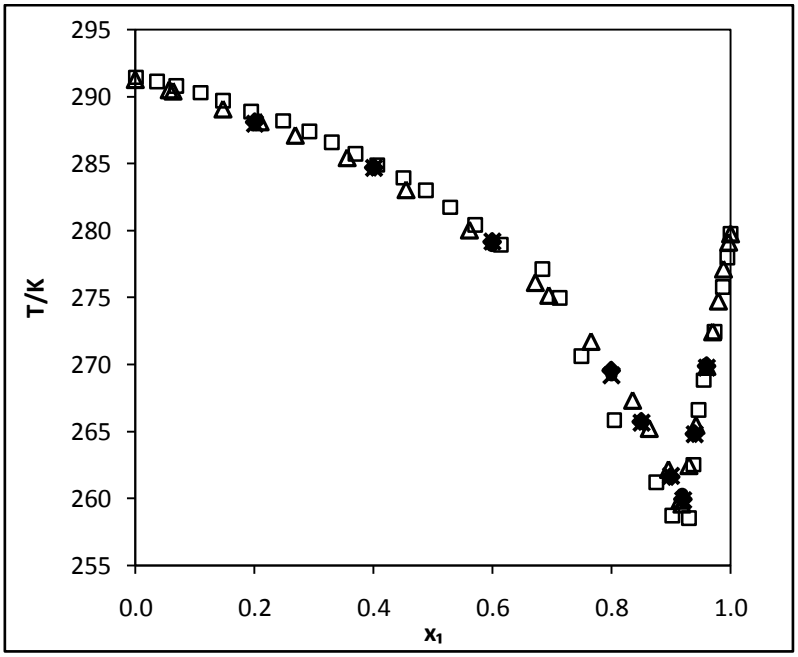

Figure 5-5: Solid-liquid equilibria temperatures for the cyclohexane (1) + hexadecane (2) system; ●, this work (Peltier); ▲, this work (Glass); □, Domanska et al. (1990); ∆, Snow et al. (1986); x, Tanaka et al. (1996).

Table 5-3: Eutectic temperatures and compositions for the cyclohexane + hexadecane systems measured.

Data	x_1	T/K
Snow et al. (1986)	0.92	259.59
Domanska et al. (1990)	0.93	258.55
Tanaka et al. (1996)	0.92	259.90
Peltier (this work)	0.92	259.94
Glass (this work)	0.92	260.29

From Table 5-3, which lists the eutectic compositions and temperatures obtained in this work and the literature, it was found that, the eutectic temperature measured by Snow and co-workers had a lower deviation compared to the experimental eutectic temperatures of both the Glass and Peltier apparati. The deviations between the eutectic temperatures measured from the Peltier and the Glass apparati, compared to the data by Tanaka and co-workers was 0.04 K for the Peltier apparatus and 0.49 K for

the Glass apparatus. The deviations for Snow and co-workers are 0.35 K and 0.70 K respectively. Larger deviations were exhibited between the data from both apparati and that by Domanska and co-workers between $x_1 = 0.68$ and the eutectic composition ($x_1 = 0.93$). However the remaining regions compared well to the data of the other literature sources as well as for this work.

The larger deviations between the measurements of this work and Snow may be attributed to different methods for analysing the melting curve. According to Snow and co-workers the average error on melting point measurements was ± 0.05 K, and in the eutectic region the deviation was ± 0.03 K. The average error for the melting points measured from the Peltier apparatus was ± 0.10 K and the uncertainty on the eutectic temperature was ± 0.05 K. For the Glass apparatus the, average error was ± 0.13 K and the uncertainty on the eutectic temperature was ± 0.02 K (refer to Appendix C for uncertainties). The accuracy of the eutectic temperatures measured by both apparati showed that the eutectic temperatures compare well with the literature values by Tanaka and those by Snow and co-workers.

Table 5-4: Experimental melting temperatures obtained for the cyclohexane (1) + hexadecane (2) test system measured on the Peltier apparatus and Glass apparatus and compared with literature data.

	T_m /K			|Δ T | /K			Relative Error/%		
x_l	Peltier	Glass	Ref[a]	Glass-Peltier	Peltier -Ref	Glass - Ref	Glass-Peltier	Peltier - Ref	Glass - Ref
0.20	288.06	288.05	288.00	0.01	0.06	0.05	0.00	0.02	0.02
0.40	284.70	284.67	284.70	0.03	0.00	0.03	0.01	0.00	0.01
0.60	279.15	278.86	279.20	0.29	0.05	0.18	0.10	0.02	0.06
0.80	269.54	269.20	269.20	0.34	0.33	0.00	0.13	0.12	0.00
0.85	265.71	265.78	265.70	0.06	0.01	0.08	0.02	0.01	0.03
0.90	261.62	261.61	261.70	0.01	0.08	0.09	0.00	0.03	0.03
0.92	259.94	260.29	259.90	0.34	0.04	0.38	0.13	0.02	0.13
0.94	264.82	264.87	264.80	0.05	0.02	0.07	0.02	0.01	0.03
0.96	269.90	270.01	269.80	0.11	0.10	0.21	0.04	0.04	0.08
Average				**0.14**	**0.08**	**0.12**	**0.05**	**0.03**	**0.05**

[a]Tanaka et al. (1996).

$|\Delta T|/K = |T_{exp} - T_{ref}|$,

Relative Error $\% = [(T_{ref} - T_{exp})/T_{ref}] \times 100$

Table 5-4 shows the deviations of the SLE temperatures measured from the Peltier and the Glass apparati compared with a literature reference (Tanaka et al. 1996), as well as the deviations when

measurements from both apparati are compared. The absolute average deviation, of the Peltier apparatus compared to the Glass was 0.14 K and is in the same range as literature values. The average absolute deviation of the Peltier apparatus with literature was 0.08 K which was lower than that for the Glass apparatus which was 0.12 K. Both apparati had relative errors of 0.05% and below. The values of these errors were in acceptable agreement with literature. In literature, average relative errors have been recorded up to 28% (Costa et al., 2007) and temperature deviations of SLE temperatures have been recorded in a range from 0.1 to 1 K (Wachter et al., 2008). From Table 5-4 the deviations between the measured data and the literature data become larger in the eutectic region for the measurements on the Glass apparatus. When both apparati were compared for this system it was found that, the melting points recorded on the Glass apparatus were lower than for the Peltier apparatus in the hexadecane rich region and higher in the cyclohexane region of the phase diagram.

5.4.3 The 2-Butanol (1) + Water (2) System

Melting point and crystallisation temperatures were measured for this system. The solid-liquid equilibria data of this work was compared to data measured by Lohmann et al. (1997) which was melting point data, and it was compared to data by Ochi et al. (1996) which was crystallisation temperatures. Both data sets were measured using the visual method. For analysis, Lohmann and co-workers determined the temperature at which the last crystal disappeared whilst Ochi and co-workers analysed the cooling curve, determining the highest temperature reached after super-cooling. The system that was measured has a region of immiscibility in which the (solid-liquid) equilibria becomes constant. Within this region the crystallisation temperature is constant. Ochi and co-workers managed to measure the SLE for the immiscibility region but Lohmann and co-workers did not include it in their measurements. The results for this system are presented in Figure 5-6 and Table 5-5.

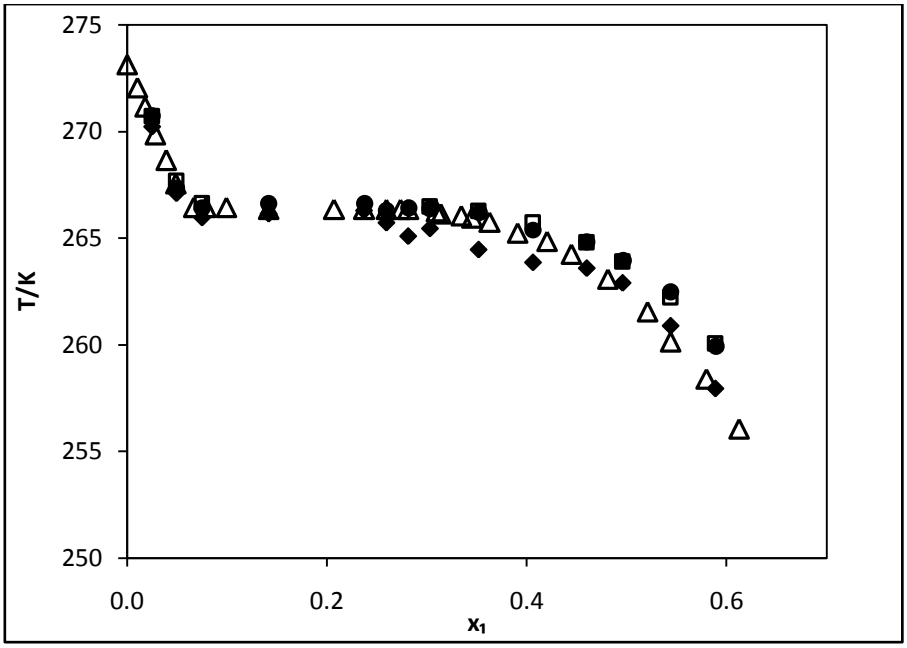

Figure 5-6: Solid-liquid equilibria temperatures for the 2-butanol (1) + water (2) system on the Peltier apparatus; ●, T_m (this work); ♦, $T_{crystal}$ (this work); □, Lohmann et al. (1997); ∆, Ochi et al. (1996).

The melting points and the crystallisation points obtained were distinctively different. This was observed for the data measured on the apparatus and for the two separate literature sources. This difference can be accounted to the effects of super-heating and super-cooling. Super-cooling is the phenomenon in which a sample remains in liquid form below the solid-liquid phase transition temperature. The super-cooled liquid reaches a temperature at which crystals begin to form spontaneously and the temperature of the sample returns to the equilibrium temperature. Super-cooling distorts the identification of the equilibrium temperature and the equilibrium form of the crystals (Nyvlt, 1977). This phenomenon may be reduced by slow rates of cooling (Wachter et al., 2008, Ochi et al., 1996). In the literature, Gimzewski and Audley (1993) have determined that for long chain organic molecules such as wax and diesel, a disparity of up to 4 K can be observed in the melting and crystallisation temperatures at the same rate of heating/cooling. Despite this however, melting temperature and crystallisation temperatures for certain systems may also be comparable as shown by Wachter et al. (2008).

The average absolute deviations of the melting points (Table 5-5) compared to literature values were within acceptable limits (range 0.03 – 0.34 K). Some of the points measured showed high deviations from the literature, up to 0.34 K. These may have arisen as a result of some of the system properties, especially the viscosity of the system. This system when measured by Lohmann et al. (1997) was found to be a viscous system. Previously it was discussed that in the calibrations for the Pt-100s, larger uncertainties were observed for temperature readings in regions of high viscosity. The same

factor may have contributed to the large deviations of the measured data from literature. The scatter of the absolute deviations showed that the deviations varied with composition, exhibiting an increase in uncertainty corresponding to increase in 2-butanol mole fraction.

The miscibility gap was existent in the system, between the composition of x_1 (2-butanol) from 0.0751 to 0.3031. The high errors that were observed for compositions before the miscibility gap may have been as a result of the mixture being close to a saturation point. This was because within the miscibility gap the SLE temperature was expected to remain constant. The measurement of the melting points within the miscibility gap was difficult due to the presence of two phases within the sample.

The comparison of the experimental data and that by Ochi and co-workers showed very large deviations. These deviations were likely to be as a result of super-cooling, resulting from differing cooling rates between the apparati. The rate used by Ochi and co-workers was not specified and the rate used in this work was not constant. Crystallisation temperatures from the apparatus were recorded to make a comparison and determine the ability of the apparatus to measure crystallisation temperatures. Hence the comparison with the experimental data by Ochi and co-workers is not considered as a measure of the accuracy of the equipment.

Table 5-5: Experimental melting point and crystallisation temperatures for the 2-butanol (1) + water (1) system measured on the Peltier apparatus and comparison with literature data.

	T/K						%	
	Experimental				|Δ T |		Relative Error	
x_1	T_m	$T_{crystal}$	T_m [a]	$T_{crystal}$ [b]	T_m	$T_{crystal}$	T_m	$T_{crystal}$
0.0251	270.74	270.24	270.71	-	0.03	-	0.01	-
0.0496	267.35	267.10	267.66	267.55	0.31	0.45	0.12	0.17
0.0751	266.43	265.95	266.63	266.45	0.20	0.50	0.08	0.19
0.1415	266.64	266.15	-	266.35	-	0.20	-	0.07
0.2375	266.64	266.30	-	266.35	-	0.05	-	0.02
0.2593	266.30	265.72	-	266.35	-	0.63	-	0.24
0.2817	266.42	265.09	-	266.35	-	1.26	-	0.47
0.3031	266.39	265.45	266.46	266.25	0.07	0.80	0.03	0.30
0.3520	266.23	264.46	266.27	265.95	0.04	1.49	0.02	0.56
0.4061	265.39	263.85	265.73	265.25	0.34	1.40	0.13	0.53
0.4600	264.84	263.60	264.78	-	0.06	-	0.02	-
0.4961	263.95	262.91	263.89	-	0.06	-	0.02	-
0.5440	262.49	260.89	262.20	-	0.29	-	0.11	-
0.5891	259.93	257.96	260.05	-	0.12	-	0.05	-
Average					**0.15**	**0.75**	**0.06**	**0.28**

Ref - T_m [a] - Lohmann et al. (1997); $T_{crystal}$ [b] - Ochi et al. (1996)
$|\Delta T|/K = |T_{exp} - T_{ref}|$
Relative Error **%** $= [T_{ref} - T_{exp} / T_{ref}] \times 100$

5.4.4 Liquid-Liquid Equilibrium

The liquid-liquid equilibrium measurements were undertaken to illustrate the versatility of the apparatus. The camera installed enabled visual identification of the cloud point. The system measured was 2-butanol (1) + water (2). This system was measured by Ochi and co-workers as well as by Hefter et al. (1991). The binodal curve for this system was reported to have a narrow section at lower temperatures giving the curve an "Ω" shape. Previous experimental measurements on this system prior to Hefter and co-workers were unable to produce the binodal curve in that region. The results for the LLE measurements on the Peltier apparatus are shown in Figure 5-7 and Table 5-6.

Table 5-6: Experimental liquid-liquid equilibria temperatures for the 2-butanol (1) + water (2) system using the Peltier apparatus.

x_1	T/K
0.0540	295.89
0.0579	291.47
0.0598	288.73
0.0654	283.33
0.0715	280.41
0.0750	275.32
0.0752	277.15
0.2722	271.71
0.2734	281.73
0.2734	271.09
0.2814	284.90
0.2926	289.59
0.2994	291.59
0.3063	295.60

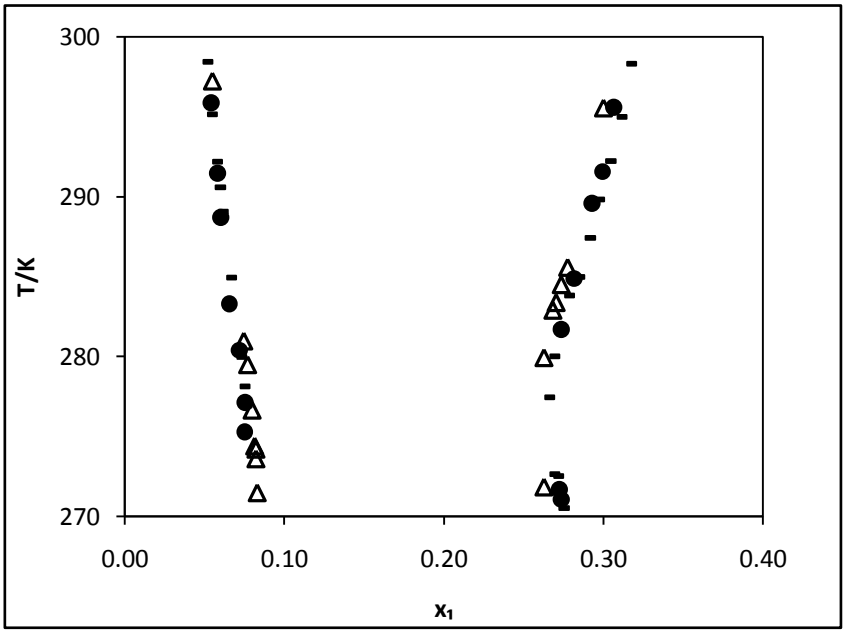

Figure 5-7: Liquid-liquid equilibria temperatures for the 2-butanol (1) + Water (2) system; ●, this work; - , Ochi et al. (1996); Δ, Hefter et al. (1991).

The experimental clear points (Figure 5-7) that have been measured in this work clearly show the distinction of the narrow region of the binodal curve. Compared to the experimental data of Hefter and co-workers, and Ochi and co-workers, the data measured in this work follows the same trend. Figure 5-7 indicates that the apparatus has the potential to produce reliable LLE data, particularly when measured in the cooling mode. The range of operation of the equipment is that it can be controlled to cool from room temperature (this is dependent on the environment) to a temperature of 253.15 K, whilst for heating, the apparatus can also be controlled to heat from ambient temperature to 373.15 K.

5.5 New Systems

Two new systems were measured in this work. These consist of n-alkyl carboxylic acid mixtures. Two binary mixtures have been investigated, heptanoic acid + butyric acid and heptanoic acid + hexanoic acid. Hexanoic acid has the lowest melting point followed by butyric acid and then heptanoic acid. Measurement of the phase data across the entire composition range was not performed using both apparati; instead melting points below 253.15 K were measured on the glass apparatus and those above 253.15 K were measured on the Peltier apparatus. The results obtained for both systems are presented in this section.

5.5.1 The Heptanoic Acid (1) + Butyric Acid (2) System

Table 5-7: Experimental solid-liquid equilibria temperatures for the heptanoic acid (1) + butyric acid (2) system.

	T/K	
x_1	**Peltier**	**Glass**
0.0000	268.64	-
0.0374	266.73	-
0.0764	263.68	-
0.1163	262.42	-
0.1587	258.52	-
0.1971	-	257.28
0.2401	-	255.48
0.2858	-	252.49
0.3282	-	250.09
0.3748	-	247.21
0.4225	-	243.53
0.4604	-	241.31
0.4743	-	242.31
0.5258	-	245.02
0.5777	-	248.32
0.6321	-	250.29
0.6882	-	254.19
0.7454	256.55	-
0.8270	259.51	-
0.8657	261.62	-
0.9271	264.00	-
1.0000	266.27	-

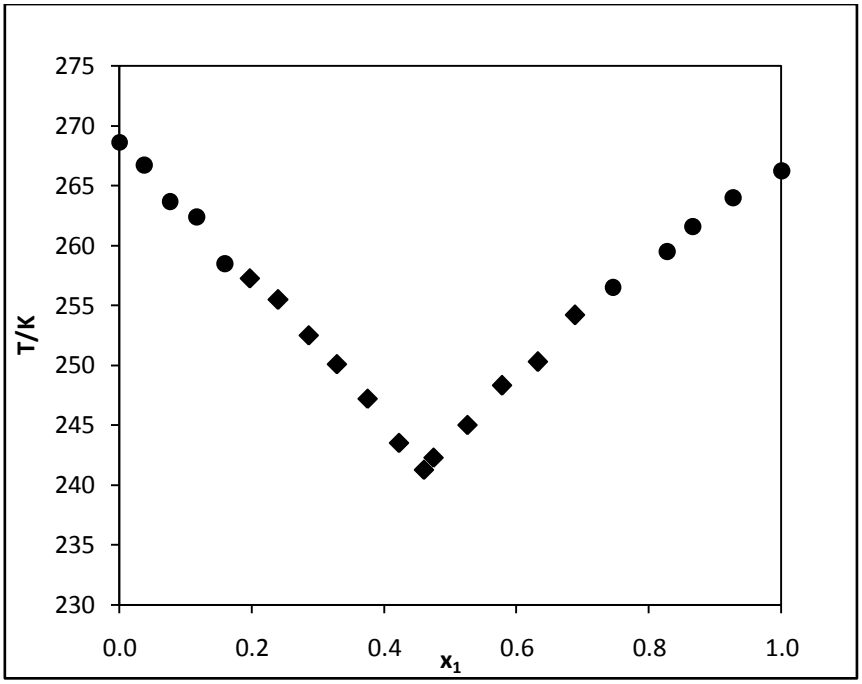

Figure 5-8: Solid-liquid equilibria temperatures for the heptanoic acid (1) + butyric acid (2) system: ●, this work (Peltier); ♦, this work (Glass).

5.5.2 The Heptanoic Acid (1) + Hexanoic Acid (2) System

Table 5-8: Experimental solid-liquid equilibria temperatures for the heptanoic acid (1) + hexanoic acid (2) system.

	T/K	
x_1	**Peltier**	**Glass**
0.0000	270.69	-
0.0501	267.64	-
0.1003	265.77	-
0.1502	263.87	-
0.2000	262.57	-
0.2500	259.25	-
0.3023	-	258.61
0.3569	-	256.33
0.4071	-	255.46
0.4497	-	255.07
0.5005	-	254.51
0.5505	-	254.94
0.5999	-	256.09
0.6506	-	257.91
0.6998	-	259.18
0.7509	259.79	-
0.8019	260.97	-
0.8521	262.84	-
0.8990	263.70	-
0.9464	264.60	-
1.0000	266.27	-

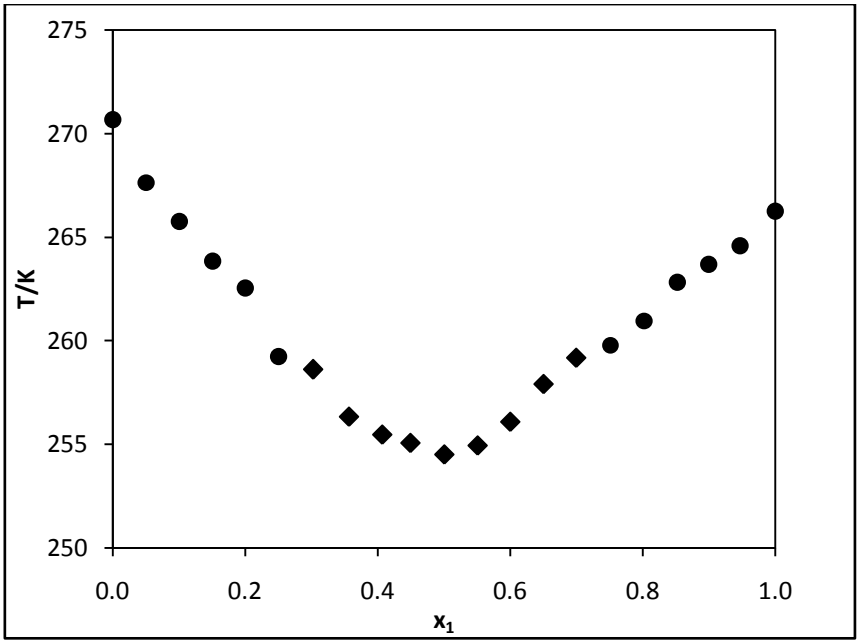

Figure 5-9: Solid-liquid equilibria temperatures for the heptanoic acid (1) + hexanoic acid (2) system: ●, this work (Peltier); ♦, this work (Glass).

5.4.3 Discussion of Results

Both systems measured exhibited eutectic behaviour and the eutectic temperatures and compositions measured are given in Table 5-9.

Table 5-9: Experimental eutectic temperatures and compositions for the measured binary acid mixtures.

Acid System	x_{eut}	T_{eut} /K
Heptanoic (1) + Butyric (2)	0.4606	241.31
Heptanoic (1) + Hexanoic (2)	0.5005	254.51

T_{eut} – eutectic temperature
x_{eut} - eutectic composition

In Figures 5-8 and 5-9 the points measured for both new systems have been presented on phase diagrams. The phase diagrams show eutectic behaviour, but there is a scatter in the points measured that is more significant in the heptanoic acid + hexanoic acid system. As previously mentioned, two different apparati were used to measure the points. An absolute temperature deviation between the apparati was reported previously as having been 0.14 K for the cyclohexane + hexadecane system. The deviation is not significant enough to result in a large scatter between the points measured by both apparati. However it can be observed that there is a temperature difference in the points

measured in the heptanoic acid (1) + hexanoic acid (2) system at the junction of the measurements by the two apparati ($0.3023 < x_1 < 0.6998$).

The scatter of the points could also have been affected by the accuracy of the temperature readings at lower temperatures. Both acid systems were measured at low temperatures from 273.15 K down to 240 K. According to Kynaston and Martin (1977) the viscosity of butyric acid is significantly lower than for hexanoic acid particularly at lower temperatures. This may have contributed to the scatter in points measured in the heptanoic + hexanoic acid phase diagram rather than with butyric acid.

In the heptanoic acid + hexanoic acid system there could have been a possibility of the existence of a peritectic point in the heptanoic acid rich branch of the phase diagram. According to literature, measurements on binary fatty acid mixtures may exhibit invariant points such as peritectic points (Costa et al., 2007). The temperature profile on the phase diagram of the heptanoic acid + hexanoic acid system resembles that of Costa and co-workers for the SLE binary system of capric acid + lauric acid (Figure 5-10).

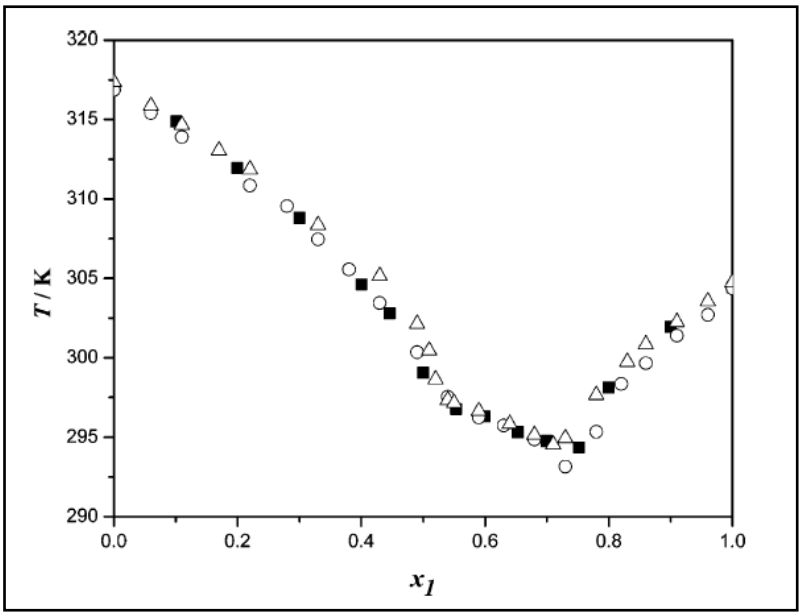

Figure 5-10: Phase diagram of binary system of Capric acid (1) + Lauric acid (2); ■, Costa et al. (2007); ○, Müller (1961); ∆, Grondall et al. (1944). Adapted from Costa et al. (2007).

Without x-ray diffraction techniques or differential methods of determining solid-liquid equilibria it is difficult to verify the presence of such a peritectic point (point at which the mixture forms an intermediate compound) within the system. According to Small (1986) cited by Costa et al. (2009), peritectic and eutectic points can both be exhibited in binary mixtures of fatty acids, where there is a carbon difference between the two acids that amounts to less than six carbons. In this same work and in previous work, Costa et al. (2007, 2009) also determined that peritectic points can also be exhibited

in binary mixtures where the carbon number difference between components is either two or four. Although this work was done for fatty acids, the properties of the fatty acids (above ten carbons) can be related to those of the saturated carboxylic acids because the behaviour of their crystal structures are similar. In his study of the carboxylic acids from C6 to C15, Bond (2004) found that the acids all solidify as dimers and that the crystals are made up of parallel chains of acids in the dimeric form. This determination is consistent with the conclusions for propionic, butyric and valeric acids, which is that they all solidify as dimers and that the crystal structure is composed of parallel dimeric chains (Strieter et al., 1962a, 1962b and Scheuerman et al., 1961). According to Larsson (1966) and later Bond (2004) the melting points of these acids which alternate between even and odd carbons was due to intermolecular attractions between layers in the crystal and alternating crystal density. All the n-alkyl carboxylic acids except for formic and acetic acid therefore exhibit similar behaviour which is only affected by the chain length on each acid.

5.5 Solid-Liquid Equilibria Modelling

5.5.1 Modelling Background

The theory for calculating solid-liquid equilibria was discussed in Chapter 2. For all systems measured in this work it was assumed that equilibrium was composed of a pure solid of either component in equilibrium with a liquid mixture. The activity coefficient of a pure solid is 1. The equation for solid-liquid equilibria for such conditions can be given as follows (Jakob et al., 1995),

$$\ln x_i^L \gamma_i^L = -\frac{\Delta H_{fus,i}}{RT}\left(1-\frac{T}{T_{m,i}}\right)-\frac{\Delta H_{trs,i}}{RT}\left(1-\frac{T}{T_{trs,i}}\right) \qquad 5\text{-}1$$

The subscripts m and t refer to melting and transition respectively. Transition refers to solid-solid transitions that occur after initial crystal formation and that are within the temperature range of the phase diagram. In this work solid-solid transitions are considered to be for pure components as it has been assumed that no solid solutions are formed.

The liquid phase activity coefficient can be calculated using the local composition models (g^E models). These models include the Wilson Model (1964), the NRTL (Non Random Two Liquid) (Renon and Prausnitz., 1968) and the UNIQUAC (Universal Quasi Activity Coefficient) model (Abrams and Prausnitz., 1975). The Wilson model has two adjustable parameters $\Lambda_{i,j}$ and $\Lambda_{j,i}$. These two parameters are energy interaction parameters between the two species and are dependent on temperature. However in most systems the temperature dependency has been found to be minimal (Prausnitz et al. 1999, Smith et al. 2001). The NRTL model also has two adjustable parameters $g_{i,j}$ and

$g_{j,i}$ which are also a measure of the energy interaction between the species in solution. A third parameter $\alpha_{i,j}$ is determined in the NRTL model. The parameter is a measure of the non-randomness of the system (Prausnitz et al., 1999 and Smith et al., 2001). It is adjustable but can be approximated to be constant. After numerous experimental measurements it was found that the value of the parameter may be approximated to be 0.3 (Prausnitz et al. 1999). The UNIQUAC model has two adjustable parameters which are $u_{i,j}$ and $u_{j,i}$, these are also energy interaction parameters (Prausnitz et al., 1999 and Smith et al., 2001). The parameters for all three models were regressed iteratively by fitting each model to the experimental data.

The software used to regress the parameters is the Dortmund Data Bank Recval3 (2009). The iteration began with the physical properties of each component (Appendix D), the experimental temperature, and composition. A thermodynamic model was used to calculate the activity coefficient of the liquid whilst that of the solid was assumed to be 1. Initial guesses for the parameters were required to begin the iteration. However these were available by default in the software used. The option to use previous parameters stored in the software as initial guesses, for the same system was available.

A new solid-liquid equilibria temperature (T_{calc}) was subsequently calculated using the activity coefficient from the thermodynamic model. T_{calc} was calculated using the following equation:

$$T_{calc} = - \frac{dH_{fus,i} + \sum_{j=1}^{H_{trs,i}} dH_{trs,i}}{R\ln x_{i,expt}\gamma_i^L - \frac{dH_{fus,i}}{T_{m,i}} - \sum_{j=1}^{htr_i} \frac{dH_{trs,ij}}{T_{trs,ij}}} \qquad 5\text{-}2$$

The Simplex Nelder-Mead algorithm was used to fit the parameters in each model by minimising an objective function. The objective function used in the software is given in Equation 5-3.

$$OF = \left(T_{exp} - T_{calc}\right)^2 \qquad 5\text{-}3$$

The convergence criterion/tolerance was 0.10E-11. If the value of the objective function was above the specified tolerance then the iteration continued but if the objective function was less than the tolerance then the software output the model parameters and the calculated temperature, T_{calc}. The composition remained the same as the experimental value. This process has been summarised as a block flow diagram in Figure 5-11.

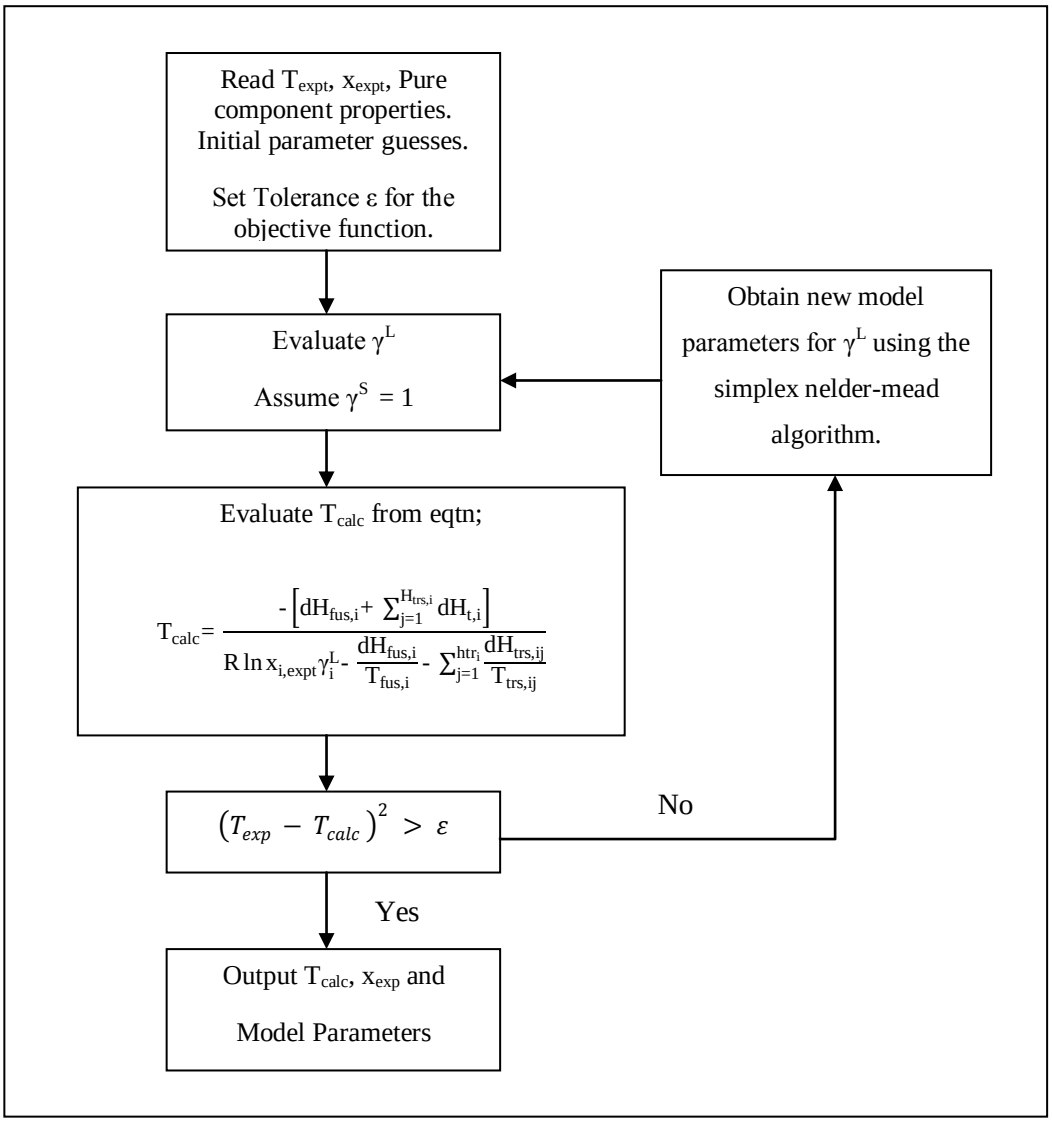

Figure 5-11: Block diagram of the solid-liquid Equilibria modelling algorithm, adapted from Dortmund Data Bank Software Manual (Dortmund Data Bank Recval3, 2009).

5.5.2 Modelling Results

Results of the modelling of the measured data for all systems using the local composition models are reported graphically in the following figures.

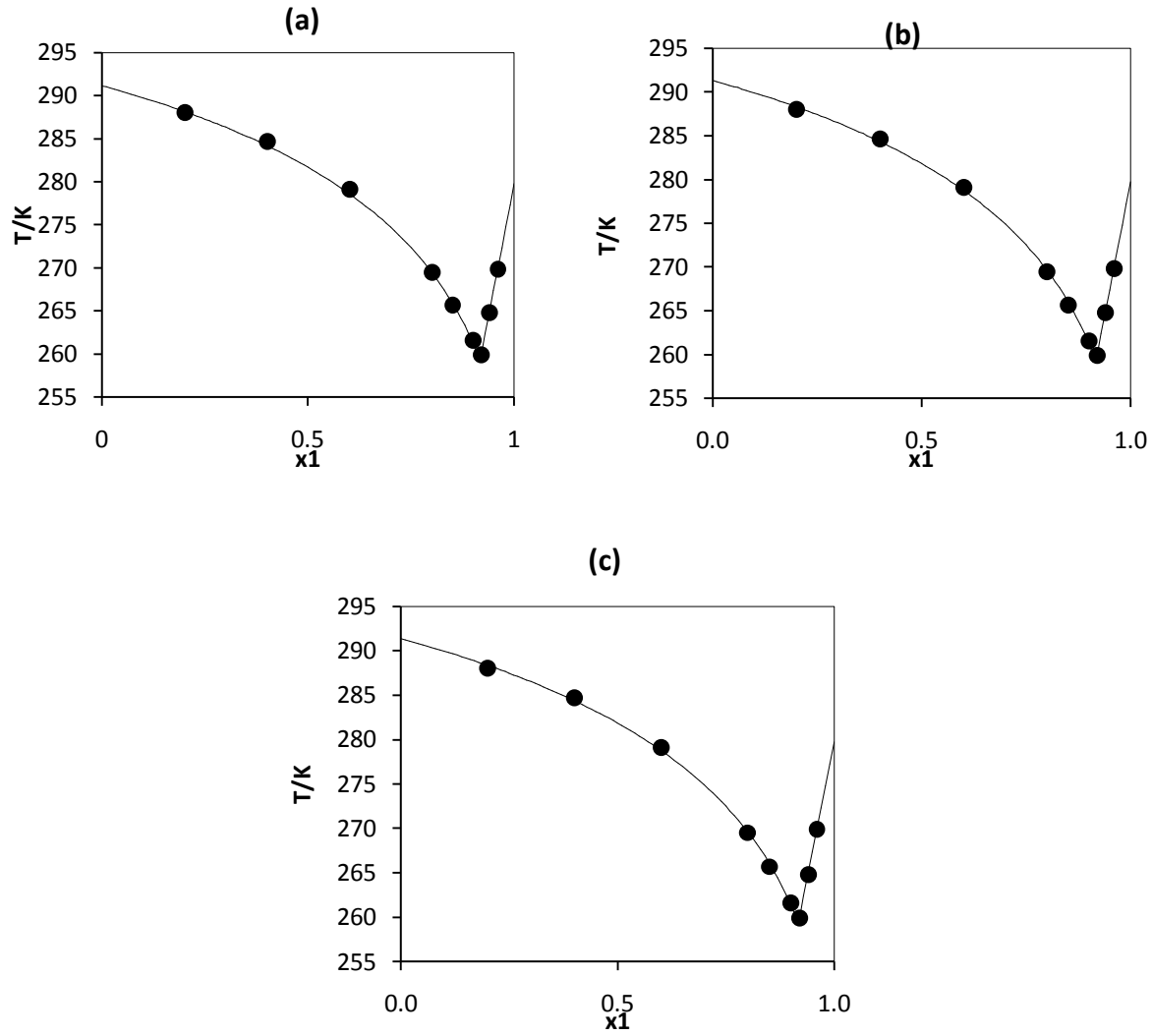

Figure 5-12: T-x plot for the solid-liquid equilibria data for the cyclohexane (1) + hexadecane (2) system. (a), Wilson model; (b), NRTL model; (c) , UNIQUAC model; ●, this work (Peltier); —, model.

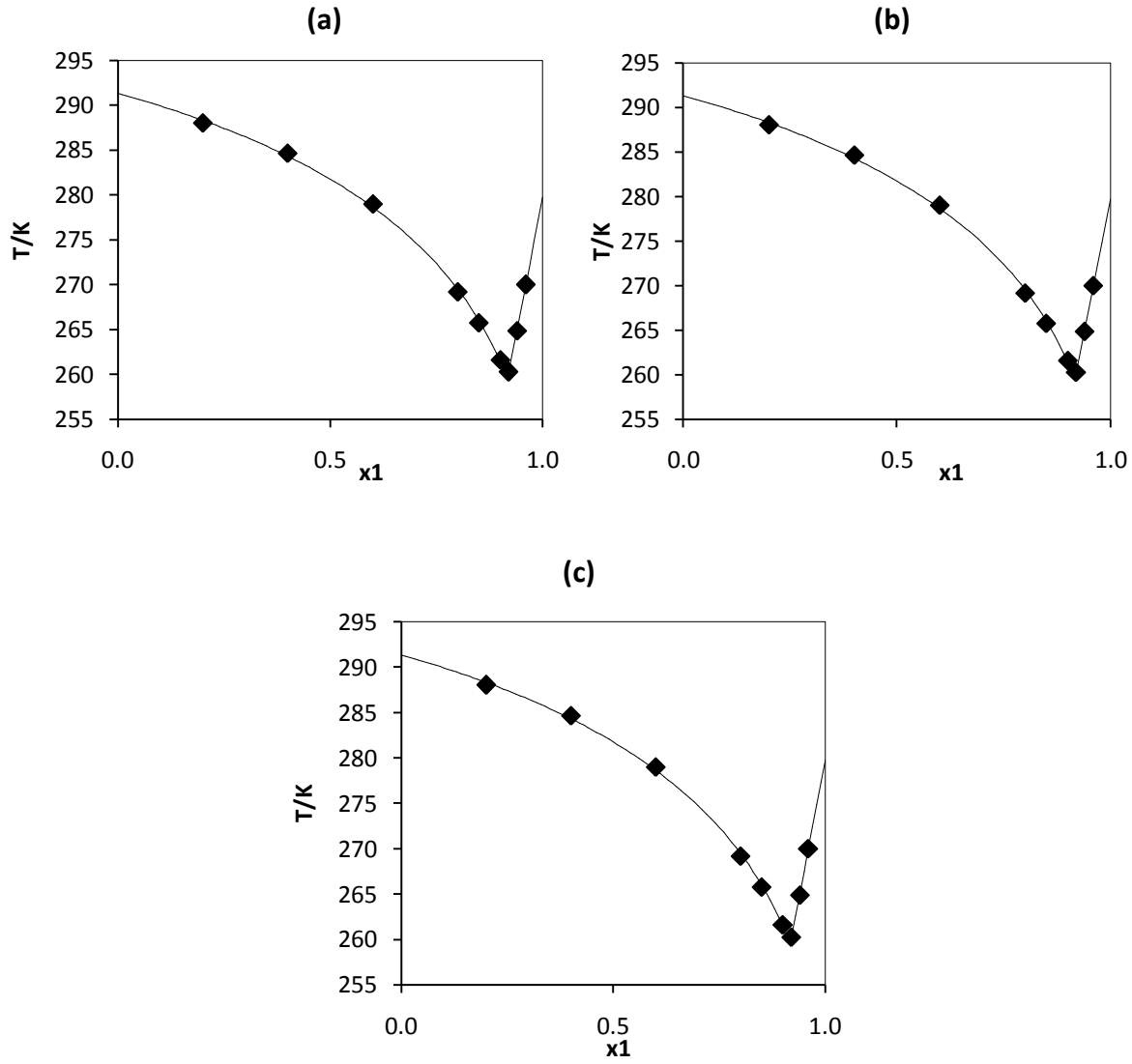

Figure 5-13: T-x plot for the solid-liquid equilibria data for the cyclohexane (1) + hexadecane (2): (a), Wilson model; (b), NRTL model; (c), UNIQUAC model; ♦, this Work (Glass); —, model.

All the models were able to fit the data measured on both apparati with high accuracy for the cyclohexane + hexadecane system. The best fit is observed in the region of the eutectic. This can be seen from Figures 5-12 and 5-13. The accuracy of the fit by the models is likely to be as a result of the cyclohexane + hexadecane system being a simple eutectic system. From the values of the activity coefficients calculated using the models it was seen that the system was almost ideal. The activity coefficients calculated by the models were almost equal to 1.

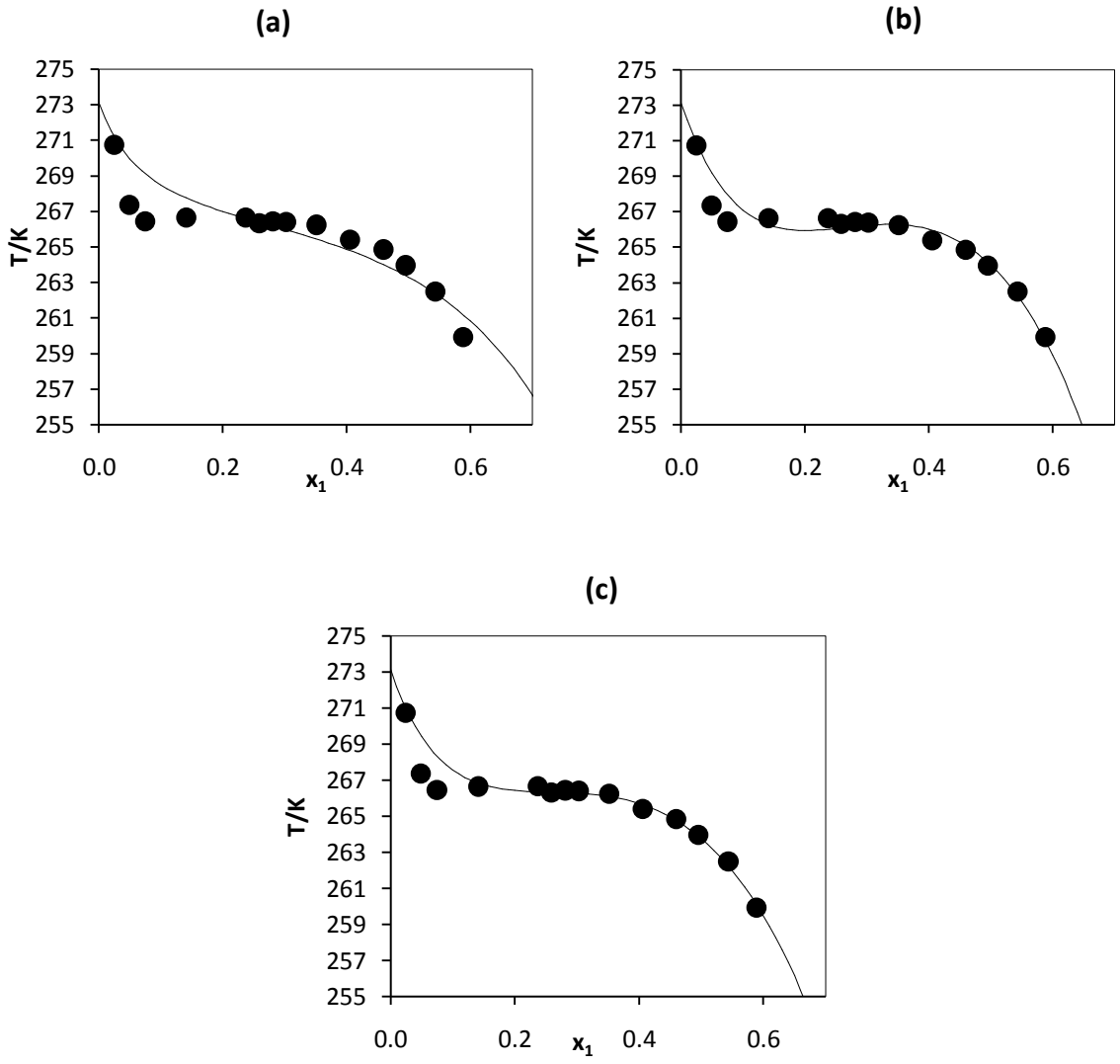

Figure 5-14: T-x plot for the solid-liquid equilibria data for 2-butanol (1) + water (2): (a), Wilson model; (b), NRTL model; (c), UNIQUAC model; ●, this work (Peltier); —, model.

For the 2-butanol-water system (refer to Figure 5-14), the Wilson equation was not able to model the data accurately. For the system, the Wilson model showed greater deviation in the region close to immiscibility. According to Prausnitz et al. (1999) the Wilson model is best suited for fitting data which is completely miscible or in regions that have complete miscibility. Conversely, the UNIQUAC and NRTL models both gave acceptable results according to the plots. The two points located directly before the immiscibility region, were found to fall outside of the fit for all the models. From Table 5-5 these two points were found to deviate from literature by as much as 0.31 K due to the proximity of the points to the immiscibility region. There is therefore a possibility of error in their temperature measurement resulting from the viscosity of the mixture as discussed previously in section 5.4.3. Overall, the UNIQUAC equation gives a more accurate fit for the data than the NRTL equation, because it was able to fit more points in the system, referring to Figure 5-14.

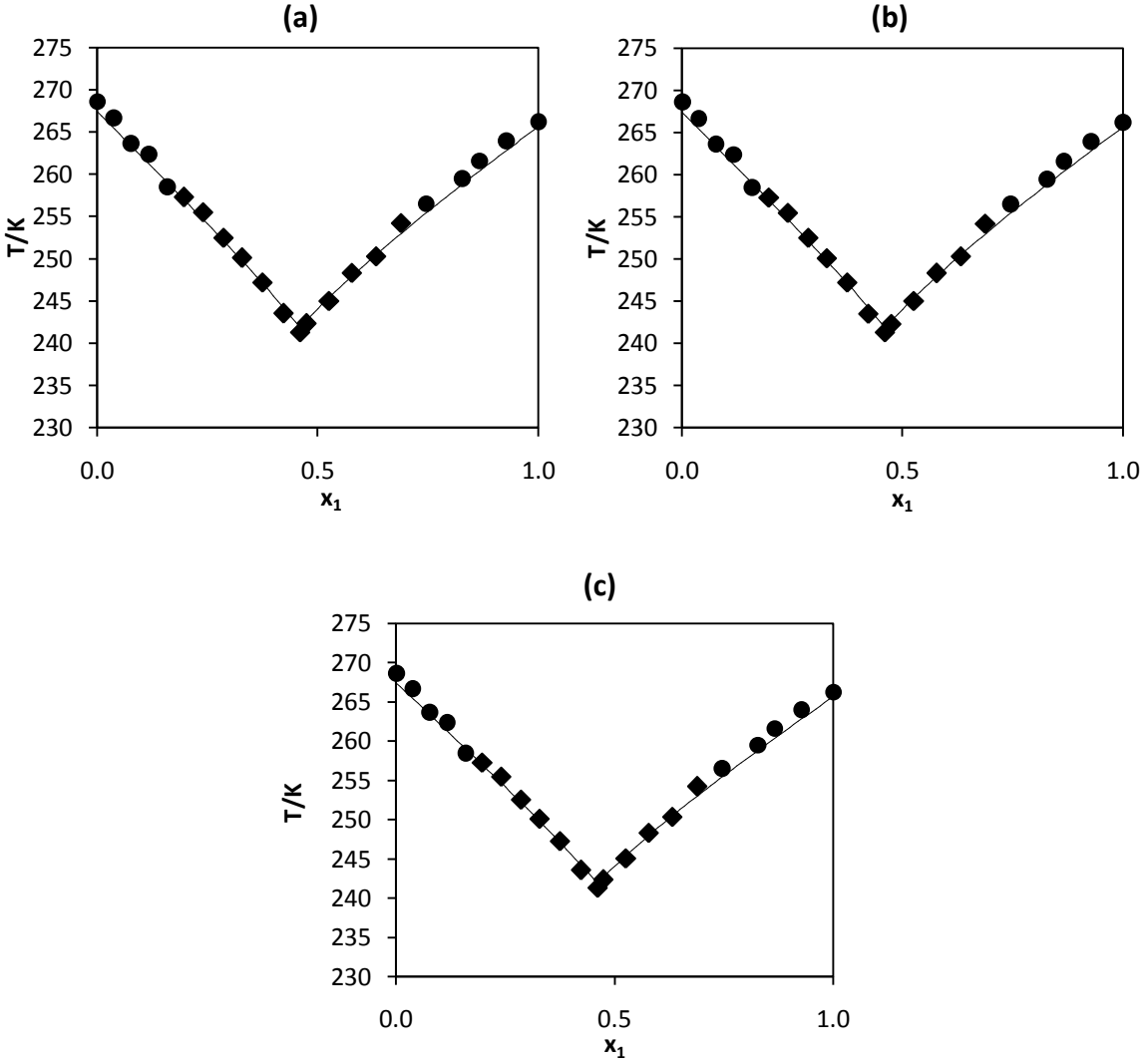

Figure 5-15: T-x plot for solid-liquid equilibria data for heptanoic acid (1) + butyric acid (2): (a), Wilson model; (b), NRTL model; (c), UNIQUAC model; ♦, this work (Glass) and ●, this work (Peltier); —, model.

From Figure 5-15 all the models follow the trend of the data. The plots also showed lower calculated values for the temperatures above 255 K, and a closer fit for the lower temperatures on the phase diagram from 255 K to the eutectic temperature. Resultantly this shows a better fit for points measured on the Glass apparatus.

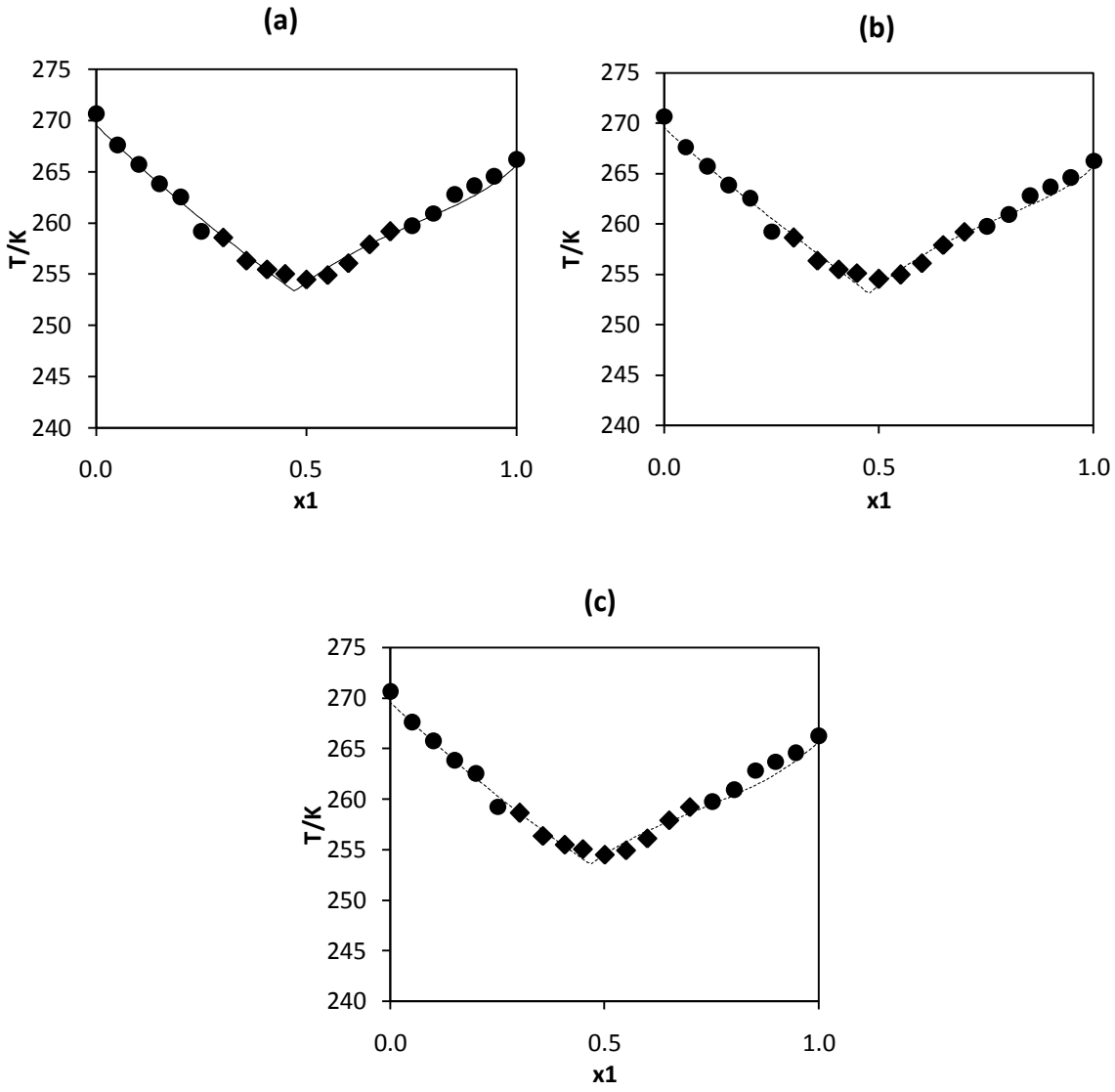

Figure 5-16: T-x plot for the Heptanoic acid (1) + Hexanoic acid (2): (a), Wilson model; (b), NRTL model; (c), UNIQUAC model; ♦, this work (Glass); ●, this work (Peltier); —, model.

Figure 5-16 shows that the models were able to fit the hexanoic acid rich branch as compared to the heptanoic acid rich branch. A wide scatter is seen on the heptanoic acid branch for all the models with the models showing a slight inflection at the point where the points measured by both apparati meet (T = 258 K). In addition the models indicate a lower eutectic temperature than the one measured in this work. This is acceptable because the eutectic temperature measured is based on the composition interval used in measuring the points on the phase diagram. The models may be used to extrapolate a true equilibrium temperature.

Table 5-10: Calculated and measured eutectic temperatures and compositions for the systems investigated.

	x_{eut}		T_{eut}/K	
System	**Exp**	**Cal**	**Exp**	**Cal**
Cyclohexane (1) + Hexadecane (2)	0.9200[a]	0.9168[c]	259.94[a]	259.16[c]
		0.9168[d]		259.23[d]
		0.9173[e]		259.26[e]
	0.9200[b]	0.9165[c]	260.29[a]	259.40[c]
		0.9167[d]		259.26[d]
		0.9166[e]		259.40[e]
Heptanoic Acid (1) + Butyric Acid (2)	0.4604[a,b]	0.4597[c]	241.31[a,b]	241.88[c]
		0.4600[d]		241.88[d]
		0.4596[e]		241.88[e]
Heptanoic Acid (1) + Hexanoic Acid (2)	0.5005[a,b]	0.4727[c]	254.51[a,b]	253.33[c]
		0.4771[d]		253.06[d]
		0.4675[e]		253.56[e]

T_{eut} – Eutectic temperature and x_{eut} is the eutectic composition
[a] Peltier, [b] Glass, [c] Wilson Model, [d] NRTL Model, [e] UNIQUAC Model

From Table 5-10 the calculated eutectic temperatures from all models deviated by less than 1 K and the compositions to 2 decimal points were the same values for the cyclohexane + hexadecane system. For the heptanoic acid + hexanoic acid system however, the eutectic temperature that has been calculated from the models showed the eutectic temperature to have occurred at a lower temperature than measured experimentally. The deviation between the measured eutectic for the heptanoic + hexanoic acid system and the calculated value is larger than for all the other eutectic temperatures and compositions. As discussed previously the difference is as a result of the choice of experimental compositions to measure.

Table 5-11: Comparison between model results and experimental data.

System	N	Wilson AAD	Wilson RMSD	NRTL AAD	NRTL RMSD	UNIQUAC AAD	UNIQUAC RMSD
Cyclohexane (1) + Hexadecane (2)	9[a]	0.21	0.54	0.22	0.57	0.21	0.53
Cyclohexane (1) + Hexadecane (2	9[b]	0.23	0.61	0.27	0.72	0.23	0.61
2-Butanol (1) + Water (2	14[a]	0.46	1.61	0.23	0.60	0.11	0.35
Heptanoic acid(1) + Butyric acid (2)	22[a,b]	0.62	2.18	0.61	2.16	0.62	2.18
Heptanoic acid(1) + Hexanoic acid (2)	21[a,b]	0.52	1.40	0.49	1.27	0.60	1.98

[a] Peltier,
[b] Glass

$AAD = \sum (|T_{exp}-T_{calc}|)/N$

$RMSD = \sqrt{(1/N)\sum_N (T_{exp}-T_{calc})^2}$

N ≡ number of points

Table 5-11 shows that the best fit, based on the average absolute deviations and the root mean square deviations, for the cyclohexane + hexadecane system was given by the Wilson and the UNIQUAC models, for both apparati. The UNIQUAC and the Wilson model gave the same results but the best results for both models were obtained from the Peltier apparatus than from the Glass according to the graphs. In the 2-butanol + water the UNIQUAC model was found to give the best results with average absolute deviations of 0.11 K and the NRTL giving deviations of 0.23 K. From these results the UNIQUAC model gave the best results as indicated from Figure 5-16.

The best fit for the new systems was given by the NRTL model. The values of the deviations between the calculated temperatures and the experimental temperatures may be attributed to dimerisation within the solid-phase, which exists for acids (Bond, 2004). This means that although solid phase non-idealities were neglected in the modelling they are existent. In addition dimerisation in the liquid phase (Bond, 2004) was also not accounted for. Based on the activity coefficients calculated for each model the systems had large positive deviations from ideality. The parameters for each of these models have been presented in Table 5-12. All the parameters were output in calories per mol from the software and are reported as such. The parameter $\alpha_{i,j}$ for the NRTL model was regressed and not kept constant. These parameters may be used for predictions in future work. The parameters are also useful for design problems in simulators for eutectic freeze crystallisation.

Table 5-12: Model parameters for the solid liquid equilibria data regression for all systems using the Wilson, NRTL and UNIQUAC models.

System	Wilson (cal/mol)		NRTL (cal/mol)			UNIQUAC (cal/mol)	
	Λ_{12}	Λ_{21}	α_{12}	Δg_{12}	Δg_{21}	Δu_{12}	Δu_{21}
Cyclohexane (1) + Hexadecane (2)	159.39	-167.75	0.30	387.74	-426.39	-65.22	97.90
Cyclohexane (1) +Hexadecane (2)	18.96	176.35	0.30	112.20	-232.36	41.81	-15.06
2-Butanol (1) + Water (2)	498.95	1512.97	0.30	105.72	1343.26	570.12	-73.64
Heptanoic acid(1) + Butyric acid.(2)	-44.61	248.72	0.70	58.62	149.77	160.11	-83.78
Heptanoic acid(1) + Hexanoic acid (2)	60.27	876.62	0.70	757.41	273.02	397.94	-165.99

Chapter 6

Conclusions

In this work two new apparati which utilise the synthetic method, have been constructed for measurement of both solid-liquid and liquid-liquid equilibria. A method has also been developed which allows the experimenter to identify the phase transition temperature for solid-liquid equilibria, through analysis of the melting curve. This method determines the SLE point from analysis of the melting curve, by calculating the gradient of the curve at a point and comparing the gradients to distinguish the phase change temperature. This method has been successfully applied to both apparati, and accurate results have been generated from both apparati for SLE data.

The first apparatus is a design that uses Peltier modules for cooling and heating. The modules are small and compact and therefore the apparatus is also a compact apparatus. It also has a small volume, which means that there are savings that can be realised on chemical costs. The uncertainty on the temperature measurement of this apparatus has been found to be ± 0.03 K. Despite a relativity high minimum temperature limit for a solid-liquid apparatus due to the cooling system, the apparatus was found to have good accuracy. Measurements made on the apparatus were compared to two binary test systems measured in literature. It was found that the absolute average deviation of this apparatus with literature values for the cyclohexane + hexadecane system was 0.08 K and with the 2-butanol + water system it was 0.15 K.

The second apparatus which is the Glass apparatus is a large volume apparatus that uses a more common technique for temperature control used in SLE and LLE apparati. This is circulation of a cooling or heating fluid in a jacket surrounding the equilibrium cell. The apparatus unlike the Peltier apparatus is able to operate at very low temperatures down to 223.15 K. The apparatus can therefore be used to measure very low melting points. This apparatus has also successfully reproduced known literature data for SLE to within absolute average deviation with literature data of 0.12 K for the cyclohexane + hexadecane system using the same method of analysis. The uncertainty on all composition measurements was calculated to be ± 0.00003 mole fraction from mass measurements, for both of the apparati.

A demonstration of the apparati's versatility has been shown by measurement of liquid-liquid equilibria cloud points for the 2-butanol + water system on the Peltier apparatus. These cloud points have been detected using a digital camera with a frame rate set to the temperature log rate, thereby allowing for precise determination of the appearance or disappearance of turbidity within the sample.

Modelling of the test systems was successfully done using the local composition models. Each system was modelled with all three models (Wilson (1964), NRTL (1968) and UNIQUAC (1975)) and it was found that the UNIQUAC model gave the overall best results for the cyclohexane + hexadecane and the 2-butanol+water test systems. From these results, different model parameters for each of the systems have been made available.

Not only have the two apparati been tested by measurement of known systems, but based on the reliability of these results these apparati have been used to generate new solid-liquid equilibria data for two binary carboxylic acid mixtures. The data has also been successfully modeled using the local composition models. The calculated deviations indicated that the NRTL model gave the best fit for the results with an average absolute deviation of 0.61 K for the heptanoic acid + hexanoic acid system and 0.49 K for the heptanoic acid + hexanoic acid system. From the measurement of these systems phase equilibria data which can be used for simulation of crystallization process and or which can be used for design purposes is made available. From the modeling of the results it can be concluded that the local composition models can be sufficiently applied to modeling of n-alkyl carboxylic acid mixtures and with these parameters it can be possible to predict the phase equilibria of similar systems.

Chapter 7

Recommendations

For the equipment it is recommended that the Peltier apparatus be used to measure systems of higher melting points than the limit of the apparatus. This will reduce errors in the determination of solid liquid equilibria for a system measured with two different apparati. When using the Peltier apparatus, extra attention concerning the external environment in which the Peltier apparatus operates, should be noted. The temperature gradient between the heat sink and the ambient temperature of the room was found to have a large effect on the minimum temperatures obtained by the apparatus. A room which is maintained at lower temperatures is best suited for the apparatus.

In order to achieve lower temperatures on the Peltier apparatus a more powerful heat dissipation system is required. A heat sink with much lower thermal conductivity may be used or a heat exchange system may be designed for the hot side of the Peltier modules.

For future developments on this apparatus it can be recommended that the software be upgraded to become fully automated. The current software works efficiently, however it is laborious to operate and this can be avoided by having a feedback control program written which will enable the software to determine parameters independently.

With the glass equipment it would be recommended that the inlet of the cryogenic fluid into the thermostat be moved to the bottom of the thermostat, to eliminate any fluid by-passing within the vessel. This avoids non-uniformity of the temperature profile of the thermostat.

For liquid-liquid equilibria measurements on both apparati it is recommended that the systems measured be systems that show distinct turbidity of the sample in the immiscibility gap. This is because the resolution in the camera is not good enough to detect small immiscibility bubbles. It is advised that if the system does not cloud then the apparati not be used to measure the LLE.

In order to achieve lower temperatures with the Glass apparatus a reliable low temperature chilling unit may be used. Otherwise an alternative means would be to design an effective low temperature heat exchange system for the bath liquid which uses a cryogenic liquid such as liquid nitrogen or a cryogenic substance such as dry ice. Dry ice was tried but was not effective due to insufficient time allowed for heat exchange and insufficient heat transfer area.

For the analysis procedure of data obtained from both apparati, the data points were found to be too many for analysis. The procedure could be improved by averaging a larger amount of data points (temperature readings) to reduce the volume of data to be analysed during analysis than the number which was being used (180 data points) which was being used.

Following on from the new systems measured the systems to be investigated as a follow on to the project are:

- Propanoic acid + (butyric acid, hexanoic acid, heptanoic acid).
- Butyric acid + (isobutyric acid, hexanoic acid).
- Hexanoic acid + (isobutyric acid, pentanoic acid).
- Heptanoic acid + (isobutyric acid, pentanoic acid).

According to the review in Table 1-1, these systems are the binary carboxylic acid mixtures that are yet to be measured for SLE. The data has thermodynamic significance in the design of separation processes such as crystallisation and will contribute to the flexibility and temperature dependency of thermodynamic model parameters. The above mentioned systems could not be accommodated due to equipment failure; the VLT unit stopped working hence it was not possible to cool to low temperatures (below 240.15 K).

The activity coefficient models were sufficient for modelling the systems. However for the acid systems, if a peritectic point is suspected or determined then the modelling results can be improved by considering the solid phase non-idealities. An example is the procedure adopted for modelling solid phase non-idealities in fatty acids, by Costa et al. (2007) from Slaughter and Doherty, (1995).

Chapter 8

References

Arce E, Earke M. J, Katdare S.P, Rodriguez H, Seddon K.R, Phase equilibria of mixtures of mutually immiscible ionic liquids, Fluid Phase Equilibria, 261 (2007) 427 – 433.

Abrams D.S, Prausnitz J.M, Statistical thermodynamics of liquid mixtures: A new expression for the excess Gibbs energy of partly or completely miscible systems, American Institute of Chemical Engineers Journal, 21 (1975) 116 – 128.

Abrman P, Malijevska I, Solid-liquid equilibria in the acetic acid-propanoic acid and propanoic acid – triflouro-acetic acid, acid systems, Fluid phase equilibria, 166 (1999) 47 – 52.

Aston J.G, Szasz G.J., Fink H.L., The heat capacity and entropy, heats of transition, fusion and vaporization and the vapour pressures of Cyclohexane. The vibrational frequencies of alicyclic ring systems. Journal of the American Chemical Society, 65 (1943) 1135 – 1139.

Bégué J.P, Bonnet-Delpon D, Recent advances (1995 – 2005) in fluorinated pharmaceuticals based on natural products, Journal of Fluorine Chemistry, 127 (2006) 992 – 1012.

Bond A.D, On the crystal structures and melting point alternation of the n-alkyl carboxylic acids, New Journal of Chemistry, 28 (2004) 104 – 114.

Clifford S.L, Low-Pressure vapour liquid equilibrium and molecular simulation of carboxylic acids, Master of Science in Engineering (Chemical Engineering) thesis, University of KwaZulu Natal, South Africa, (2004).

Costa M C, Rolemberg M.P, Boros L.A.D, Krahenbuhl M.A, de Olivieira M.G, Meirelles A.J.A, Solid-liquid equilibrium of binary fatty acid mixtures, Journal of Chemical and Engineering Data, 52 (2007), 50 -56.

Costa M.C, Sordo M, Rolemberg M.P, Coutinho J.A.P, Meirelles R.P, Krahenbuhl M.A, The solid-liquid phase diagrams of binary mixtures of consecutive even fatty acids, Chemistry and Physics of Lipids 160 (2009) 85-97.

Coutinho J A P, Ruffier-Meray V, A new method for measuring solid-liquid equilibrium phase diagrams using calorimetry, Fluid Phase Equilibria, 148 (1998) 147-180.

Coutinho J.A.P, Stenby E.H, Predictive local composition models for solid-liquid equilibrium in n-Alkane systems: Wilson equation for multi-component systems, Industrial and Engineering Chemistry Research, 35 (1996) 918 – 925.

Cvahte M, Strnad J, A thermoelectric experiment in support of the second law, European Journal of Physics, 9 (1998) 11-17.

Di Nicola G, Santori G, Stryjek R Solid liquid equilibrium for the carbon dioxide + 1,1-tetrafluoroethane and nitrous oxide + 1,1-tetraflouroethane systems, Journal of Chemical Engineering Data, 8 (2008) 53.

Domanska U, Vapour-Liquid-Solid Equilibrium of eicosanoic acid in one – and two component solvents, Fluid Phase Equilibria, 26 (1986) 201 – 220.

Domanska U, Kniaz K, Solid-liquid equilibria in some normal alkanes (C16, C22, C28) + 2 – methylpentane, + 3 – methylpentane, + 2,2 – dimethylbutane, or + cyclohexane, International Data Series Selected Data on Mixtures, Series A, 3 (1990) 194 – 206.

Domanska U, Measurement and correlation of the solubility of 1-alkanols (C14, C16) in n-alkanes (C7 – C16), Fluid Phase Equilibria, 114 (1996) 175-178.

Domanska U, Lachwa J, Solid-liquid phase equilibria of binary mixtures containing N-methyl-2-pyrrolidone and long chain n-alkanols at atmospheric pressure, Fluid Phase Equilibria 198 (2002) 1-14.

Dortmund Data Bank (DDB) version 2009, DDBST Software and Separation Technology GmbH, Oldenburg, Germany.

Erkey C, Rodden J.B, Matthews M.A, Akgerman A, Application of rough hard-sphere theory to diffusion in n-alkanes, International Journal of Thermophysics, 10 (1989) 953 – 962.

Fridrihsberg D.A, (translated by Leib G), A course in colloid chemistry, Leningrad, Mir Publishers Moscow, (1986).

Gimzewski E and Audley G, Monitoring wax crystallisation in diesel using differential scanning calorimetry (DSC) and microcalorimetry, Thermochimica Acta, 214 (1993) 149 – 155.

Goates J.R., Ott J.B., Moeller J.F., Farrell D.W., (Solid + Liquid) phase equilibria in n-hexane + cyclohexane and benzene + cyclohexane, Journal of Chemical Thermodynamics, 11 (1979) 709 – 711.

Goff M.J, Suppes G.J, Dasari M.A., Interpreting freezing point depression of stearic acid and methyl stearate, Fluid Phase Equilibria, 238 (2005) 149 – 156.

Grondal B.J, Rogers D.A, Melting points of binary fatty acid mixtures C_6 to C_{12} and their application in the determination of Purity, Oil Soap, 21 (1944) 303 – 305.

Hammammi A, Ratulowski J, Coutinho J.A.P, Cloud Points: Can we measure or model them? Petroleum Science and Technology, 21 (2003) 345 – 358.

Haruki M, Iwai Y, Nagao S, Arai Y, Measurement and correlation of liquid-liquid equilibria for water + aromatic hydrocarbon binary systems at high temperatures and pressures, Journal of Chemical and Engineering Data, 46 (2001) 950 – 953.

Haruki M, Iwai Y, Nagao S, Yahiro Y, Airai Y, Measurement and correlation of phase equilibria for water+ hydrocarbon systems near the critical temperature and pressure of water, Industrial and Engineering Chemistry Research, 39 (2000) 4516 – 4520.

Hefter G.T, Barton A.F.M, Chand A, Semi-Automated apparatus for the determination of liquid solubilities: mutual solubilities of water and butan-2-ol, Journal of the Chemical Society, Faraday Transactions, 87 (1991) 591-596.

Hohne G.W.H., Hemminger W.F, Flammerseim H.J, Differential Scanning Calorimetry, Springer (2003) 9-10, 230-231.

Huang T.C, Kang B.C, Naphthalene hydrogenation over Pt/Al_2O_3 catalyst in a trickle bed reactor, Industrial & Engineering Chemistry Research, 34 (1995) 2349 – 2357.

Iwarere S.A, Measurement of phase equilibria for oxygenated hydrocarbon systems, Master of Science in Engineering (Chemical Engineering), University of KwaZulu Natal, South Africa, (2009)

Jakob A, Joh R, Rose C, Gmehling J, Solid liquid equilibria in binary mixtures of organic compounds, Fluid Phase Equilibria 113 (1995) 117-126.

Kirk K.L, Fluorine in medicinal chemistry: Recent therapeutic applications of fluorinated small molecules, Journal of Fluorine Chemistry, 127 (2006) 1013 – 1029.

Knauth P, Sabbah R.J., Development and applications of a low temperature differential thermal analyzer (77<T, K< 330), Journal of Thermal Analysis and Calorimetry, 36 (1990) 969 – 977.

Kurosawa I, Solid Liquid equilibrium in multi-solute systems, PhD thesis Georgia Institute of Technology, United States of America (2004).

Kynaston W, Martin J.F, Thermal conductivity and viscosity of normal $C_2 – C_6$ aliphatic carboxylic acids, Journal of Applied Chemistry and Biotechnology, 27 (1977) 296 – 302.

Larsson K, Alternation of melting points in homologous series of long-chain compounds, Journal of the American Oil Chemists Society, 43 (1996) 559 – 562.

Lazzaroni M.J, Bush D, Jones R, Hallet J.P, Liotta C.L, Eckert C.A, High pressure phase equilibria of some carbon dioxide – organic – water systems, Fluid Phase Equilibria, 224 (2004) 143 – 154

Lobbia G., Berchiesi G, Vitali G, Crystallisation curve of hexadecane in mixtures with methyl nonadecanoate, methyl octadecanoate, ethyl octadecanoate andmethyl hexadecanoate. A comparison of the experimental and calculated curves, Thermochimica Acta, 65 (1983) 29 - 33

Lohmann J, Joh R, and Gmehling J, Solid-liquid equilibria of viscous binary mixtures with alcohols, Journal of Chemical Engineering Data, 42 (1997) 1170-1175.

Lohmann J, Joh R, Gmehling J, From UNIFAC to Modified UNIFAC (Dortmund), Industrial & Engineering Chemistry Research, 40 (2001) 957 – 964.

Marsh K.N, Boxall J.A, Lichtenhaler R, Room temperature ionic liquids and their mixtures – A review, Fluid Phase Equilibria, 219 (2004) 93 – 98.

Matsuoka M, Garside J, Davey R.J, Jones A, Advances in industrial crystallisation, Butterworth Henemann Ltd, (1991) 229

Mohan R, Lorenz H, Myerson A, Solubility measurement using differential scanning calorimetry, Industrial & Engineering Chemistry Research, 41 (2002) 4854-4862.

Müller E, Stage H, Experimental determination of vapour-liquid-phase equilibria, Springer-Verlag, (1961).

Müller K, Christoph F, Diedrich F, Fluorine in pharmaceuticals: Looking beyond intuition, Science, 317 (2007) 1881.

Ndlovu M, Development of a dynamic still for measuring low pressure vapour-liquid equilibria (systems of partial liquid miscibility), Master of Science in engineering (Chemical Engineering), University of KwaZulu Natal, South Africa, (2005).

Novak J P, Matous J, Pick J, Studies in Thermodynamics 7, Liquid-liquid equilibria, Elsevier, (1987) 68 – 71.

Nyvlt J, Solid Liquid Phase Equilibria, Elsevier (1977).

Ochi K, Momose M, Kojima K, Lu B.C.Y, Determination of mutual solubilities in aniline + n-hexane and furfural + cyclohexane systems by a laser scattering technique, Canadian Journal of Chemical and Engineering Data, 73 (1993) 982-985.

Ochi K., SaitoT., Kojima K., Measurement and correlation of solubilities in 2-butanol+water, Journal of Chemical and Engineering Data, 41 (1996) 361 – 364.

Poole C.F, Poole S.K, Extraction of organic compounds with room temperature ionic liquids, Journal of Chromatography A, 1217 (2010) 2268 – 2286.

Prausnitz J M, Lichtenhaler R N, de Azevedo E G, Molecular thermodynamics of fluid phase equilibria 3rd edition, prentice Hall PTR (1999).

Provost E, Chevallier V, Bouroukba M, Petitjean D and Dirand M, Solubility of some n-alkanes (C-23 ,C25 ,C26 ,C28) in heptane, methylcyclohexane and toluene, Journal of Chemical and Engineering Data, 43 (1998) 745 – 749.

Qingzhu J, Peisheng M.A, Shaona M.A, Chang W, Solid-liquid equilibria of benzoic acid derivatives in 1-octanol, Chinese Journal of Chemical Engineering, 15 (2007) 710 – 714.

Raal J.D, Muhlbauer A.L, Phase Equilibria: Measurement and Computation, Taylor and Francis, (1998).

Renon H , Prausnitz J.M, Local compositions in thermodynamic excess functions for liquid mixtures, American Institute of Chemical Engineers Journal, 14 (1968) 135 – 144.

Rossi G.S, Dixon H.D, Purity analysis of highly purified materials by time-temperature cryometry, Journal of research of the National Bureau of Standards-A, Physics and Chemistry, 67A, (1963) 247 – 251.

Scheuerman R.F, Sass R.L, The crystal structure of valeric acid, Acta Crystallographica, 15 (1961) 1244.

Schroder B, Santos L.M.N.B.F, Marrucho I.M, Coutinho J.A.P., Prediction of aqueous solubilities of solid carboxylic acids with Cosmo-RS, Fluid Phase Equilibria, 289 (2010) 140 – 147.

Schrodle S, Buchner R, Kunz W, Automated apparatus for the rapid determination of liquid-liquid and solid liquid phase transitions, Fluid Phase Equilibria 216 (2004) 175-182.

Sewnairan R, Multipurpose Separation and Purification Facility, Master of Science in Engineering (Chemical Engineering), University of KwaZulu Natal, South Africa, (2001).

Sirota E.B, Supercooling, nucleation, rotator phases and surface crystallisation of n-alkane melts, Langmuir, 14 (1998) 3133 – 3136.

Slaughter D.W, Doherty M.F, Calculation of solid-liquid equilibrium and crystallisation paths of melt crystallisation processes, Chemical Engineering Science, 50 (1995) 1679 - 1694

Small D.M, The physical chemistry of Lipids: From alkanes to phospholipids, Plennum Press New York, 4 (1986) 587.

Smith J.M, Van Ness H.C, Introduction to chemical engineering thermodynamics, McGraw- Hill, 5th Edition (1996).

Smith J.M, Van Ness H.C, Introduction to chemical engineering thermodynamics, McGraw- Hill, 6th Edition (2001).

Snow R.L, Ott J.B, Goates J.R, Marsh K.N, Stokes R.H, O'Shea S, (Solid+Liquid) and (Vapour+Liquid) phase equilibria and excess enthalpies for (benzene+n-tetradecane),(benzene+n-hexadecane),(cyclohexane+n-tetradecane), and (cyclohexane + n-hexadecane) at 392.15, 298.15 and 308.15K. Comparison of GEm calculated from (vapour+liquid) and (solid+liquid) equilibria, Journal of Chemical Thermodynamics, 18 (1986) 107 – 130.

Strieter F.J, Templeton D.H, Crystal Structure of Propionic Acid, Acta Crystallographica, 15 (1962a) 1233.

Strieter F.J, Templeton D.H, Crystal Structure of Butyric Acid, Acta Crystallographica, 15 (1962b) 1240.

Tanaka Y, Kawakami M, Solid – liquid phase equilibria in binary (benzene, cyclohexane + n-tetradecane, n-hexadecane) systems at temperatures 230 – 323K and pressures up to 120MPa, Fluid Phase Equilibria 125 (1996) 103-114.

Torzo G, Soletta I, Branca M, Using Peltier cells to study solid liquid vapour transitions and super cooling , European Journal of Physics, 28 (2007) S13-S27.

Van Miltenberg J.C, van den Berg G.J.K, van Genderen A.C.G, An adiabatic calorimeter for small samples. The solid-liquid system Naphthalene-Durene, Thermochimica Acta 383 (2002) 13-19.

Wachter P, Schweiger H, Wudy F, Gores H J, Efficient determination of crystallization and melting points at low cooling and heating rates with novel computer controlled equipment, Journal of Chemical Thermodynamics, 40 (2008) 1542-1547.

Wahayudi B, Gupta S, Mclaughlin E, Solid-liquid phase diagrams of binary aromatic hydrocarbon mixtures from calorimetric studies, Journal of Chemical and Engineering Data, 34 (1989) 223-226.

Weast R.C, Handbook of Chemistry and Physics, CRC Press, 64th Edition (1983-1984).

Weir R.D, De Loos TH W, Measurement of the thermodynamic properties of multiple phases, Elsevier Amsterdam (2005).

Wilson G.M, Vapour-liquid equilibrium XI: A new expression for the excess free energy of mixing, Journal of American Chemical Society, 86 (1964) 127 – 130.

Yang M, Narita T, Tanaka Y, Sotani T, Matsuo S, Solid-Liquid phase equilibria in binary (1-octanol + n-alkane) mixtures under high pressure: Part 2 (1-octanol + n-octane, n-dodecane) systems, Fluid Phase Equilibria 204 (2003) 55 – 64.

Yoo K-P, Shin H.Y, Lee C.S, Approximate non-random two-fluid lattice hole theory. Thermodynamic properties of real mixtures. Bulletin of the Korean Chemical Society, 18 (1997) 841 – 851.

Zhang L, Gui Q, Lu X, Wang Y, Shi J, Lu B C Y, Measurement of solid-liquid equilibria by a flow cloud point method, Journal of Chemical and Engineering Data, 43 (1998) 32 – 37.

Appendix A

Thermodynamic Theory

A.1 Gibbs Phase Rule

The Gibbs phase rule is used to determine the number of intensive properties which can be determined in a system at equilibrium. The rule states that (Prausnitz et al., 1999);

Number of Intensive Properties = Number of components – Number of Phases + 2

The number of independent variables (intensive properties) in a system is called the degrees of freedom of that system. The number of degrees of freedom in a heterogeneous (multiphase) system depends on the state of equilibrium. A phase is described as having (m + 2) variables, but of these variables (m + 1) are independent (Nyvlt, 1977). The number of independent variables (degrees of freedom) in a heterogeneous system, which is in internal equilibrium and having π phases, is given by π (m + 1). If the entire system is described as being in a state of internal equilibrium, then among the [π(m + 1)] variables, there are [(π-1)(m+2)] equilibrium relations (Nyvlt, 1977).

The number of degrees of freedom F is the number of intensive variables used to describe the system less the number of relations or restrictions connecting them (Nyvlt, 1977);

$$F = \pi(m + 1) - (\pi - 1)(m + 2) \qquad \text{A-1}$$

$$F = m + 2 - \pi \qquad \text{A-2}$$

F - The degrees of freedom. The number of independently variable intensive properties required for the determination of the state of the system.

π - The number of phases or the number of mutually different parts of the system

m - The number of components or the number of stoichiometrically independent chemical species characterizing the system.

A.2 Chemical Potential

As mentioned before, real systems are described thermodynamically by abstract properties which are then translated to measurable properties. The abstract property that describes equilibrium is the chemical potential. This is an intensive property which is dependent on temperature, pressure and

composition. With the chemical potential it is possible to describe phase equilibria with measurable properties. The equation describing chemical potential comes from the description of the Gibbs energy (Prausnitz et al., 1999);

$$dG = -SdT + VdP + \sum_i \mu_i dn_i \qquad \text{A-3}$$

Resultantly the chemical potential is described as;

$$\mu_i = \left(\frac{\partial G}{\partial n_i}\right)_{T,P,n_i} = \overline{G} \qquad \text{A-4}$$

Where $\overline{G}$ is the partial molar Gibbs energy.
Most importantly for a heterogeneous system of π phases in a state of equilibrium, the following relation applies.

$$\mu_m^1 = \mu_m^2 = \ldots = \mu_m^\pi \qquad \text{A-5}$$

The equation applies for m components and π phases.

A.3 Fugacity and Activity

In order to relate chemical potential to real systems G.N Lewis, introduced the concept of fugacity (Smith et al., 2001 and Prausnitz et al., 1999). Fugacity is an auxiliary function which translates chemical potential to a function with properties that can be measured within the system. Through fugacity and another quantity know as activity, it is possible to calculate the properties of a system at equilibrium using the equilibrium criterion described through chemical potential (Equation A-5).

The simplest system to describe in terms of properties is the ideal gas state; hence the chemical potential was first related to an ideal gas state. The relation between ideal gas state and real state can then be obtained by applying a factor of deviation. For an ideal system (Prausnitz et al., 1999);

$$\mu_i - \mu_i^0 = RT\ln\frac{P_i}{P_i^0} \qquad \text{A-6}$$

Fugacity exists for any system with different phases (solid, liquid or gas), which is pure or mixed, ideal or non-ideal and undergoes an isothermal change. The relationship between fugacity and chemical potential is given by the relation (Prausnitz et al., 1999 and Nyvlt, 1977);

$$\mu_i - \mu_i^0 = RT \ln \frac{f_i}{f_i^0} \quad \text{A-7}$$

Where f_i is the fugacity of the system

Superscript ^{0} refers to the property at the standard state

The ratio of fugacity and fugacity at its standard state is known as the activity (a) i.e. (Prausnitz et al., 1999);

$$\frac{f_i}{f_i^0} = a \quad \text{A-8}$$

The activity is a measure of the systems fugacity relative to its standard state, and provides a difference between the substances chemical potential at required state and at its standard state.

A.3.1 Fugacity in Phases

For a binary system with two phases α and β the fugacity relationship is given by the following equations for each phase (Prausnitz et al., 1999);

$$\mu_i^{\alpha} - \mu_i^{\alpha 0} = RT \ln \frac{f_i^{\alpha}}{f_i^{\alpha 0}} \quad \text{A-9}$$

$$\mu_i^{\beta} - \mu_i^{\beta 0} = RT \ln \frac{f_i^{\beta}}{f_i^{\beta 0}} \quad \text{A-10}$$

According to Equation A-5 the equilibrium criterion therefore becomes;

$$\mu_i^{\alpha 0} + RT \ln \frac{f_i^{\alpha}}{f_i^{\alpha 0}} = \mu_i^{\beta 0} + RT \ln \frac{f_i^{\beta}}{f_i^{\beta 0}} \quad \text{A-11}$$

If fugacity in the standard states is equal then the following equation exists and is known as the iso-fugacity criterion. This equation describes equilibrium between two phases. According to Equation A-8, this implies that the activity of species i in any two phases are equal provided that the standard fugacity is the same;

$$f_i^{\alpha} = f_i^{\beta} \ldots \quad \text{A-12}$$

A.3.2 Fugacity in Solution, Excess Properties and Activity Coefficients

The deviation of a property from ideal behaviour is expressed in terms of the excess property. It is from the excess property that the activity coefficient is defined. The activity coefficient is a factor which represents the deviation of a property from the ideal property.

By definition the excess property in summary is given as (Smith et al., 2001);

$$M^E \equiv M_{(\text{actual solution at T ,P and x})} - M_{(\text{Ideal solution at same T ,P and x})}$$

Where M represents a property e.g. Gibbs Energy, G

The activity coefficient is derived from the excess Gibbs energy property because of the definitions of chemical potential and resultantly fugacity and activity. When equations A-4 and A-7 are combined and integrated the partial Gibbs property is described in the following equation (Smith et al., 2001);

$$\overline{G}_i = \Gamma_i(T) + RT \ln \hat{f}_i \qquad \text{A-13}$$

For an ideal solution;

$$\overline{G}_i^{id} = \Gamma_i(T) + RT \ln x_i f_i \qquad \text{A-14}$$

The fugacity is replaced by the Lewis/Randall rule (Smith et al., 2001), the excess Gibbs property is thus defined as (Smith et al., 2001);

$$\overline{G}_i^E = \overline{G}_i - \overline{G}_i^{id} = RT \ln \frac{\hat{f}_i}{x_i f_i} \qquad \text{A-15}$$

From this equation we define the activity coefficient γ_i (Smith et al., 2001); the activity coefficient is a measure of the deviation of a system from the ideal solution state;

$$\gamma_i = \frac{\hat{f}_i}{x_i f_i} \qquad \text{A-16}$$

The main function of excess functions has been to determine relations for multi-component mixtures. This can be done through liquid phase excess function property models such as the Wilson model.

Appendix B

Experimental Solid-Liquid Equilibria Apparati

B.1 Caloric Methods

B.1.1 Adiabatic Calorimetry

This is a method of measuring SLE data that is known for accuracy and precision in producing results. This is because the sample can be heated gradually and systems with low or infinitesimal heat flux during phase transition can be measured (Hohne et al., 2003). The technique is by application of a known heat flux and maintenance of adiabatic conditions, such that the change in temperature that arises in the sample is known to be entirely due to the applied heat.

Adiabatic calorimetry has evolved from being a time consuming technique which could take as long as 24 hours for generation of results, to being one which is faster and less labour intensive. The experimental procedure and operation of the apparatus of an adiabatic calorimeter can be described by experiments conducted by P.R van der Linde, described by Weir and de Loos (2005).

An example of an adiabatic calorimeter is the calorimeter designed by van Miltenburg et al. (2002) which could measure samples as small as 0.6 cm^3. The operating temperature range for this apparatus was 10 – 420 K and has an accuracy of 0.2 % for specific heat capacity measurements. Excess Gibbs energy was calculated from experimental data, for naphthalene – durene system and results yielded a relative error of 24.2% from literature values.

B.1.2 Differential Scanning Calorimetry (DSC)

Over the years improvements have been made to make DSC's more accurate. Automation has increased the speed at which results are generated and thereby reducing the work required by the experimenter (Mohan et al. (2002)). For accuracy, according to Hohne et al. (2003) correctly calibrated DSC's can measure specific heat capacity up to an accuracy of 1 to 2% and even better.

B.1.2.1 Apparatus by Wahayudi et al. (1989)

The apparatus by Wahayudi et al. (1989) used differential scanning calorimetry. Experiments were conducted on binary aromatic compounds, namely flourene - dibenzofuran, dibenzothiophene - dibenzofuran, flourene - dibenzothiophene as follows:

- The apparatus was a calorimeter with two identical heat flow detectors, surrounded by a heat conducting block.
- The temperature of the block was controlled by a programmable controller and it was assumed that the temperature of the block and the sample were the same (recorded temperatures were corrected after calibration).
- Heat was transferred from the heat flow detectors to two identical tubes, one filled with sample and the other empty.
- Detectors were differentially connected and thermal perturbations to the block eliminated. As a result only the signal to the sample was generated. During phase transition the heat flux rose above the applied heat, due to latent heat of transformation.

From the generated thermogram Wahayudi et al. reported a precision of ±0.3 K for temperature readings obtained from the calorimeter.

B.1.3 Other Caloric Equipment

Apart from obtaining phase diagrams through thermograms using DSC, more analytical methods can be used. An example is the apparatus of Coutinho et al. (1998) which uses the caloric measurements to define a eutectic point, and then by use of the lever rule construct the phase diagram.

B.1.3.1 Apparatus of Coutinho et al. (1998)

Measurements taken were the amount of liquid formed during melting as a fraction of the initial sample. This was determined by analysis of the change in enthalpy during heating/melting of the solid. The phase diagram was then formed by using the lever rule. The method was applicable to systems which exhibited no solid phase solubility. The caloric measurements are used to define the eutectic point composition and the temperature. The composition is determined by the total liquid fraction at this point, with enthalpies calculated from the generated thermogram.

- The apparatus used 150 μl equilibrium trays filled to 66% volume.
- The DSC was a Mettler TA 3000.
- Temperatures were measurable up to 150 K through a refrigeration system that used liquid nitrogen for cooling.
- The heating rate used on the apparatus was 1 K/min over a temperature range of 150 K – 320 K. Every 0.75 K enthalpy changes were registered.

Results obtained from this apparatus were reported to be low compared to other DSC apparati. However the apparatus was cheap and easy to use.

B.2 Synthetic Methods

B.2.1 Apparatus of Di Nicola et al. (2008)

This apparatus was for measurement of solid-liquid equilibria of gases in liquids, namely refrigerants such as carbon dioxide + diflouroethane, nitrous oxide + 1,1 – diflouroethane, up to temperatures of 132 K.

- The equilibrium cell was a stainless steel cylinder with a volume of 43 cm^3. It was fitted with a stainless steel stirrer rod which was driven by a magnet, for homogenising the sample from the centre of the cell. From the top of the cell a temperature sensor was inserted and in another opening, gas was introduced into the cell.
- The apparatus comprised a two stage cooling system. This was heat exchange of the sample cell with compressed air by means of copper tubing covering the sample cell. Compressed air was passed through the tubes for cooling. The air was then subsequently cooled in a two stage cooling system, firstly through a heat exchanger with air circulating on the tube side and then through heat exchange with liquid nitrogen. Liquid nitrogen was used to achieve the low temperatures required to crystallise the sample.
- The phase transition temperature was determined by studying the cooling curve generated. Temperature was measured using a platinum resistance 100 Ω Minco sensor and the calculated uncertainty on temperature reading was ±0.023 K

B.2.2 Apparatus of Domanska (1996)

Domanska (1986) has used a dynamic (Synthetic) method, in which the disappearance of the last crystal was observed as the SLE point. The details of the apparatus are reported Domanska (1996):

- The equilibrium cell was a pyrex cell which had temperature control provided by immersion in a thermostat.
- Temperature was measured by a calibrated Aschutz thermometer with 0.1 K subdivisions and immersed in the thermostatting liquid.
- The accuracies obtained on temperature measurements were ±0.1 K and mole fractions were measured with an accuracy of ±0.0005 K.
- The mixture of solute and solvent was heated at a rate of <2 Kh^{-1} at the equilibrium temperature, and the last crystal disappearance was observed by the experimenter.

B.2.3 Apparatus of Zhang et al. (1998)

The apparatus designed was used for measurement of solubility of salts in water. It has been described as follows:

- The apparatus comprised of a thermostated glass equilibrium flask immersed in a thermostat. It also consisted of a water addition section followed by a phase change detection section.
- Phase change detection was achieved by shining a beam of single-coloured laser through the sample.
- The analysis of phase change was by the Tyndall Effect which was discovered by Fridrihsberg (1986). This says that a solution can undergo three states during crystallisation. These are; saturation with crystals, equilibrium, and sub-saturation. Each state is characterised by a specific image when light passes through the sample (Zhang et al., 1998).
- For solubility measurements, the sample was a mixture of water and salt crystals. The mixture was gradually heated and stirred. A continuous beam of light was passed through the mixture and corresponding temperatures recorded to indicate the phase transition point.
- Equilibrium was taken to be the point of first crystal appearance when the apparatus was cooling and as the point of complete dissolution when the apparatus was heating. In their results a maximum deviation with literature values of 0.043 mol/kg_{H2O} was calculated.

B.2.4 Apparatus of Schrödle et al. (2004)

An automated apparatus was designed by Schrödle and co-workers which used the principle of optical effects to obtain solid-liquid equilibria data. Phase transition temperature was determined by identifying the temperature at which a change in turbidity occurred i.e. cloud point. The apparatus was fully automated and was able to process up to six samples simultaneously without input from the experimenter. The main features and operation are described;

- The apparatus consisted of a sample holder which had a magnetic stirrer immersed inside it. The sample holder was positioned inside a Dewar vessel which was filled with Silicon oil as the fluid medium. Temperature was measured by an RTD which was immersed in the oil surrounding the sample cell. The temperature probe used was from the National Institute of Standards and Technology (NIST) and was reported to have an accuracy better than 0.01 K. (The temperature measured by the probe is taken as the sample temperature). The apparatus was designed to simultaneously measure up to six samples with a volume of 2.75 ml.
- Heating and cooling of the sample was achieved either automatically using a resistance heater or manually via an external thermostat.

- For determining phase transition, six light emitting diodes (LED) were used to deliver light into the sample cell. Transmitted light was picked up by photo detectors which were either LDR's or photodiodes. The photo detectors were part of a circuit which converts the light flux into a voltage signal U_{det}.
- For analysis of data, turbidity was measured as a function of temperature and a turbidity temperature graph was generated.
- The apparatus was used to successfully measure critical temperatures and melting points for binary and single component samples. It was reported to measure temperatures with a resolution of 1 mK (0.001K) and with an accuracy of 0.01 K.

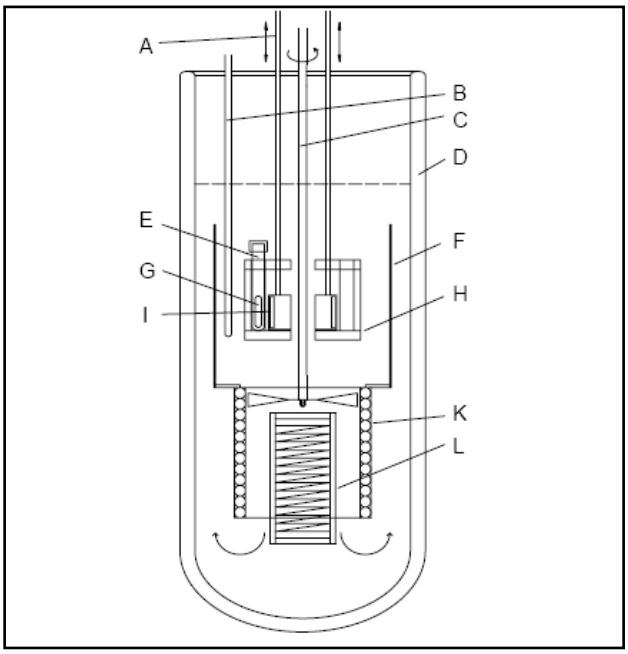

Figure B-1: Cross Sectional view of apparatus of Schrödle et al. (2004). Adapted from Scrödle et al. (2004).

Figure B-1 shows a cross sectional view of the apparatus designed and the components labelled in the diagram are as follows: solenoid rod (A), temperature sensor (B), stirrer (C), dewar vessel (D), sample cell (E), flow controller/heat conductor (F), magnetic follower (G), sample cell holder (H), magnet (I), heat exchanger (K) and resistance heater (L) (Schrödle et al., 2003).

Equipment Summary

- Equipment was operable from -20^{o}C to 80^{o}C
- Temperature reading accuracy: > 0.01K

To evaluate the apparatus they measured the critical temperature of the 2,6 lutidine + water system was measured. They also measured the solid –liquid equilibria of ethylene carbonate and the solid-

liquid equilibria of the pentaethylene glycol dodecyl ether + water system. Experimental results were compared against literature values and the results reported were as follows (Schrödle et al., 2004);

- Critical temperature of the 2,6-lutidine + water system was found to have an accuracy of ±0.01 K and the reproducibility was ±0.003 K
- Individually measured melting points were accurate to ±0.0007 K
- Phase transition temperatures with accuracies that were greater than 0.1 K were obtained.

B.2.5 Apparatus of Wachter et al. (2008)

The apparatus measured solid-liquid as well as liquid-liquid equilibria using the visual method by analysis of the temperature profile.

- The equilibrium cell was a transparent glass tube with a Teflon coated magnetic stirrer bar inside. A temperature measuring, glass encased, home built precision thermometer was immersed inside the sample. The entire assembly was sealed and placed in an empty air chamber (outer tube) that acted as thermal insulation. This equilibrium cell assembly then fit into a magnetic stirrer device designed to hold up to thirty equilibrium cells (sample tubes). The entire assembly was then placed in a thermostat which controlled cooling and heating rates.
- The thermostat was made up of a bath with silicon oil as the fluid medium. In it was a stirring mechanism, a platinum resistance thermometer and a heat source and heat exchanger immersed in it. Cooling was achieved through a cryostat coupled to the thermostat via the heat exchanger. Variable cooling rates were applied.
- The operating temperature range for the thermometer was 193 K – 313 K. It was connected to a computer using homebuilt software which could measure data, at a rate of one point per second.

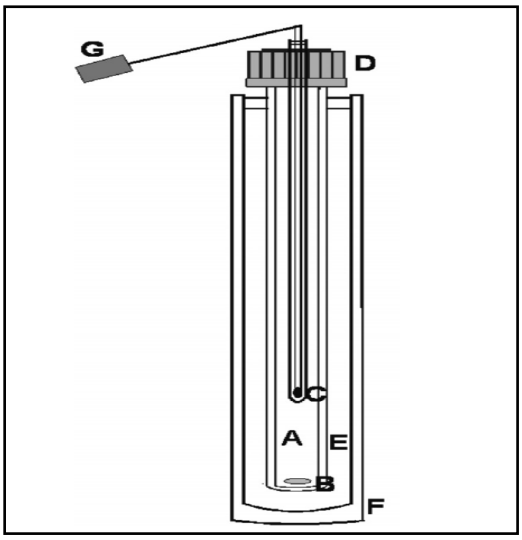

Figure B-2: Sample holder assembly of the apparatus of Wachter et al. (2008). Adapted from Wachter et al. (2008).

Figure B-2 shows the sample holder assembly of the apparatus which is comprised of: Inner pyrex tube (A), magnetic stirrer (B), glass tube with thermistor (C), SQ18 closure with Teflon coated rubber seal (D), thermal insulation (E), Outer Pyrex tube (F), and the connector for the thermistor (G). The measuring cell above is fitted into a magnetic stirring device which can hold up to 21 measuring cells (Wachter et al., 2008).

Equipment Summary

Temperature Range: 223 K – 283 K, (thermometer could measure up to range of 193 K-313 K with accuracy > 0.03 K)

To determine the accuracy and operability of the equipment, experiments were undertaken to determine critical temperatures and melting points of various chemicals. These were acetonitrile, dimethyl carbonate and methoxy propionitrile. The results reported were (Wachter et al., 2008):

- Standard deviations of measurements between 0.03 and 1 K compared to literature values.
- For low rates there was difficulty in evaluating the cooling and heating curves, and concluded that this was due to diffuse transitions taking place.

Appendix C

Uncertainties in System Measurements

The uncertainty in each measurement for a system was measured by calculating the standard deviation of the repeat measurements on each composition measured. The uncertainties have been discussed in the results and discussion chapter. Standard deviation is defined as:

$$\text{Standard Deviation }, \boldsymbol{\sigma} = \sqrt{\Sigma\left(T_{exp} - \mu\right)^2 / N} \qquad \text{C-1}$$

Where μ is the mean of T_{exp}

N is the number of data points measured

The standard deviation is therefore applied as a measure of the reproducibility of the individual temperature measurements and the results are presented as follows.

C.1 Uncertainties in Test System Measurements

Figures C-1, C-2 and C-3 show the uncertainties that are calculated for the points measured in the cyclohexane + hexadecane systems on the Peltier and Glass apparati and the 2-butanol + water system measured on the Peltier apparatus.

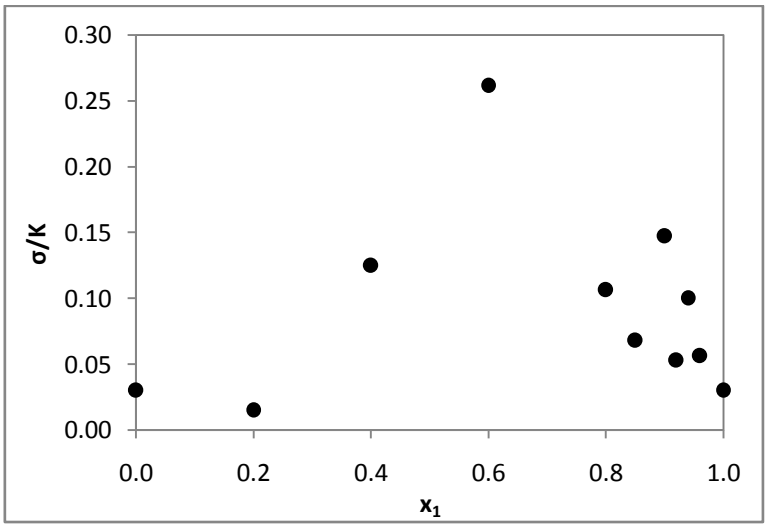

Figure C-1: The scatter plot for the errors in terms of standard deviation on the melting point measurements of the cyclohexane (1) + hexadecane (2) test system measured on the Peltier apparatus.

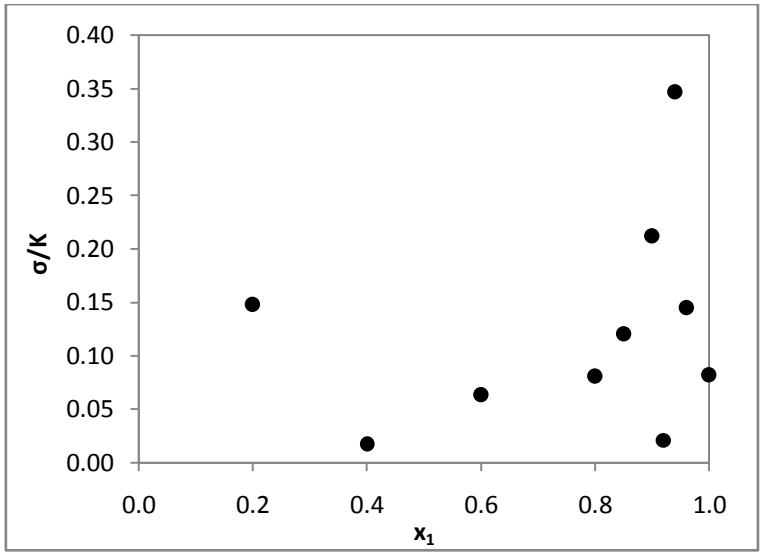

Figure C-2: The scatter plot for the errors in terms of standard deviation on the melting point measurements of the cyclohexane (1) + hexadecane (2) test system measured on the Glass apparatus.

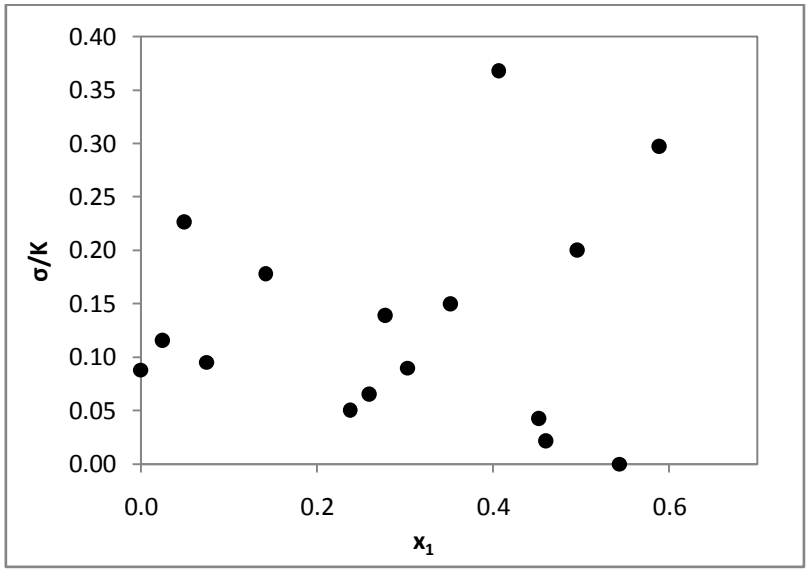

Figure C-3: The scatter plot for the errors in terms of standard deviation on the melting point measurements of the 2-butanol (1) + water (2) test system.

C.2 Uncertainties in New System Measurements

Figures C-4 and C-5 show the uncertainties measured for each SLE point for the new systems measured.

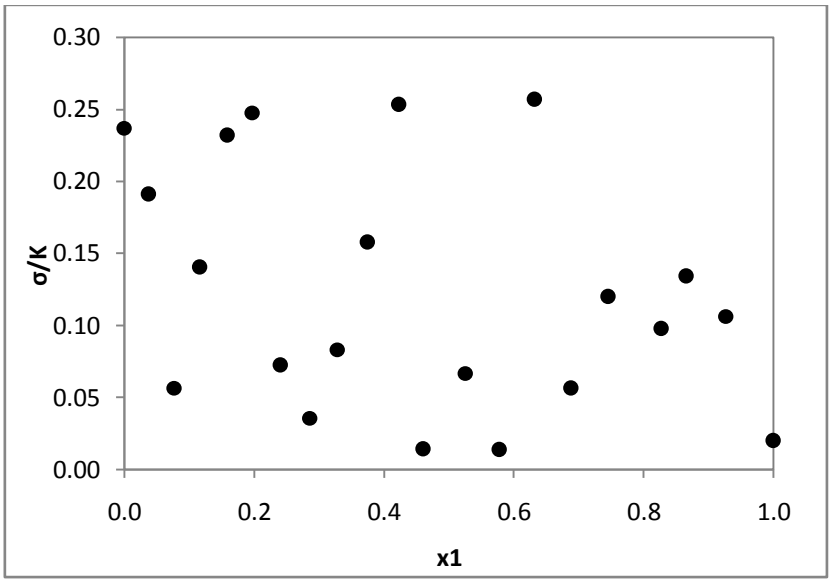

Figure C-4: The scatter plot for the errors in terms of standard deviation on the melting point measurements of the heptanoic acid (1) + butyric acid (2) system.

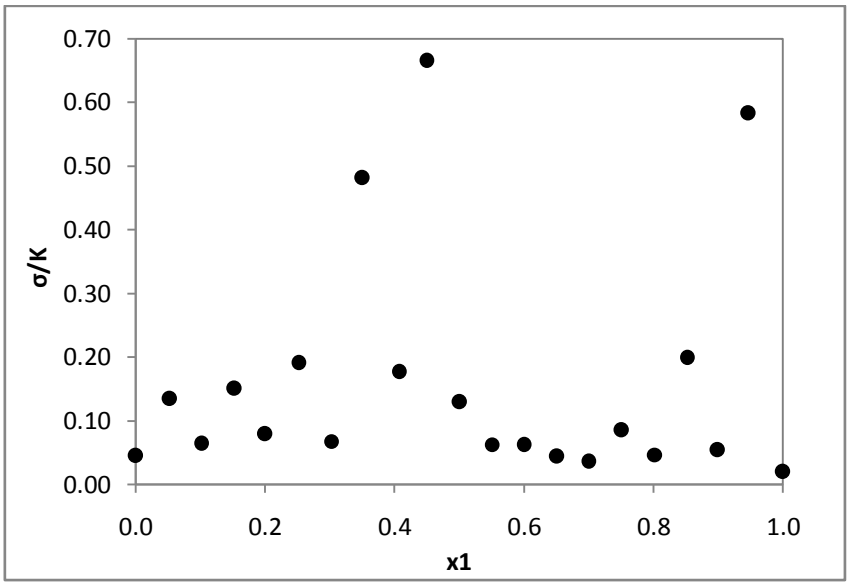

Figure C-5: The scatter plot of the errors in terms of standard deviation on the melting point measurements of the heptanoic acid (1) + hexanoic acid (2) system.

Appendix D

Pure Component Properties

The pure component properties that were used in the modelling were obtained from the Dortmund Data Bank (DDB) software (2009) and are given in Table D-1.

Table D-1: Pure Component Properties of the Chemicals Used.

	T_m /K	H_m J/mol	T_t/K	H_t J/mol
Water	273.15	6000.11	-	-
2-Butanol	158.50	5970.79	-	-
Butyric acid	267.45	11074.91	-	-
Cyclohexane	279.80	2630.16	186.10	6740
Heptanoic acid	265.65	15010.14	-	-
Hexadecane	291.15	53394.31	-	-
Hexanoic acid	269.55	15110.20	-	-